STUDIES OF MESENCHYMAL AND AMOEBOID

MIGRATION ON COMPLIANT SUBSTRATES

YIP AI KIA

B. Eng. (Hons.), NUS

A THESIS SUBMITTED FOR THE DEGREE OF

DOCTOR OF PHILSOPHY

NUS GRADUATE SCHOOL FOR INTEGRATIVE SCIENCES

AND ENGINEERING

NATIONAL UNIVERSITY OF SINGAPORE

2013

DECLARATION

I hereby declare that this thesis is my original work and it has been written by

me in its entirety. I have duly acknowledged all the sources of information

which have been used in the thesis.

This thesis has also not been submitted for any degree in any university

previously.

_____

Yip Ai Kia

30 May 2013

ACKNOWLEDGEMENTS

TABLE OF CONTENTS

SUMMARY

Studies have reported that cells utilize two different migration strategies: Mesenchymal cell migration, commonly utilized by fibroblasts and epithelial cells, is characterized by actin polymerization driven protrusions and dependent on cell-matrix adhesiveness. In contrast, amoeboid cell migration, observed in the migration of leukocytes and tumor cells through three-dimensional (3D) extracellular matrix (ECM), is characterized by rapid shape changes and its independence from cell-matrix adhesion. Tumor cells have also been shown to switch between the two modes of migration depending on factors present in the ECM. Unfortunately, mechanisms underlying amoeboid cell migration remain vague and little is known about the interplay of physical variables of the ECM, in determining cellular response and migration strategies.

During mesenchymal cell migration, ECM rigidity appears to be an important physical variable sensed by cells. I found that maximal mesenchymal cell migration speed occurred at intermediate rigidities (6-16 kPa). The biphasic behavior of cell speed with substrate rigidity likely results from a balance between force generation within a cell, and the amount of resistance against cell migration provided by cell-matrix adhesions. However, details of the rigidity sensing mechanism remain elusive. Using traction force microscopy, I reported two-dimensional (2D) traction stress measurements of

fibroblasts, on polyacrylamide gels with Young's moduli varying from 6-110 kPa. On soft gels (rigidity < 20 kPa), cell-exerted substrate deformation remained constant, independent of the substrate rigidity, suggesting that cells adapt to increasing substrate rigidity by generating more forces to conserve strain. In contrast, on stiff gels (rigidity > 20 kPa), traction stress plateaus at a limiting value, suggesting that cells are limited by the maximum amount of force cells can generate.

I have also quantified amoeboid and mesenchymal migration in confined environments using 3D traction force microscopy. Neutrophil-like, differentiated human promyelocytic leukemia (HL60) cells confined between two pieces of polyacrylamide gels, with varying gap sizes, were found to exhibit two modalities during migration: Cells formed blebs (amoeboid mode) on non-fibronectin coated gels, and lamellipodia (mesenchymal mode) on fibronectin coated gels. In the amoeboid mode, cells migrate via a 'chimneying' mechanism by generating anchoring stresses normal to the confining gels, and shearing stresses at bleb protrusions. Bleb growth shifted the anchoring stress forward resulting in cell movement. On the other hand, cells in the mesenchymal mode generated contractile, opposing shearing stresses at the cell front and rear during protrusion and retraction, respectively. Based on these traction stress differences, I proposed quantitative measures which may be used to classify cells into the amoeboid or mesenchymal mode of migration.

In addition, I found that, unlike mesenchymal cell migration, amoeboid cell migration speed is not affected by gel rigidity. Instead, amoeboid cells appear to sense the amount of confinement cells experience, as maximal amoeboid migration speed occurred at an intermediate gap size. A computational model was used to explain this biphasic behavior, and the model predicted that this optimum gap size can be increased by weakening the cell membrane-cortex adhesion strength. Collectively, my results highlight clear mechanistic differences underlying mesenchymal and amoeboid cell migration.

LIST OF TABLE

LIST OF FIGURES

LIST OF ABBREVATIONS

2D   Two-dimensional

3D   Three-dimensional

ACA   N-acryloyl-6-aminocaproic acid

ADAM   A disintegrin and metalloprotease

AFM   Atomic force microscope

ARP2/3   Actin-related-protein 2/3

BIS   N,N'-methylenebisacrylamide

CV   Coefficient of variance

dHL60   Differentiated human promyelocytic leukemia

DIC   Differential interference contrast

DMSO   Dimethyl sulfoxide

DNA   Deoxyribonucleic acid

DVC   Digital volume correlation

ECM   Extracellular matrix

ERM   Ezrin Radixin Moesin

F-actin	Filamentous actin
FAK	Focal adhesion kinase
FFT	Fast Fourier Transform
fMLP	Formyl-Methionyl-Leucyl-Phenylalanine
G-actin	Globular actin monomers
GFP	Green fluorescent protein
HEPES	4-(2-hydroxyethyl)-1-piperazineethanesulfonic acid
HL60	Human promyelocytic leukemia
ICAM-1	Intercellular Adhesion Molecule 1
mDia2	Mammalian diaphanous-related formin-2
MAT	Mesenchymal to amoeboid transition
MDCK	Madin-Darby canine kidney
MEF	Mouse embryonic fibroblasts
MES	2-(N-morpholino)ethanesulfonic acid
MMP	Matrix metalloproteinase
NA	Numerical aperture
NBT	Nitroblue tetrazolium

NIH3T3 cells	National Institutes of Health 3-day transfer, inoculum 3 x 10^5 cells
RNA	Ribonucleic acid
ROCK	Rho kinase
PBS	Phosphate buffered saline
PGCs	Primordial germ cells
SE	Standard error
Sulfo-SANPAH	Sulfo-succinimidyl-6-(4-azido-2-nitrophenyl-amino) hexanoate
TEMED	N,N,N',N'-tetramethylethylenediamine
UPAR	Urokinase plasminogen activator surface receptor
UV	Ultraviolet

1   INTRODUCTION AND LITERATURE REVIEW

1.1   The importance of studying cell migration

The study of cell migration originated from observations of bacteria and protozoa movement, during the 17th century, when observations of cells were made using simple light microscope by Leeuwenhoek (1-4). In the 19th century, Nobel Prize laureate Mechnikov observed a mass of mobile cells surrounding foreign bodies introduced in the larvae of starfishes, and deduced that these mobile cells fight against the foreign bodies introduced, as part of the organism's first immune response in a process termed as phagocytosis (5). However, it was not until the 20th century, when further improvements to the optical microscopy such as phase contrast, differential interference contrast (DIC), fluorescence, and time-lapse microscopy were introduced, that cell migration was studied in greater details, quantified and properly documented (2,3).

Today, cell migration has been found to be a fundamental process in the development and normal functioning of multicellular organisms. For example, in embryonic development and morphogenesis, cells have to move either collectively or independently during gastrulation to specific locations to establish the basic body plan essential for the organism's survival (6,7,8). In another example, upon skin injury which exposes the organism to the

pathogens in the external environment, epithelial cells have to migrate towards the injury site to close the wound as part of the wound healing process (9,10). Leukocytes also have to migrate to the site of infection as part of the body's immune response against foreign bodies (11,12). Defects in the cells' ability to migrate can have serious consequences leading to developmental defects in the embryo (7,8), impaired wound healing (9), or bacterial infections (11). In cancer metastasis, tumor cells also have to migrate into and out of the lymphatic and blood vessels in order to invade other distant organs and cause secondary growth (13,14). Once the cancer cells have metastasized, a patient's survival rate is known to greatly reduce (15). Understanding how cells migrate would therefore not only aid in developing therapies to restore normal functioning of the organisms, but also in developing anti-tumor drugs that stop malignant cells from spreading to other sites.

1.2   Cells: The structural unit of living organisms

An understanding of cell migration first requires knowledge of what a cell is. Cells are the basic building blocks of living organisms. Living organisms can be classified as unicellular (comprising of only one-cell, e.g. bacteria and protozoa) or multicellular (comprising of more than one cell, e.g. most plants and animals) organisms. In addition, there are two types of cells with different structural compositions: the prokaryotic cell (e.g. bacteria), and the eukaryotic cell (e.g. protozoa and most multicellular organisms). I will

only further elaborate on the eukaryotic cell components as the focus of this thesis is on eukaryotic cell motility.

The eukaryotic cell (Figure 1) comprises mainly of a fluid known as the cytoplasm, enclosed within a lipid bilayer known as the plasma membrane. Another compartment within the cell is called the cell nucleus where the chromosomes, which contain genetic information for cell replication and function in the form of deoxyribonucleic acid (DNA), can be found. The cell nucleus is enclosed by two lipid bilayer membranes known as the nuclear envelope. The cell transcripts the genetic information in the nucleus into shorter sequences called the ribonucleic acid (RNA) to be transported out of the nucleus to other organelles (e.g. endoplasmic reticulum and the Golgi apparatus) in the cytoplasm. These organelles can then synthesize proteins in a process known as RNA translation.

In addition, the cell cytoplasm also contains a meshwork of three different kinds of filamentous proteins, namely actin filaments, microtubules and intermediate filaments. These filaments are collectively known as the cytoskeleton and form the skeleton of a cell. They have multiple functions in cells, some of which include maintaining the cell shape, intra-cellular transport and cell migration processes. In particular, the actin filaments (F-actin), formed from the polymerization of globular actin monomers (G-actin), have been associated with multiple processes during cell migration, most of which will be elaborated on in Sections 1.3 and 1.4.
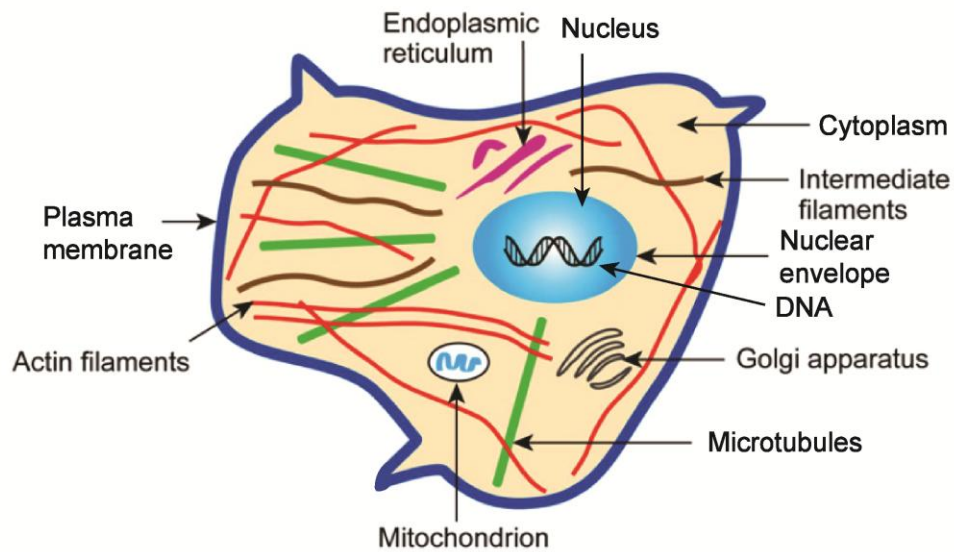
Figure 1 Ilustration of a typical eukaryotic cell. Figure adapted from reference (16).

1.3   Mesenchymal cell migration: Actin polymerization driven motility

One of the significant milestone in cell migration studies occurred in the mid 20th century, when Abercrombie and Heaysman set up the first time-lapse experiment to study chicken fibroblasts' migration patterns on a planar surface (17). Abercrombie et al. also first described the dynamic movements of the leading edge of the chicken fibroblast in the 1970s. The fibroblast's flatten leading edge (termed lamella) was found to form repetitive cycles of protrusions and withdrawals (sometimes accompanied by appearance of ruffles), with a greater time spent in protrusion than withdrawal, hence resulting in a forward movement of the cell (18,19). Particles which happened to attach to the dorsal surface of the cell were also observed to move

4

backwards during cell locomotion, leading to the idea that new materials are constantly made at the cell's leading edge which then caused excess membrane and particles on the membrane, to move backwards (20). Using the electron microscope to visualize sections of fibroblasts which were moving on a flat substratum, Abercrombie et al. showed that the cell's lamellipodia are of constant thickness (100-200 nm in thickness) and contains a fibrillar cytoplasm (21). These fibrillar structures were later identified as actin filaments (22,23). Abercrombie et al. also observed that the cell closely approach the substratum at localized regions in the cell, thus forming adhesions. In the cytoplasm near these adhesions, electron-dense plaques containing long filaments are found, suggesting that these adhesions link up to the fibrillar network within the cell (21).

These observations by Abercrombie et al. formed the basis for our understanding of what is later termed mesenchymal cell migration. Since then, cell migration has been widely studied on 2D surfaces and it has been established that during mesenchymal cell migration, cells move via a five-step migration cycle summarized in Figure 2. The first step involves the protrusion of the cell's leading edge where the growing actin filaments connect to adaptor proteins and push the cell membrane outwards. Step two involves cell-matrix interaction and formation of focal contacts via integrin receptors on the cell membrane and its ligands in ECM. The integrins cluster in the cell membrane and recruit adaptor and signaling proteins, thereby inducing phosphorylation

5

and dephosphorylation signals into the cell. The third step involves the recruitment of surface proteases to substrate binding sites to cleave ECM components such as collagen, fibronectin and laminins. Step four involves cell contraction triggered by the contraction of active myosin-II that are bound to the actin filaments (acto-myosin). The last step in the migration cycle involves focal contact disassembly and detachment at the trailing edge. The integrins detach from the substrate and are either endocytosed for recycling towards the leading edge or deposited onto the substrate (14).
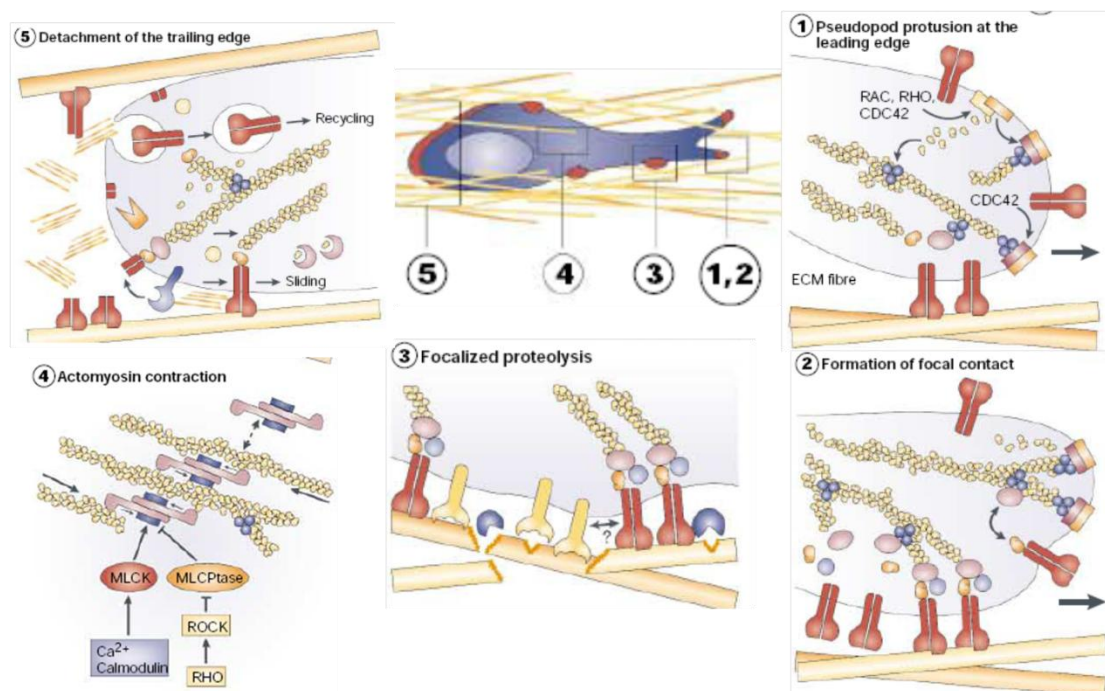
Figure 2 Five step model of mesenchymal cell migration in 3D. Figure adapted from reference (14).

1.3.1 Lamellipodia, filopodia, podosomes and invadopodia: Actin rich protrusions

The first step involved in cell migration often requires cell protrusion at the cell front. In mesenchymal cell migration, such protrusions are known to be enriched with F-actin. Specifically, these actin-based structures are known as lamellipodia, filopodia, podosomes and invadopodia (Figure 3).

Lamellipodia (Figure 3*A*), first observed by Abercrombie et al. in chicken fibroblasts, are thin sheet-like protrusions comprising of dense and dynamic branch networks of F-actin (18,21-23). These branched F-actin networks results from actin polymerization mediated by the actin nucleator known as actin-related-protein 2/3 (ARP2/3) on existing actin filaments, resulting in a meshwork with angles of typically 70º between each branch of the filaments (23,24). The polymerization of new actin filaments then drives the extension of the cell membrane forward (23), hence forming the flat sheets of membrane protrusions known as lamellipodia.

Filopodia (Figure 3*B*) are finger-like protrusions which help the cell to sense its immediate surroundings (25,24). These finger-like protrusions, unlike the flat, sheet-like lamellipodia, comprise of tight parallel bundles of F-actin, likely nucleated by formins such as mDia2 (mammalian diaphanous-related formin-2) (24). Filopodia act as potential sites for signal transduction as it contains receptors which can pick up a variety of signaling molecules (24).

The tip of filopodia may also contain cell adhesion molecules like integrins and cadherins which help the cell to probe its environment and form initial adhesion sites (24).
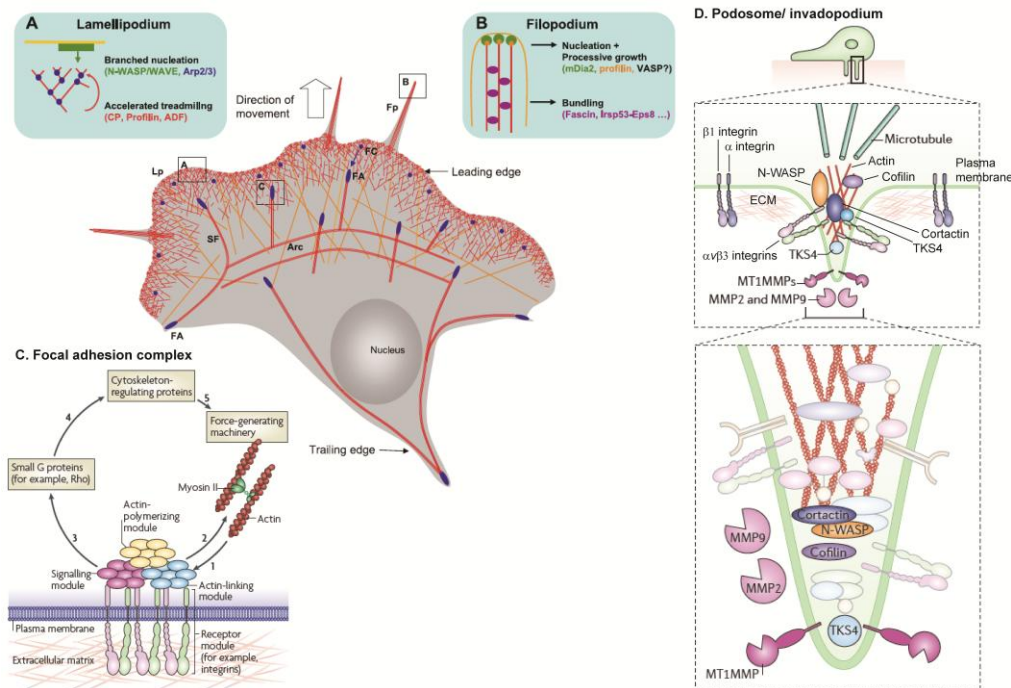
Figure 3 Schematic illustrations of (*A*) lamellipodium, (*B*) filopodium, (*C*) focal adhesion complex, and (*D*) podosome and invadopodium. Figure adapted from references (26,27,29).

Podosomes and invadopodia (Figure 3*D*) are actin rich, adhesive structures found on the ventral surface of the cell, and both are characteristically comprised of an actin rich core, surrounded by a ring of adhesion proteins (26-28). These structures are termed podosomes in normal cells such as macrophages, dendritic cells, endothelial cells and vascular smooth muscle cells, and invadopodia in cancerous cells (26,28). Formation of

podosomes and invadopodia has been associated with matrix remodeling, cancer cell invasion and metastasis, by degrading the ECM through the secretion of proteases (26).

1.3.2 Focal adhesion complexes: Anchoring cells to the ECM

After the cell protrudes, another important step during mesenchymal cell migration involves the formation of cell-matrix adhesions to stabilize the protrusions. Cell-matrix adhesions, known as focal adhesion complexes (Figure 3*C*), are usually mediated by integrin receptors via their extracellular domains while the intracellular domains either interact with the actin cytoskeleton to strengthen the mechanical ECM to cytoskeleton linkage, or participate in adhesion mediated signaling events (29,30).

These integrin-mediated cell-matrix adhesions can be classified into three stages of interaction with the ECM: Focal contact, focal adhesion and fibrillar adhesion (30,31). Small and short-lived cell-matrix interactions called focal contacts (*FC* in Figure 3) are usually found at the cell periphery, along the leading edge of migrating cells. Focal contacts contain proteins such as β3-integrin, vinculin, paxillin, α-actinin, low levels of FAK (focal adhesion kinase) and possibly Arp2/3. These focal contacts may grow in size and mature to form stable focal adhesions. Focal adhesions (*FA* in Figure 3 and Figure 3*C*) contain proteins such as αVβ3 integrin, zyxin, vinculin and paxillin, and are highly tyrosine phosphorylated. Fibrillar adhesions arise from

focal adhesions and are located at the central positions within the cell. They contain little or no phosphor-tyrosine, and are associated with fibronectin fibrils, $\alpha 5\beta 1$ integrin and tensin (30).

These cell-matrix adhesions help to anchor the cell to the ECM, as the cell's contractile acto-myosin machinery pull the cell body and trailing edge forward (30). Cell-matrix adhesions can also enable cells to sense the extracellular environment, such as the chemical, geometrical, and physical properties of the ECM, and trigger the appropriate cellular response through activation of signaling events associated with the adhesion complexes (29).

Although cell-matrix adhesions can aid cell migration by anchoring the cell to the ECM, very strong adhesion can also hinder the cell from detaching efficiently from the ECM at the trailing edge. Palecek et al. have shown that cell migration speed exhibit a biphasic relationship with substrate adhesiveness, with the maximal speed occurring at intermediate substrate adhesiveness (32). Palecek et al. have also proposed, through a kinetic model, that when strong focal adhesions are present, separation of the integrins from the ECM cannot occur (33). This slows the cell migration speed and integrins remain on the ECM because the integrins rip from the cell's trailing edge during detachment as observed experimentally (34).

1.3.3   Pericellular proteolysis: Remodeling the ECM

ECM remodeling is also another important step in mesenchymal cell migration particularly to overcome structural barriers posed by the ECM to cell migration in 3D environments, and also during tumor cell invasion and metastasis. During ECM remodeling, cells overcome barriers and create space for cells to migrate by secreting proteases to cleave ECM components such as collagen, fibronectin, and laminins (14,35). In many tumor cell types, the ability of cancer cells to invade and metastasize is often associated with the upregulation of protease production (14). These cells form invadopodia which secretes proteases, such as matrix metalloprotease (MMP), seprase, urokinase plasminogen activator surface receptor (UPAR), and a disintegrin and metalloprotease (ADAM), at the site of ECM adhesion to degrade the ECM (26).

1.3.4   Physical cues in the ECM: how do mesenchymal cells 'feel' their physical environment?

Although the mechanisms and components of mesenchymal cell migration have been well-studied, how cells respond and adapt to physical changes in the ECM, remains unclear. Throughout their lifetime, cells need to interpret and respond to mechanical signals from their extracellular environment, caused by geometrical constrains and rigidity of the extracellular ECM, in order to proliferate, migrate or undergo programmed cell death.

Mechanical interactions between cells and their environment therefore play an important role in the regulation of biological processes. However, these interactions are far less well understood and appreciated as compared to the biochemical interactions governing these processes.

In recent years, some research groups have began to investigate how cells response to their physical environment such as cell-substrate adhesion strength. Palecek et al (32) reported that cell migration speed of chinese hamster ovary cells exhibit a biphasic dependence on ECM ligand concentration (fibronectin) which determines how well the cell adheres to the substrates. At low ECM ligand concentration, the short-term cell-substratum adhesion energy is low, causing the cell to exert lesser traction force and lower migration speed. However, at higher ECM ligand concentration migration speed is also low as the cell adheres too strongly to the substratum, preventing it from detaching from the substratum at the trailing edge of the cell, thus slowing cell migration.

In addition, it has also been shown that physiologically, biological tissues have varying stiffness depending on the location of the tissues (55). Cells cultured in vitro are also found to sense and respond to variations in stiffness during cell migration and differentiation. For example, Lo et al reported that fibroblasts tend to migrate from a softer substrate towards a stiffer substrate, and termed this phenomenon durotaxis (65). In a separate study, AJ Engler et al (55) have shown that mesenchymal stem cells

differentiate into different lineages depending on the rigidity of the polyacrylamide gels on which these cells are grown. Cells cultured on soft substrates committed into neurogenic lineages while cells cultured on stiff substrates committed into myogenic lineages.

Although these studies have suggested the importance of external physical cues in determining cellular response, the mechanism of how cells sense and convert these mechanical stimuli into chemical signaling within the cells, remains poorly understood.

1.4   Amoeboid migration: Intracellular pressure driven motility

Although cell migration has been commonly linked to changes that are associated with actin polymerization, focal adhesion formation and protease secretion (mesenchymal cell migration), there is another type of migration termed amoeboid cell migration. In recent years, many research groups have shown that mesenchymal cell migration by F-actin polymerization does not fully explain all cell migration phenotypes. Instead, amoeboid-like motility was observed in the cells of multicellular organisms, such as leukocytes, zebrafish primordial germ cells (PGCs) and in some tumor cells (14,36-42). This mode of motility was termed amoeboid motility as cells were found to move via rapidly alternating cycles of morphological expansion and contraction, and relatively low-affinity substrate binding, like the amoebae (36-42). Amoeboid cell motility is also sometimes termed blebbing cell

motility as cells were sometimes seen to migrate using bleb-like protrusions (36,39,40,42). The growth of these bleb-like protrusions, unlike protrusions formed in mesenchymal cell migration, is proposed to be driven by hydrostatic pressure generated through myosin contraction (40,43). Unfortunately, the exact mechanism underlying this amoeboid type of migration remains unclear and very often, amoeboid migration is loosely used to describe any cell migration which appears to be non-mesenchymal in nature.

1.4.1 Motility of the amoebae

The study of migration of single cell eukaryotic organisms known as amoebae was popular in the 20th century, as amoebae are more similar to cells in multicellular organisms, as compared to bacteria. The large sizes of amoebae also allowed experiments to be conducted, which would otherwise be challenging in smaller tissue cells from multicellular organisms in those days (2). In addition, amoebae move quickly, unlike most tissue cells, hence permitting the study of amoebae migration without the use of time-lapse recording (3).

Amoebae were observed to migrate by extending pseudopodia forward, attaching to the substratum and coordinating cytoplasmic streaming which results in a displacement of the cell (2,4). This cytoplasmic streaming can be observed from movement of visible particles within the cytoplasm that is being carried forward by the streaming of the cytoplasm (4). Several

hypotheses have been proposed in the past regarding the motive force for cytoplasmic streaming but there have been no conclusive experimental establishment of a particular theory (2,45,46). Models based on surface tension were popular in the early 1900s when Bernstein showed that both amoebae movement and phagocytosis could be reproduced using a mercury drop (2,46). However in later years, surface tension models were shown to be unrealistic in their predictions of amoebae movement as the amoebae were deemed to be too rigid to be influenced by surface tensions (2).

The discovery of contractile filamentous structures in amoebae formed the basis of contraction based models but the site of contraction reminded unclear (45,46). The tail contraction model proposed that contractions at the cell rear generate an internal pressure gradient within the cell thus driving cytoplasmic streaming and pseudopodia formation (2). Pantin and Mast proposed that amoeboid movement results from pressure induced flow caused by contractions in the 'outer layer of the cytoplasm' (probably referring to the cell's acto-myosin cortex) at the cell rear, coupled with a cycle of gel-sol changes (46,47). The gel-sol theory proposed that these contractions at the cell rear disrupt actin cross-linking, cause solation and hence recycling of actin to the cell front. This results in further gelation at cell front to drive movement of the amoebae (2,47,48). However, capillary suction experiments showed that high negative pressure applied to the tip of one pseudopodium does not stop other pseudopodia from extending (2,45). Destruction of the tail by

microsecond laser beam also does not instantaneously disrupt the rate of cytoplasmic streaming (2). These experiments implied that the motive force for cytoplasmic streaming does not originate from contractions in the cell rear.

On the other hand, Odell and Frisch proposed the frontal contraction model which states that the site of contraction is located at each pseudopodium tip (49). This contraction at the cell front applied tension to the viscoelastic endoplasm (inner cytoplasm), increasing both viscosity and elastic modulus of the endoplasm near the pseudopodia tip. The contraction at the cell front pulls the cytoplasm forward and forms the ectoplasmic tube of the advancing pseudopodium (2,3,49). However, before scientists can come to a consensus regarding the motive force for cytoplasmic streaming, studies on amoebae locomotion gradually lost interest in the 1980s, after the first time-lapse observation of fibroblast motility by Abercrombie et al.

1.4.2   Cellular blebs: A role in cell motility

Cellular blebs are spherical membrane protrusions, formed through contractions by the cell's acto-myosin cortex (43,44). Blebs are commonly associated with cell death via the apoptotic pathway, but in recent years, experimental observations have suggested that blebs may also contribute to cell motility in normal healthy cells (36,39,40,42).

For example, Blaser et al. (40) observed zebrafish PGCs in vivo and found that migration of these cells was guided by bleb-like protrusions, as no

enrichment of actin at leading edge was initially seen. This is in contrast to the actin-polymerization driven cellular protrusion such as lamellipodia or filopodia, observed in mesenchymal cells. Cytoplasmic streaming into the cell protrusion was also observed, suggesting that the bleb growth was driven by movement of the cytoplasm. The motive force for this cytoplasmic streaming likely comes from contractions in both the cell front and rear as myosin light chain activity was found to be elevated at both the front and rear ends of the migrating cell.

Interstingly, Blaser et al. (40) proposed that different kinases are likely to be responsible for the myosin light chains activation in the front and rear ends of the cell. The contractility at the cell front was proposed to be caused by the myosin light chain kinase which is in turn activated by calcium ions (Ca^{2+}). This hypothesis was supported by the observation of localization of the myosin light chain kinase and higher Ca^{2+} concentrations at the cell front. The higher calcium concentration at cell front is proposed to cause contractions in the acto-myosin network, causing a tearing of the cell membrane, away from the cell cortex. This is followed by flow of cytoplasm into the region of weakened membrane-cortex attachment, causing inflation of the bleb. The authors' hypothesis, that the free calcium levels drive formation of the bleb-like protrusion, is supported by the observation that cell blebs are formed at the back of the cell if that part of the cell is expressing a mutant stromal interaction molecule 1, which increases calcium influx at that location. Cells

expressing cell membrane bound buffers against calcium ions, such as Parvalbumin or CalbindinD28k which lower free calcium levels in the pseudopodia, were also found to have lower cell migration speed.

Charras and Paluch (42) proposed that bleb nucleation is initiated by a weakening of the cell's membrane-cortex adhesion at the site of bleb formation (Figure 4). This occur either due to myosin-driven contraction of the actin cortex at the cell front, or the rupture of the actin cortex at the site of bleb formation. The cell membrane subsequently expands as cytoplasmic fluid flows towards the site of membrane-cortex detachment. The cytoplasmic fluid flow is driven by the pressure difference between the high intracellular pressure exerted by the acto-myosin cortex, and the lower pressure at the site of membrane-cortex detachment. This pressure driven bleb growth is not supported by an actin cytoskeleton initially, but an actin cortex subsequently reassembles under the cell membrane, leading to bleb retraction. Before the bleb retracted fully, new blebs can also form subsequently after the actin cortex have reformed under the cell membrane, as the newly formed leading edge cortex tends to be more fragile (43).
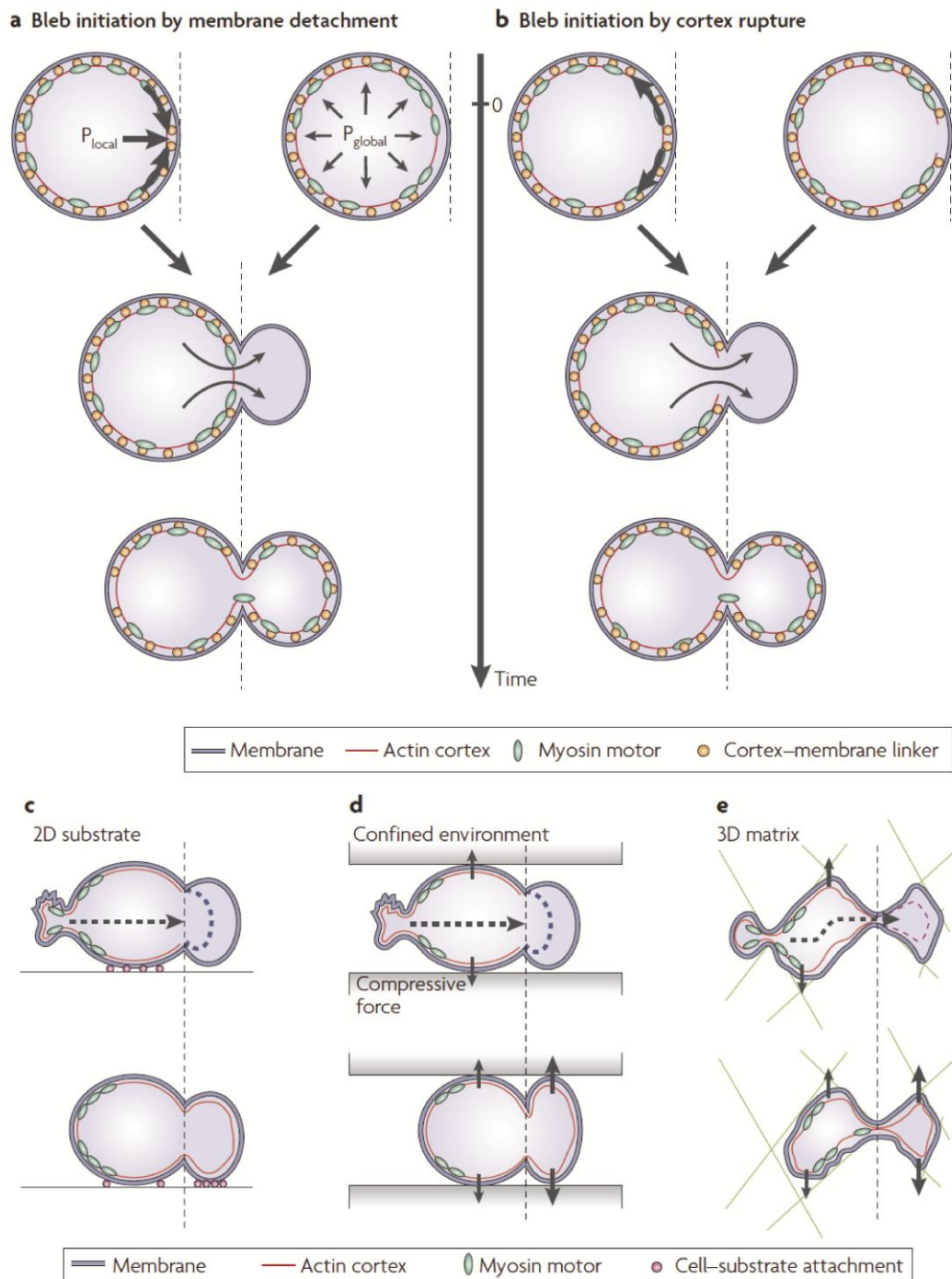
Figure 4 Schematic illustrations of bleb formation, with blebs initiated by either (*a*) membrane-cortex detachment, or (*b*) actin cortex rupture. (*c-e*) Schematic illustrations of cell migration using blebs, (*c*) on a 2D substrate, (*d*) in a confined environment between two walls and (*e*) in 3D matrix. Figure adapted from reference (43).

1.4.3   Membrane-cortex linkers: Ezrin, Radixin and Moesin

Formation of cellular bleb depends on not only on the hydrostatic pressure, but Charras et al. (44) have showed that weaker membrane-cortex adhesion and higher membrane tension contributes to increased bleb formation as well. These factors are likely to influence blebbing motility as well. In fact, it has been hypothesized that the amoeboid cell polarization may be achieved by polarizing the distribution of membrane-cortex linkers such as ezrin, radixin and moesin (collectively known as ERM proteins) to the cell rear. The localization of the membrane cortex linker, ezrin, at the cell rear has also been observed experimentally in blebbing cells (50,51).

Diz-Munoz et al. have also found that zebrafish mesoderm-endoderm germ-layer progenitor cells which possess a dominant-negative ezrin domain produced more blebs than wild type cells due to the weakened membrane-cortex adhesion. However, despite producing more blebs, these cells do not migrate faster and are less directed than wild-type cells.

Overall, these studies suggest that membrane-cortex linkers could potentially play a role in determining the polarization of bleb formation and directionality of migration in amoeboid cells.

1.4.4 'Chimneying': migration without cell-substrate adhesions

Charras and Paluch (44) also hypothesized that for cell migration to occur on 2D substrates, cell adhesion to the substrate must occur in order to translate polarized blebbing into movement (Figure 4*C*). New cell-substrate adhesions are formed as the new bleb comes into contact with the substrate and the cell mass can stream forward. If however, the cells are in confined environments (for example, between two glass coverslips or in a thin microfluidic channel, Figure 4*D*), the cell can migrate in the absence of receptor-ligand mediated cell–substrate adhesion via a mechanism termed 'chimneying'. This chimneying mechanism was hypothesized by Malawista et al. (52), who observed experimentally that leukocytes with β2-integrin adhesion deficiency are able to migrate efficiently in confined environment. It is thought that the cell can migrate in the absence of cell–substrate adhesions as the cell pushes perpendicularly to both sides of the glass surfaces to anchor itself while the cell squeezes itself forward.

1.4.5 Physical cues in the ECM: do amoeboid cells 'feel' their physical environment?

Although many studies have looked into how mesenchymal cells respond to the physical environment, few studies have explored how amoeboid cell migration is influenced by mechanical stimuli in the ECM. Interestingly, amoeboid cell migration seems to be uninfluenced by changes in

cell-substrate adhesiveness, unlike mesenchymal cells. Malawista et al (52) noted that leukocytes with adhesion deficiency are able to migrate efficiently in confined environment in the absence of cell–substrate adhesions. However, the authors also note that these leukocytes are unable to migrate efficiently when they are not confined between two coverslips suggesting that the extent of cell confinement may be an important physical factor influencing amoeboid cell migration. Unfortunately, there has been no systematic and quantitative study reported to investigate amoeboid cell response to physical cues in the ECM, and the mechanisms used by these cells to sense these physical cues.

1.5 Mesenchymal to amoeboid transition: Plasticity of migration modes

Cells do not migrate exclusively with only the mesenchymal or the amoeboid modes of migration under all circumstances. In fact, some cells have been shown to be capable of switching between the mesenchymal and amoeboid mode of cell migration depending on the environment (43). For example, it has been reported that adding protease inhibitors to cells which under normal circumstances migrate using the mesenchymal mode is not sufficient to stop cancer cell migration (35). These mesenchymal cells undergo a mesenchymal to amoeboid transition (MAT) to continue migrating using the amoeboid mode, thus highlighting the plasticity of cell migration modes.

However, how and why cells choose one mode of motility over another remained unclear.

1.5.1 Inhibition of MMP activity

Mesenchymal cells are known to migrate in 3D environments by secreting proteases such as MMPs to cleave the surrounding fibers and create spaces for the cell to move through. The upregulation of proteases production in metastatic tumor cells have prompted the use of MMP inhibitors to prevent tumor cell migration. However, clinical trials using MMP inhibitors for late-stage cancer treatment have turned in discouraging results as significant tumor progression continues in most cases despite treatment with MMP inhibitors (14,35). This suggests a possible escape mechanism which tumor cell use to disseminate after inhibition of proteolysis.

In a separate experiment, Wolf et al. (35) added protease inhibitors to cancer cells in 3D collagen matrix, which normally migrate using the mesenchymal mode, to prevent cells from cleaving physical barriers impeding cell movement. However, the cells were found to undergo MAT instead, where cells change from an elongated morphology to a spherical morphology and continue to migrate by amoeboid type motility. Instead of degrading the matrix to create space for cell migration, the cells can squeeze through pre-existing gaps between the collagen fibers by changing cell shape in an amoeba-like manner.

1.5.2 Increase in acto-myosin activities

Sahai and Marshall (53) have also demonstrated that tumor cells in 3D matrigel can switch between the two modes of cell migration by changing the Rho, Rho Kinase (ROCK) and Rac activities. Bleb formation was found to be inhibited in tumor cell lines, which were initially producing blebs during cell migration, when RhoA or ROCK inhibitors were added. The inhibition of RhoA and ROCK likely lowered the strength of acto-myosin contractile force produced. In these amoeboid tumor cell lines, it was also found that ROCK expression levels are high, suggesting that increase in acto-myosin activities favor amoeboid cell migration. On the other hand, these bleb protrusions were not suppressed when Rac1 activation was blocked in these cells. In contrast, tumor cell lines which produced elongated actin rich protrusions remained unaffected when RhoA or ROCK activity was inhibited. These cells however switched to a spherical morphology when Rac1 activity was blocked or when protease inhibitors were added. The authors hypothesized that the switch between the two migration modes is dependent on the levels of Rho/ROCK and Rac activity within the cells. The authors also proposed a combined treatment of protease and ROCK inhibitors, to stop tumor cells from switching between different modes of motility and to completely prevent tumor cell metastasis and invasion.

1.5.3 Absence of cell-matrix adhesions

Another experimental result by Bergert et al. (54) showed that cell-matrix adhesions can also be a factor triggering the switch of one migration mode to another. By selecting Walker 256 carcinosarcoma cells for, or against adhesion, two different phenotypic sublines, namely a suspension subline (suspension cells) and an adhesion subline (adhesive cells) of the Walker cells were obtained. The suspension cells formed bleb-like protrusions while the adhesive cells formed lamellipodia-like protrusions during migration. Using micropipette aspiration to measure cortical tension in the cells, the suspension cells were found to have a higher cortical tension than the adhesive cells, an observation attributed to the higher myosin activity in the suspension cells.

The authors have also shown, similar to what Sahai and Marshall (53) have reported, that increasing ROCK activity induced a switch from lamellipodia to bleb formation in adhesive cells and increasing Rac1 activity caused suspension cells to switch from bleb to lamellipodia formation. In addition, when untreated suspension cells were placed on adhesive surfaces, the adhesive surfaces can trigger lamellipodia formation in these cells, suggesting that changes in adhesiveness of the ECM can cause immediate changes in the protrusion types which could be reversed.

1.5.4 Decrease in ECM rigidity

ECM rigidity may also be a factor that potentially triggers a change in migration phenotype. Numerous experiments have shown that cells sense and respond to changes in the rigidity of the ECM. For instance, AJ Engler et al. (55) have demonstrated that mesenchymal stem cells can differentiate into lineages specified by the ECM. Cells which were grown on soft substrates committed into neurogenic lineages while cells grown on stiff substrates committed into myogenic lineages. However, the question of whether changes in ECM rigidity can contribute to MAT remains largely unknown.

One possible hint that cells adapt and change their phenotype depending on the rigidity of their environment comes from the experiment by Tang et al. (56,57). Tang et al. have reported that human colon carcinoma cells which were cultured on soft substrates (21 kPa) transformed from an elongated to a rounded morphology after 7 days of culture on the soft substrate. These rounded cells were also found to have weak cell-cell and cell-matrix adhesions and were liken to a metastasis-like phenotype, although the metastatic ability was not quantified by the authors. The change in phenotype was also shown to be irreversible even when these cells are later grown on rigid substrates. However, the author did not further compare and elaborate on whether the migration morphologies adopted by these cells were different from the elongated cells which are grown on stiffer substrates, and the effects of ECM rigidity on MAT remains largely unknown.

1.6   Quantifying cellular force

Cell migration is essentially a physical process with the cell front exerting a protrusive force, and the cell rear a retraction force for forward migration, regardless of the migration mode used by the cell. Since cell migration is fundamentally a mechanical process, the amount of traction force a cell exerts on the ECM can provide valuable clues into mechanisms of cell locomotion and motility, and the underlying process of cytoskeletal force generation or intracellular pressure generation.

The first visual observations of this traction force was by Harris et al. (58), who grew cells on very thin film of silicone rubber and saw that locomoting cells exert forces on the substrates to cause wrinkling of the thin film. Quantitative measurements of the cellular traction force were proposed by Lee et al. (59), through embedding beads on the silicone films. However, wrinkling on silicone films due to the cells exerting a complex, non-isotropic force, is a highly nonlinear problem and mathematical solutions to quantify the wrinkles caused by such a force field remains unknown (60).

Pelham and Wang provided a solution to this problem, through a method known as 2D cell traction force microscopy, in which cells are cultured on flat, elastic polyacrylamide gels with fluorescent beads embedded (61). The beads on the surface of the gel are first imaged with cells attached and detached. Bead displacement between these two states can then be used to

27

calculate substrate strains and subsequently, the traction stresses which cell exert on the substrates, using the Boussinesq's equation as proposed by Dembo and Wang (62). Since then, 2D cell traction force microscopy has been used to characterize cell generated forces in numerous cell behaviors. Examples include the phenomenon of cell migration towards more rigid substrates known as durotaxis (65), amoebae development (67), changes in cell spreading areas (66), and focal adhesion formation (68,72,73). It is now recognized that cells actively probe the mechanical attributes of their environment by applying forces at the sites of substrate adhesion (63).

These traction force calculations can also be extended to 3D by imaging the 3D positions of the beads within the polyacrylamide gels, with the cells attached and detached, using the confocal microscope. After obtaining the beads displacements, 3D traction stresses can then be computed using either a finite elements method (74-77) or in a forward manner as proposed by Frank et al. (78-80).

1.7   Thesis overview

A review of past literatures has revealed that the cellular responses such as cell migratory behavior are sensitive to the mechanical factors present in their external environment (63). For example, physical barriers such as the pore size of the matrix, the strength of cell-matrix adhesions, and also the substrate rigidities, seemed to play a role in determining the cell speed,

migratory directions and even the choice of migration mechanism to employ. However, little is known about the underlying mechanism which the cells use to sense their physical environments and whether mesenchymal and amoeboid cells sense and respond to similar physical cues. The objectives of this thesis is therefore to probe the differences in mesenchymal and amoeboid cell response when physical factors in the ECM, namely cell-substrate adhesiveness, substrate rigidity, and degree of cell confinement, is systematically varied. The results presented in this thesis will therefore allow us to propose possible mechanisms that the mesenchymal and amoeboid cells employ in sensing their physical environments.

In the first study, I explored the response of cells to changes in the ECM substrate rigidity and cell-matrix adhesiveness during mesenchymal migration on polyacrylamide substrates with variable elasticity and adhesiveness (with varying ligand concentration). Fluorescent beads were also embedded within the polyacrylamide gels to determine the cell-exerted stresses on the substrate by traction force microscopy, thus allowing me to probe the mechanical adaptation within the cells in response to changes in the ECM rigidity. On soft substrates, cells were found to adapt to increase in substrate rigidity by increasing cell-generated force to conserve strain in their environment. However, on stiff substrates cells are stress-limited, due to the limit in the amount of force the cells' force-generating machineries are capable of, while focal adhesion sizes continued to increase.

In the second study, I explored how mesenchymal and amoeboid cells sense the mechanical properties of their environment. To achieve this, I first quantitatively characterized, through 3D traction force microscopy, the differences in the mechanism used in the two migration modes in confined environments between two pieces of elastic gels. Cells in the amoeboid and mesenchymal modes were found to exert distinct stresses in the confined environment, thus allowing us to distinguish between the two different migratory modes quantitatively. By varying the substrate rigidities and the degree of cell confinement (through varying the distance between the two pieces of gels), I was able to conclude that the two modes of migration are regulated by different physical properties of the extracellular environment. Mesenchymal cell migration was found to exhibit a biphasic relationship with gel rigidity, while amoeboid cell migration exhibits a biphasic relationship with degree of cell confinement. In addition, the membrane-cortex adhesion strength was also found to be crucial in determining amoeboid migration speed and directionality.

1.7.1 Investigating the effects of substrate rigidity on 2D mesenchymal migration

In this chapter, I first quantified the cell migration speed of fibroblasts with varying substrate adhesiveness and substrate rigidity. I found that cell migration speed exhibits a biphasic relationship with substrate adhesiveness and substrate rigidity. The value of the optimum substrate rigidity (16 kPa)

was also found to occur at a lower substrate rigidity (6 kPa) as the strength of cell-substrate adhesion increase from 25 µg/ml to 75 µg/ml. The cells' focal adhesion areas were found to increase with increasing substrate rigidity up to a substrate rigidity of 60 kPa, after which focal adhesion areas were found to remain at a constant level regardless of substrate rigidity. These results illustrate that mesenchymal cells sense and respond to the underlying substrate rigidities.

Traction stress measurements carried out also revealed that on soft polyacrylamide gels (Young's modulus < 20 kPa), cell-exerted substrate deformation remains constant, independent of the substrate Young's modulus, while on stiff substrates (Young's modulus > 20 kPa), traction stress plateaus at a limiting value with increasing substrate rigidity.

I proposed that sustained substrate strain on soft substrates and sustained traction stress on stiff substrates may be factors governing how cells sense the underlying substrate rigidity. On soft substrates, cells are possibly strain-limited and adapt to increasing substrate rigidity by increasing cell-generated force to conserve strain in their environment. However, on stiff substrates, cells could be stress-limited, due to a limitation in the amount of force the force-generating machineries, within the cells, are capable of.

In addition, the traction stress and focal adhesion sizes were found to saturate at different substrate rigidity (20 kPa and 60 kPa respectively), and a linear correlation analysis shows only weak linear correlation between the two

measurements. The difference in the substrate rigidity where traction stress and focal adhesion sizes saturate suggest that traction stress magnitudes and mature focal adhesion sizes is likely to be regulated by two different mechanisms. This may help to explain the biphasic relationship between cell migration speed and substrate rigidity. At substrate rigidities below 20 kPa, the increasing cell traction force allowed cells to migrate faster with increasing substrate rigidities. However, at substrate rigidity above 20 kPa, the larger focal adhesions serve to slow down cell migration while traction stress saturates.

1.7.2 Investigating mechanistic differences between amoeboid and mesenchymal migration

Migration of leukocytes and tumor cells through the 3D ECM has been shown to be amoeboid-like, characterized by its independence from integrin-mediated cell-substrate adhesions (amoeboid cell migration). This is different from mesenchymal cell migration, characterized by actin polymerization and focal adhesion assembly. However, amoeboid cell migration mechanisms and classification remained vague.

In this chapter, I have quantified amoeboid cell migration in confined environments. Neutrophil-like, differentiated human promyelocytic leukemia cells confined between two pieces of polyacrylamide gels, with varying gap sizes, were found to exhibit two modalities during migration: Cells formed

blebs (amoeboid mode) on non-fibronectin coated gels, and lamellipodia (mesenchymal mode) on fibronectin coated gels.

In the amoeboid mode, cells migrate via a 'chimneying' mechanism by generating anchoring stresses normal to the confining gels, and shearing stresses at bleb protrusions. Bleb growth shifted the anchoring stress forward resulting in cell movement. On the other hand, cells in the mesenchymal mode generated contractile, opposing shearing stresses at the cell front and rear during protrusion and retraction, respectively.

Amoeboid migration speed was also found to peak at an intermediate gap size. A computational model was used to explain this biphasic behavior, and the model predicted that this optimum gap size can be increased by weakening the cell membrane-cortex adhesion strength.

1.7.3   What have we learnt?

Overall, through the work presented in this thesis, we can improve our understanding of how cells in general sense and respond to the mechanical cues present in their external environments. Such knowledge is crucial in designing the appropriate therapies during disease progressions where mechanical factors in the ECM may change. My results have shown that mesenchymal and amoeboid cells sense different physical parameters in their environment.

In mesenchymal cell migration, migration speed is biphasic with cell substrate rigidities, together with cell-matrix adhesions. These mechanical factors likely contribute through signaling events triggered by mechano-sensors which are capable of sensing strains of the ECM on soft substrates (< 20 kPa) and stress applied to the ECM on stiffer substrates (> 20 kPa). The weak linear correlation between traction stress and focal adhesion areas suggest that this strain and stress sensing mechanism is likely to be independent from the cellular mechanism that regulates mature focal adhesion sizes.

On the other hand, amoeboid cell migration speed is biphasic with degree of cell confinement. I proposed that amoeboid cells can feel the degree of cell confinement likely through an increase in their contact area with the gel surface, and the intracellular pressure, as the amount of confinement increases. The strength of the cell membrane to actin cortex adhesion can also determine the location of bleb formation and directionality of migration, thus suggesting a possible mechanism an amoeboid cell may use to sense and respond to degree of confinement in its ECM.

I therefore suggest that different parameters in the cell's mechanical environment stimulate distinct signaling pathways within the cell, thereby allowing the cell to migrate with the most favorable mode of migration that is best suited for navigating through that particular physical condition of the ECM. Although the identity of the molecular switch that determines the

migratory mode of the cell remain to be elucidated by future studies, the results and tools for quantitative analysis presented in this thesis can contribute valuably in deciphering the complex mechanisms behind cell migration regulation.

1.7.4 Publications

The publications that arise due to this work in the thesis are listed as follows. Part of the study of the effects of substrate rigidity on mesenchymal cell migration, as described in Section 1.7.1, have been written and published as an article in the January 2013 issue of the Biophysical Journal, where I am a co-first author:

[1] Ai Kia Yip*, Katsuhiko Iwasaki*, Chaitanya Ursekar*, Hiroaki Machiyama, Mayur Saxena, Huiling Chen, Ichiro Harada, Keng-Hwee Chiam, and Yasuhiro Sawada. Cellular response to substrate rigidity is governed by either stress or strain. *Biophysical Journal* **104**: 19-29. (2013).

The investigation on the mechanistic differences between amoeboid and mesenchymal migration, as described in Section 1.7.2, is being prepared for publication.

[2] Ai Kia Yip, Keng-Hwee Chiam and Paul Matsudaira. Amoeboid cell migration in confined environment occurs via chimneying. In preparation.

2 INVESTIGATING THE EFFECTS OF SUBSTRATE RIGIDITY ON 2D MESENCHYMAL MIGRATION – THE ROLE OF STRAIN AND STRESS

2.1 ECM rigidity – mechanical regulator of biological events

Biological tissues and cells are constantly subjected to external mechanical forces caused by geometrical constrains and rigidity of the extracellular environment and it has been shown that cells are able to sense and respond to differences in ECM rigidity during cellular differentiation and migration. For example, AJ Engler et al. (55) have shown that mesenchymal stem cells can differentiate into lineages specified by the ECM. Cells which were grown on soft substrates committed into neurogenic lineages while cells grown on stiff substrates committed into myogenic lineages. In addition, Pelham et al. (61) observed that cells migrate faster on substrates with Young's modulus of 15 kPa as compared to stiffer substrates. Lo et al. (65) also reported that cells tend to migrate towards the more rigid substrate, and termed this phenomenon durotaxis. Despite these observations, specific details on the rigidity sensing mechanism have yet to be fully elucidated. How substrate rigidity is gauged by cells remains elusive.

Actin stress fibers (70,81,82), focal adhesions (73,83,84) or mechano-sensitive ion channels (85) have been proposed to act as rigidity sensors and guide cellular responses. Some have hypothesized that these rigidity sensors allow cells to sense substrate rigidity either via stress or strain sensing proteins which then activate the related signaling pathways, thereby influencing cell migration behavior. For example, De et al. theorized that cells may readjust their contractile activity and cytoskeleton to maintain either optimal strain or optimal stress (86). However, experiments addressing this issue have produced conflicting results, with some suggesting that cells maintain a constant traction stress (87), whilst others propose that cells sustain a constant substrate deformation (69,70,88).

Therefore, we have performed traction force microscopy on continuous polyacrylamide substrates to address the issue of whether cells sense stress or strain. By varying the concentrations of monomer (acrylamide) and cross-linker (N,N'-methylenebisacrylamide, BIS), we prepared substrates with rigidities covering a wide range, from 6 to 110 kPa, which spans the entire range of physiologically relevant matrix rigidities from brain tissue (1 kPa) to bone (100 kPa) (55).

Using these polyacrylamide gels, we measured the two physical variables that may play important roles in the rigidity sensing mechanism of cells: traction stress and substrate strain. We observed that cells generated sustained substrate strain on soft substrates and sustained traction stress on

stiff substrates. This suggests that depending on the substrate rigidity, either strain or stress could influence cell behavior. The switch from sustained substrate strain to sustained substrate stress at substrate rigidities of about 20 kPa, also appears to coincide with the range where maximal cell migration speed occurred. Traction stress and focal adhesion area was also found to be weakly correlated, suggesting that this strain to stress switch is likely to be regulated independently from the size of mature focal adhesions. It is possible that while increasing cell traction force allowed cells to migrate faster with increasing substrate rigidities, the larger mature focal adhesions slowed down cell migration at large substrate rigidities where traction stresses saturates, hence resulting in a biphasic relationship between cell speed and substrate rigidity.

2.2   Methods and materials

2.2.1   Preparation of polyacrylamide substrates

To activate glass coverslips for gel attachment, coverslips (25 mm diameter) were silanized by incubating in silane solution (2% acetic acid (Schedelco, Singapore, Singapore) and 1.2% 3-methacryloxypropyltrimethoxysilane (Shin-Etsu Chemical, Tokyo, Japan)) for 2 hours at room temperature. The coverslips were then washed with ethanol and air dried. Polyacrylamide gels were prepared with varying concentrations

of acrylamide (Bio-Rad, Hercules, CA) and BIS (Bio-Rad) to vary rigidity.

For the traction force measurements, N-acryloyl-6-aminocaproic acid (ACA; Tokyo Chemical Industry, Tokyo, Japan) solution (500 mM, pH 7) was added to the acrylamide-BIS mixture such that the final concentration of the ACA monomer was 100 mM. In addition, green fluorescent beads of 0.2 µm diameter (Polysciences, Warrington, PA) were added to the mixture to allow visualization of substrate deformation and calculation of traction stresses exerted by the cell. The relationship between acrylamide, BIS and ACA concentrations, and Young's modulus of gels is shown in Table 1.

Polymerization was initiated with 0.2% ammonium persulfate (Bio-Rad) and catalyzed with 0.2% *N,N,N',N'*-tetramethylethylenediamine (TEMED) (Bio-Rad). 4.52 µl of gel solution was placed onto the silanized coverslips and the drop was covered with a non-treated circular coverslip (12 mm diameter). After polymerization, the top coverslip was carefully removed and gels were fully hydrated in MES buffer (0.1 M 2-(N-morpholino)ethanesulfonic acid, 0.5 M sodium chloride, pH 6.1; Sigma-Aldrich, St. Louis, MO). Fully hydrated gels were approximately 50 µm thick.

For measurement of cell migration speed, fibronectin was immobilized on the polyacrylamide gel surface using Sulfo-succinimidyl-6-(4-azido-2-nitrophenyl-amino) hexanoate (sulfo-SANPAH). 0.5 mg/ml sulfo-SANPAH (Pierce, Rockford, IL) in HEPES buffer (50 mM 4-(2-hydroxyethyl)-1-

Table 1 Concentration of acrylamide, BIS and ACA, and the corresponding Young's modulus of the gels.

Acrylamide (%)	BIS (%)	Young's modulus (kPa)	
		100 mM ACA	0 mM ACA
3.0	0.13	6.2	
4.0	0.17	14.4	
4.3	0.18	16.7	
4.6	0.20	19.4	
4.9	0.21	22.5	
5.5	0.23	31.6	
6.5	0.28	45.1	
7.5	0.32	60.7	
10.0	0.43	110.5	
5.0	0.05		1.2
8.0	0.07		3.5
8.0	0.1		6.2
8.0	0.2		16.6
10.0	0.26		31.6

piperazineethanesulfonic acid, pH 8.5; Sigma-Aldrich) was placed onto the surface of each gel and exposed to ultraviolet (UV) light in a sterile hood for 15 minutes. The darkened sulfo-SANPAH solution was removed and gels were rinsed twice with HEPES for 10 minutes and incubated in 0.01-0.1 mg/ml fibronectin (Sigma-Aldrich) at 4ºC overnight.

For traction force measurements, collagen was conjugated with the polyacrylamide gel surface using a dehydration condensation reaction with water soluble carbodiimide. First, carboxyl groups of the ACA gels were activated with 0.2 M 1-ethyl-3-(3-dimethylaminopropyl) carbodiimide hydrochloride (Dojindo Laboratories, Kumamoto, Japan) and 0.5 M *N*-hydroxysuccinimide (Wako Pure Chemical Industries, Osaka, Japan) in MES buffer for 30 minutes at room temperature. Gels were then washed with cold 60% methanol diluted with phosphate buffered saline (PBS; 1st Base, Singapore, Singapore), before being reacted with 0.2 mg/ml type I collagen (Koken, Tokyo, Japan) in HEPES buffer (0.5 M HEPES, pH 9.0) overnight at 4ºC. Finally, gels were transferred to 0.5 M ethanolamine hydrochloride (Sigma-Aldrich) diluted by HEPES buffer for 30 minutes at 4ºC. The gels were washed once with HEPES buffer at 4ºC and then washed three times with PBS.

All gels were exposed to UV light in a sterile hood for 15 minutes. Before plating cells, gels were equilibrated in cell culture medium for 30–45 minutes at 37°C.

2.2.2 Measuring rigidity of polyacrylamide gel

Gel rigidity was determined by the penetration method (**95**). The Young's modulus (E) was obtained using the Hertz sphere model,

$$h = bf^{2/3}, \qquad (1)$$

where $b = (9/(16ER^{1/2}))^{2/3}$, and assuming a value of 1/2 for the Poisson ratio. The indentation profiles were obtained from fully hydrated 2 to 3 mm gel samples with a stainless steel sphere (3 mm radius (R)) (Figure 5).
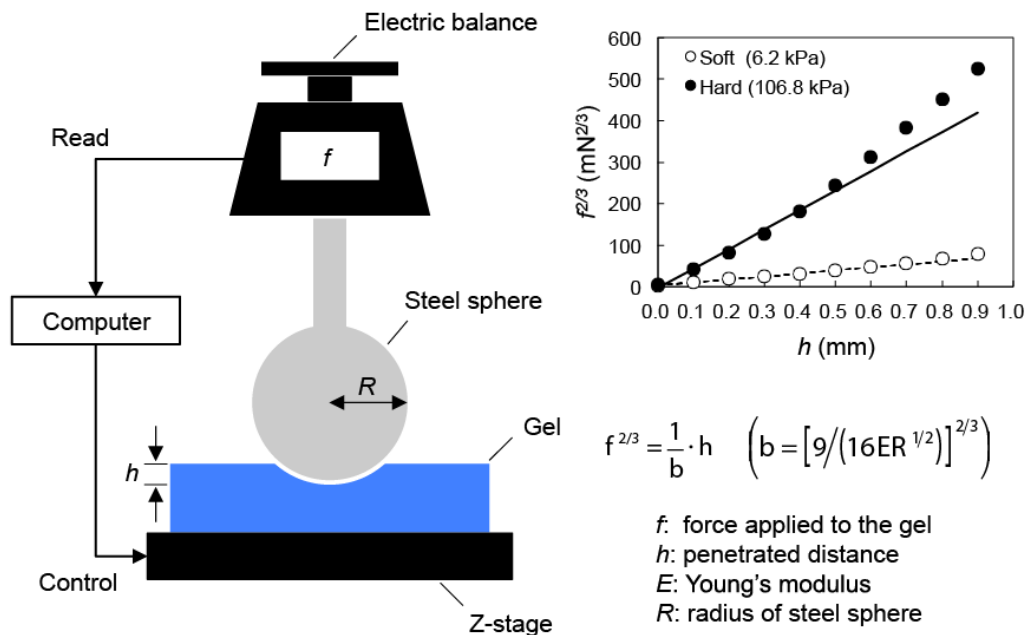
Figure 5 Schematic illustration of the penetration method to measure the gel elasticity. A gel placed on a z-axis stage (resolution of step: 0.1 mm) was compressed with a steel sphere (6 mm in diameter), which was directly connected to an electric balance. The penetrated distance (*h*) was controlled and the force applied to the gel (*f*) was measured. The Hertz model was applied to fit the first linear section in the plot $f^{2/3}$ against the indentation depth to ensure that the estimation was consistent with the linear approximation. The plots from a soft (6.2 kPa) gel (*open circles*) and a stiff (106.8 kPa) gel (*solid circles*) are exemplified.

To measure the force exerted on gels (f), individual gels were placed on a custom-designed electronic balance (Shimadzu, Kyoto, Japan), and indentation of the sphere (h) was monitored using a z-axis stage (Chuo Precision Industrial, Tokyo, Japan). The Hertz model was then applied to fit the first linear section in the plot $f^{2/3}$ against indentation depth to ensure that the estimation was consistent with the linear approximation as illustrated in Figure 5.

2.2.3 Cell culture

Mouse embryonic fibroblasts (MEFs) and National Institutes of Health 3T3 (NIH3T3) cells were cultured in Dulbecco's modified Eagle's medium (GIBCO, Grand Island, NY) supplemented with 10% fetal bovine serum (GIBCO) and 1% penicillin-streptomycin (GIBCO) at 37°C, 5% CO_2 and 100% humidity. MEFs expressing mCherry-tagged paxillin and NIH3T3 cells expressing mCherry-tagged zyxin were provided by A/P Sawada's laboratory in the Mechanobiology Institute, Singapore.

2.2.4 Live cell imaging and detection of fluorescent beads embedded in polyacrylamide gels

Cells on polyacrylamide substrates and beads embedded in polyacrylamide gels were viewed 12 hours after cell plating. For cell migration speed analysis, DIC images were obtained at regular intervals

43

(every 6 minutes for 3 hours) with PerkinElmer Ultraview spinning disk at 10x air objective lens (numerical aperture (NA) 0.4) and a stage incubator.

For traction force measurements, images were obtained with the PerkinElmer Ultraview spinning disk using a 60x water objective lens (NA 1.2) and a stage incubator. For each data set a number of images were obtained. Specifically, a DIC image indicating cell position; an image of the green fluorescent beads (excitation 488 nm, emission 516 nm) embedded in the polyacrylamide substrate; and an image of the mCherry-tagged focal adhesion proteins (excitation 561 nm, emission 640 nm). Cells were subsequently detached from the substrate using trypsin and another image of the green fluorescent beads was obtained to determine bead position in the unstrained substrate.

2.2.5 Quantification of cell migration speed

Cell migration speed was determined with time-lapse DIC images recorded over a period of 180 minutes. Using the Image Processing Toolbox in Matlab, the cells were segmented from the images by applying a Sobel filter to obtain the cell outlines. The cells which are connected to the borders are removed and cell centroid positions were determined. A MATLAB tracking program which computes the correlation of centroid positions between time frames was then used to find the cell displacement and hence the cell speeds (133). For each data point, approximately 30 cells were counted.

2.2.6 Quantification of focal adhesion size

mCherry-tagged zyxin and paxillin expressed in NIH3T3 cells and MEFs, respectively, were used as focal adhesion markers. Focal adhesion area was defined as the region with fluorescence intensity higher than the threshold determined in each individual cell. A relative intensity was defined as:

$$relative\ intensity = (i\text{-}i_{min})/(i_{max}\text{-}i_{min}), \qquad (2)$$

where i represents the measured intensity, i_{max} the maximum intensity, and i_{min} the minimum intensity within the cell. The relative intensity of 0.25 was used to threshold the fluorescence images in PerkinElmer's Volocity to quantify the area of individual focal adhesion.

2.2.7 Calculation of 2D traction stress magnitudes

2D traction force microscopy has become a common technique and its experimental procedures have been well documented (68,71,98,99,100). Cell-induced substrate deformations can be identified by comparing images of the fluorescent beads embedded in the substrate before and after the cell is detached by trypsinization.

The bead displacements were obtained by a method known as digital image correlation. The images acquired before and after cell detachment were first divided into a set of sub-areas. Using each pair of corresponding sub-area images, the respective local displacement vector was obtained by maximizing

the cross-correlation function of the sub-areas. The cross correlation function was obtained efficiently using the Fast Fourier Transform (FFT) algorithm and the displacement vector was estimated from the location of the cross-correlation peak (101,102). The mean displacement at cell-free regions, where the cell was at least 5 μm away, was subtracted from the calculated displacements, to correct for sample drift during image acquisition. The resultant displacement matrix approximates the local substrate deformation for each sub-area which best fit the strained image to the unstrained image.

Once the entire displacement field $\boldsymbol{u}$ was calculated, the traction stress field $\boldsymbol{F}$ was obtained as the solution to the inverse Boussinesq problem (95,62). We have assumed that the substrate is an infinite half-plane and response of the substrate is linear. Displacements from the various traction points can then be superimposed. The Boussinesq equations relate the displacement (u_x, u_y) at location (x, y) on the surface of the substrate to an imposed point stress (F_x, F_y) at location (x', y'),

$$u_x = \frac{1+v}{2\pi E}\left\{\frac{2(1-v)F_x}{r} + \frac{2v(x-x')\left[(x-x')F_x+(y-y')F_y\right]}{r^3}\right\}, \tag{3a}$$

$$u_y = \frac{1+v}{2\pi E}\left\{\frac{2(1-v)F_y}{r} + \frac{2v(y-y')\left[(x-x')F_x+(y-y')F_y\right]}{r^3}\right\}, \tag{3b}$$

where $r^2 = (x - x')^2 + (y - y')^2$, ν is the Poisson ratio and E the Young's modulus of the gel. A matrix equation comprising Eq. (3) at all locations was then formed and inverted. To prevent the matrix from being singular, owing to presence of the $1/r$ and $1/r^3$ terms, the grid (x, y) of the displacement field was staggered in both x and y directions from the grid (x', y') of the stress field by a small percentage (7.5%) of the grid spacing.

2.3   Results

2.3.1   Cell migration speed has a biphasic relationship with substrate stiffness and ligand concentration

To study the effect of substrate stiffness and cell-substrate adhesiveness on the cell migration speed, a series of polyacrylamide gels with different substrate stiffness and fibronectin coating, varying from 1-31 kPa, and 0.01-0.1 mg/ml respectively, was prepared. NIH3T3 cells were plated onto these substrates for at least 15 hours and DIC time-lapse images were acquired. Based on these time-lapse images, cell centroid positions were obtained as described in Section 2.2.5. The cell migration speed was calculated based on the centroid positions over time.

It was observed that cells migrate fastest on substrates of intermediate stiffness of either 7 kPa or 13 kPa, depending on the fibronectin concentration which was coated on the polyacrylamide gels (Figure 6). At low fibronectin

47

coating (0.025 mg/ml), the optimum substrate stiffness for maximum migration speed of 1.62 µm/minutes occurred at substrate stiffness of 16 kPa. On the other hand, at higher fibronectin coating (0.075 mg/ml), the maximum migration speed of 1.75 µm/minutes occurred at substrate stiffness of 6 kPa.
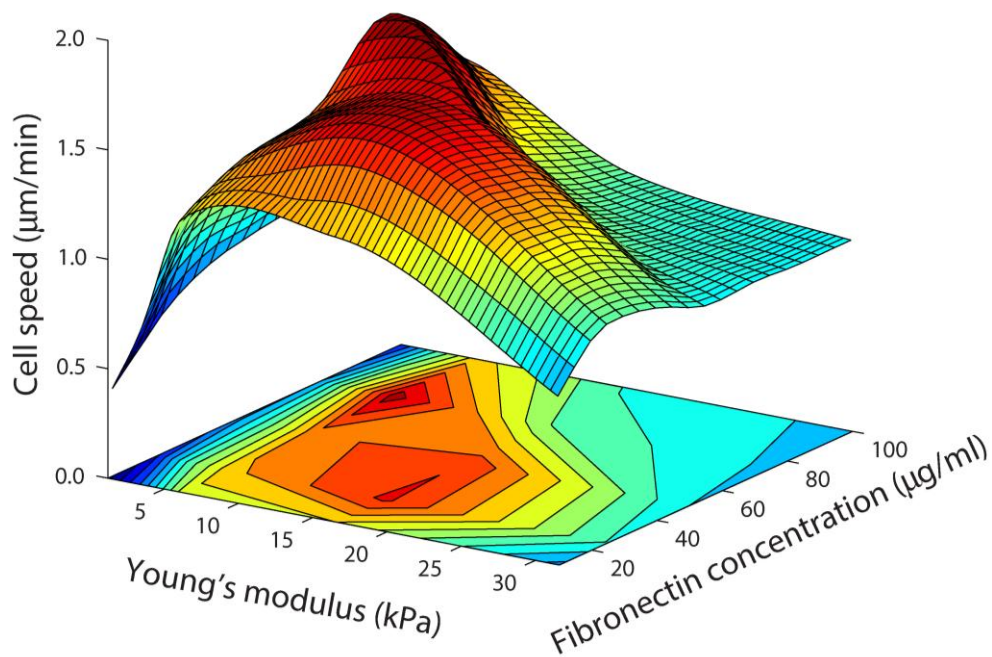
Figure 6 3D contour plot of cell speed vs. fibronectin coating and substrate rigidity.

2.3.2 Substrate deformation is sustained on soft substrates whereas traction stress is constant on stiff substrates

Traction force microscopy was used to measure traction stress magnitudes exerted by cells on polyacrylamide gels of varying rigidity. Figure 7 shows the results from traction force microscopy of MEFs on a soft gel with

48

Young's modulus of 6.2 kPa (panels *A-D*), and on a stiff gel with Young's

modulus of 60.7 kPa (panels *E-H*). The traction stress magnitudes averaged

over the whole cell on the soft and on the stiff gels were 0.099 ± 0.0035 kPa

and 0.53 ± 0.011 kPa (mean $\pm$ standard error (SE)) respectively, whilst the

maximum traction stress magnitudes were 1.14 kPa and 3.86 kPa respectively.

Both our mean and maximum traction stress magnitudes support previous

traction force studies using fibroblasts (65,68,72,101,105).

We found that for gels with Young's modulus below 20 kPa, the mean

bead displacement was sustained at approximately 0.34 μm for NIH3T3 cells,

and 0.38 μm for MEFs (Figure 8*A*). Correspondingly, traction stress increased

with substrate rigidity up to 20 kPa. The mean traction stress exerted by

NIH3T3 cells and MEFs increased from 0.19 to 0.38 kPa, and 0.20 to 0.35 kPa

respectively as substrate rigidity was increased from 6.2 to 19.4 kPa (Figure

8*B*).

In contrast, at substrate rigidities above 20 kPa, traction stress did not

show a marked increase, suggesting that there is a maximal force with which

cells can pull on the substrate. The mean traction stresses leveled off at

approximately 0.38 kPa for NIH3T3 cells and MEFs. Conforming to this

trend, the mean bead displacement decreased with increasing rigidity beyond

20 kPa.

6.2 kPa
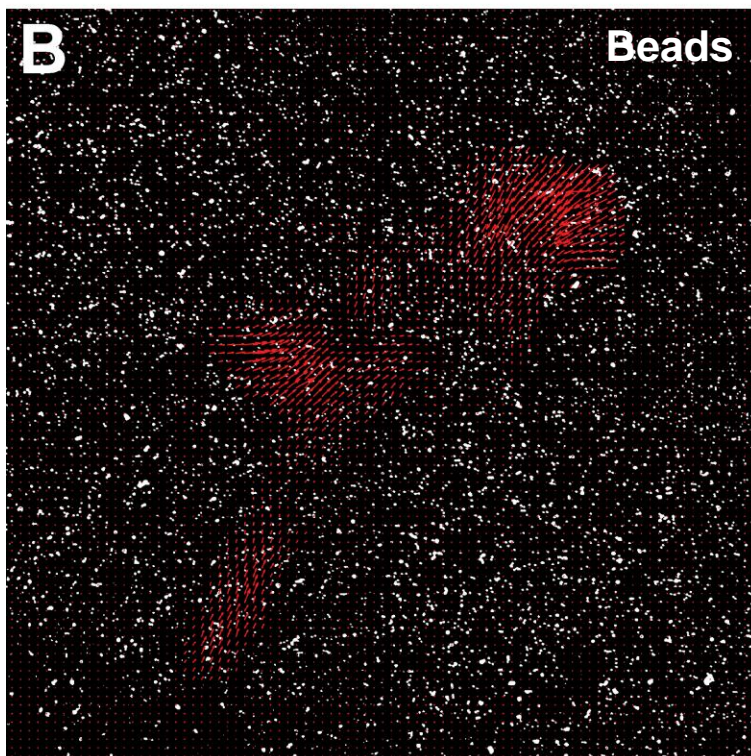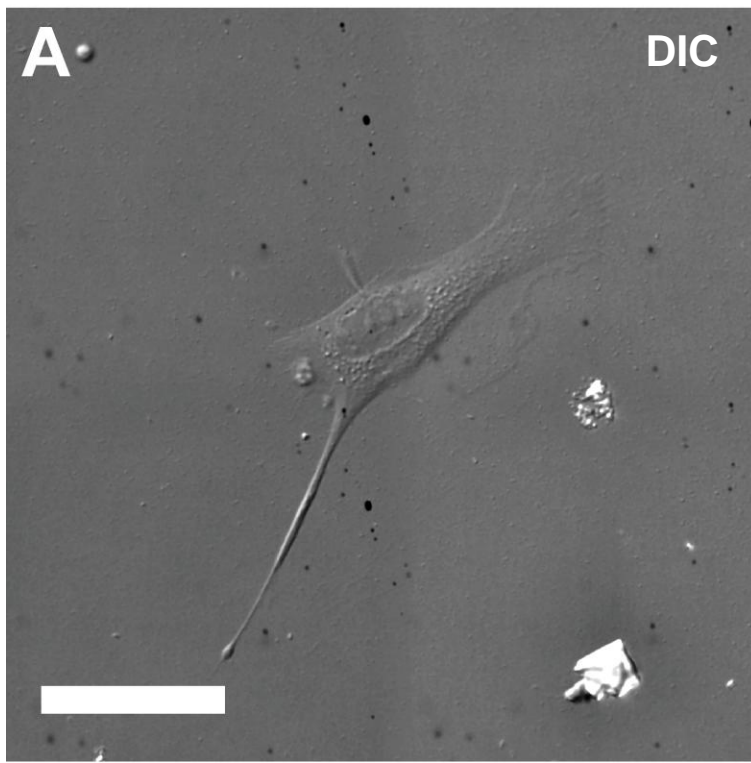
6.2 kPa
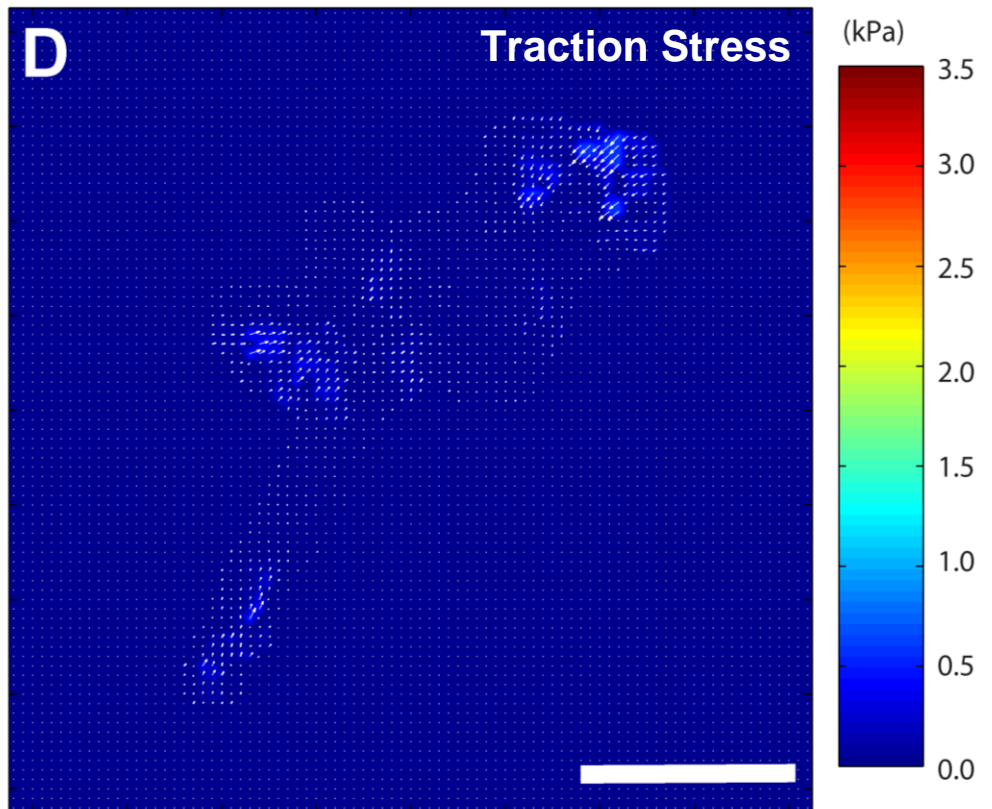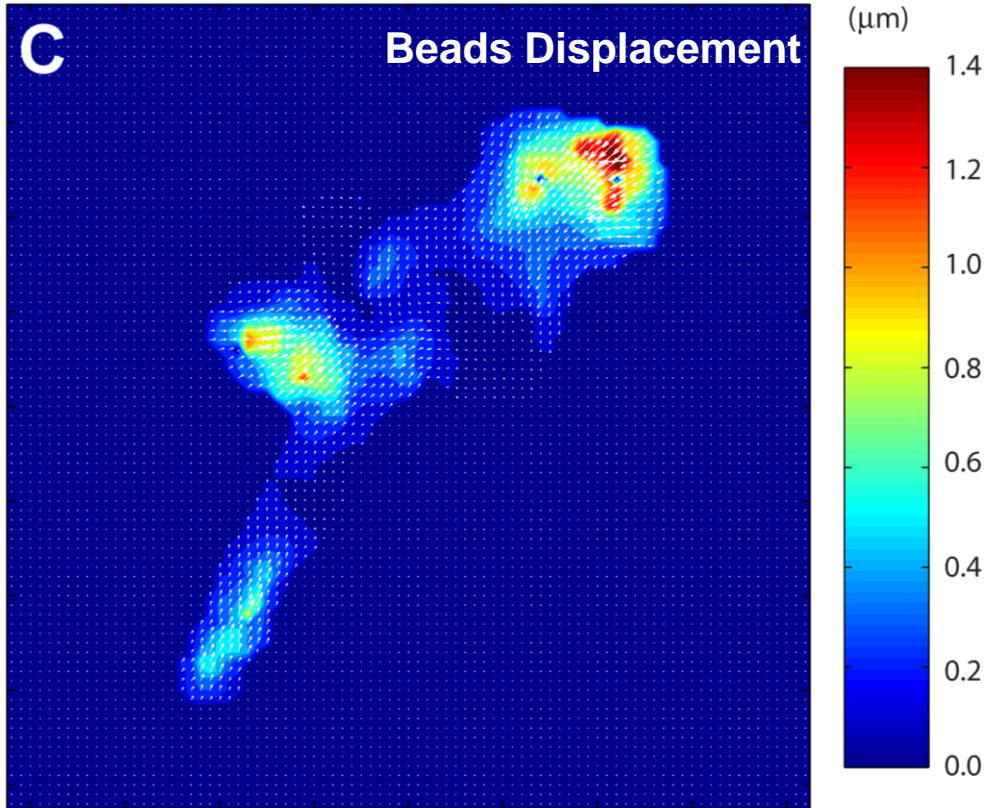
60.7 kPa
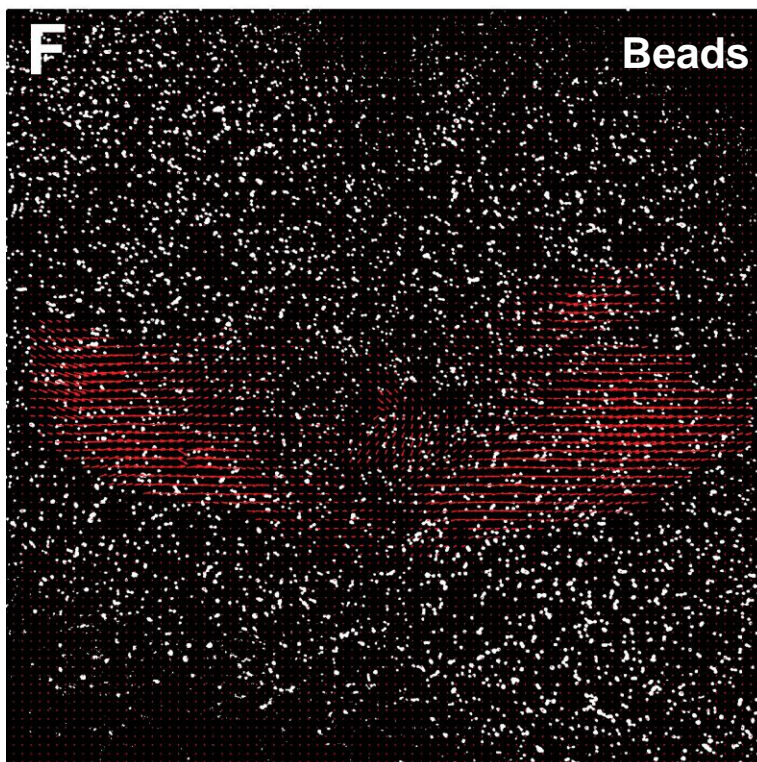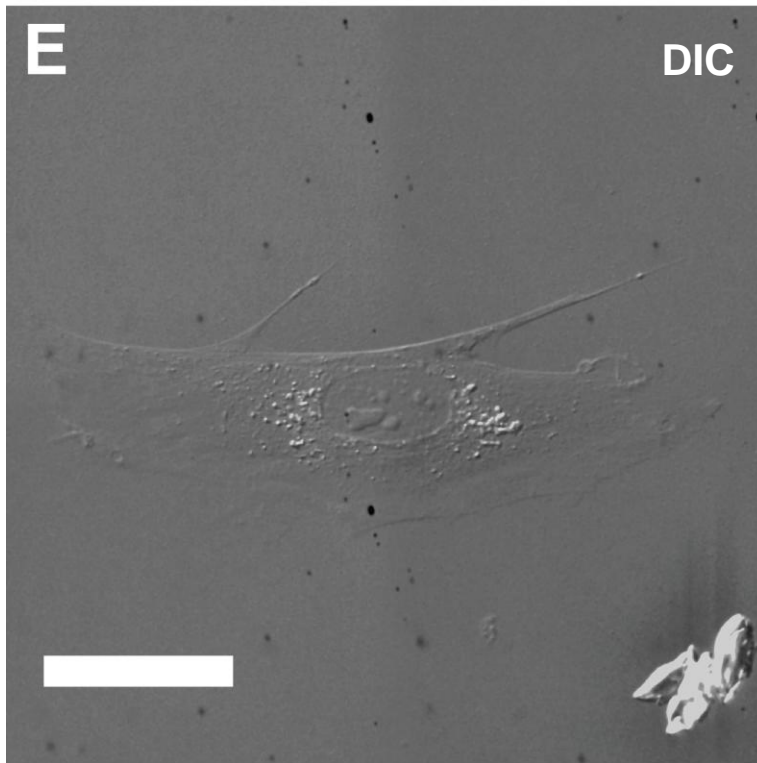
60.7 kPa
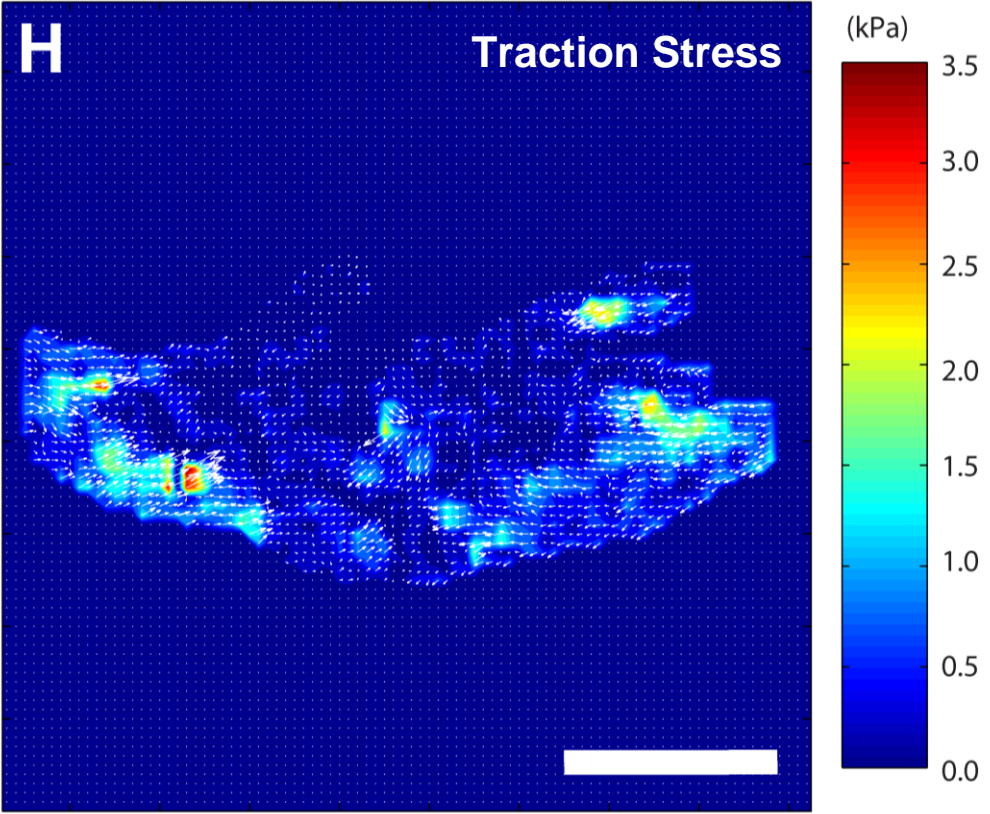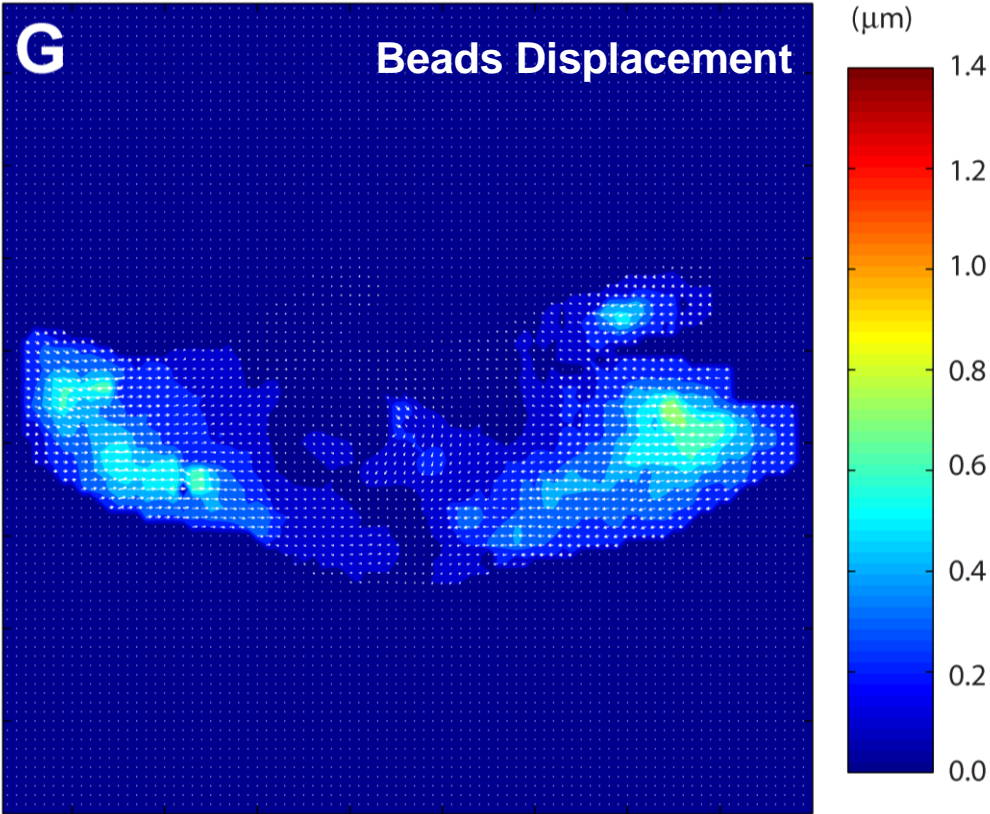
Figure 7 Traction force microscopy. DIC images of MEFs on gels with Young's modulus of (*A*) 6.2 kPa and (*E*) 60.7 kPa. Thresholded images of beads with red arrows showing bead displacements due to the traction exerted by a cell on the substrate of Young's modulus (*B*) 6.2 kPa and (*F*) 60.7 kPa. Displacement maps obtained from digital image correlation, for Young's modulus of (*C*) 6.2 kPa and (*G*) 60.7 kPa. Color bar is in units of micrometers. Traction stress maps for Young's modulus of (*D*) 6.2 kPa and (*H*) 60.7 kPa. Color bar is in units of kPa. The traction stress magnitude averaged over the whole cell is 0.099 ± 0.0035 kPa in (*D*) and 0.53 ± 0.011 kPa in (*H*). Scale bar represents 50 μm.
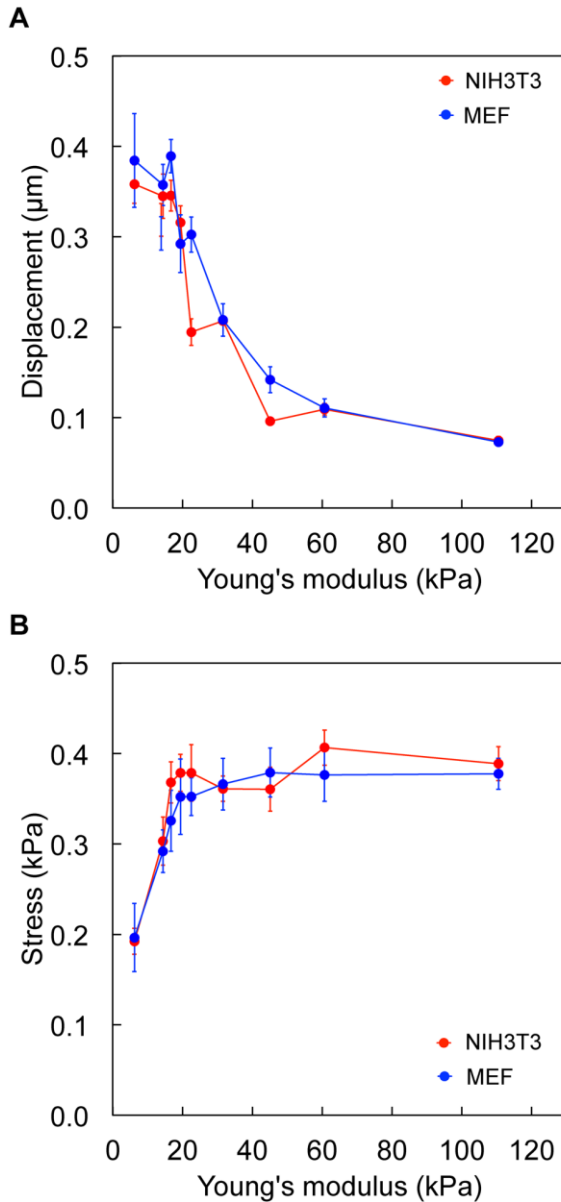
Figure 8 Cell-generated substrate deformation and traction stress. Graphs of (*A*) mean bead displacement magnitude vs. substrate elasticity, and (*B*) mean traction stress magnitude vs. substrate elasticity. (*NIH3T3 cells: red solid circles, MEFs: blue solid circles*) Error bars represent SE of the mean. For each substrate rigidity value, 10-20 cells were analyzed.

2.3.3   Focal adhesion areas increase with increasing substrate rigidity

From the analysis of cell migration speed, it was observed that the substrate stiffness at which the maximum speed occurs can be altered by changing the fibronectin concentrations, which in turn would affect the cell-substrate adhesion. This suggests that ability of the cell to adhere to the substrate could be altered by changing the substrate stiffness, and thereby affecting the cell migration speed. We then analyzed the size of focal adhesion, which has been reported to be modulated by externally applied forces (73,106).

When we performed live cell imaging of NIH3T3 cells and MEFs expressing mCherry-tagged zyxin and paxillin, respectively, the mCherry-tagged proteins was also found to form more elongated assemblies in cells on stiff (60 kPa) substrates (Figure 9*A*) compared to cells on soft (6 kPa) substrates (Figure 9*B*). We found that as the Young's modulus increased from 6.2 to 60.7 kPa, the mean area of individual focal adhesion also increased from approximately 0.81 to 1.2 μm^2. This was observed in both NIH3T3 cells and MEFs. At larger substrate rigidities however, focal adhesion area did not increase further (Figure 9*C*).

2.3.4 Focal adhesion size is not correlated with the magnitude of traction stress

We found that both the mean traction stress magnitude and the mean focal adhesion area increased with increasing substrate rigidity but in distinct fashions (compare Figure 8*B* and Figure 9*C*). Although the mean traction stress magnitude did not increase with substrate rigidity on polyacrylamide gels stiffer than 20 kPa (Figure 8*B*), the mean focal adhesion areas continued to increase with substrate rigidity up to 60 kPa (Figure 9*C*). These results suggest that traction stress may not be directly correlated with the size of mature focal adhesions.

To address this, we performed linear regression analysis between the mean focal adhesion area and the mean traction stress for each individual cell. When linear regression was applied individually for each substrate rigidity, low R^2 values (0.001 to 0.26) were obtained, suggesting little or no linear correlation (Figure 10). Nonetheless, when data from all rigidities were analyzed together, there were weak but positive linear correlations between the focal adhesion area and the stress magnitude (R^2 values were 0.38 for NIH3T3 cells and 0.22 for MEFs) (Figure 10).
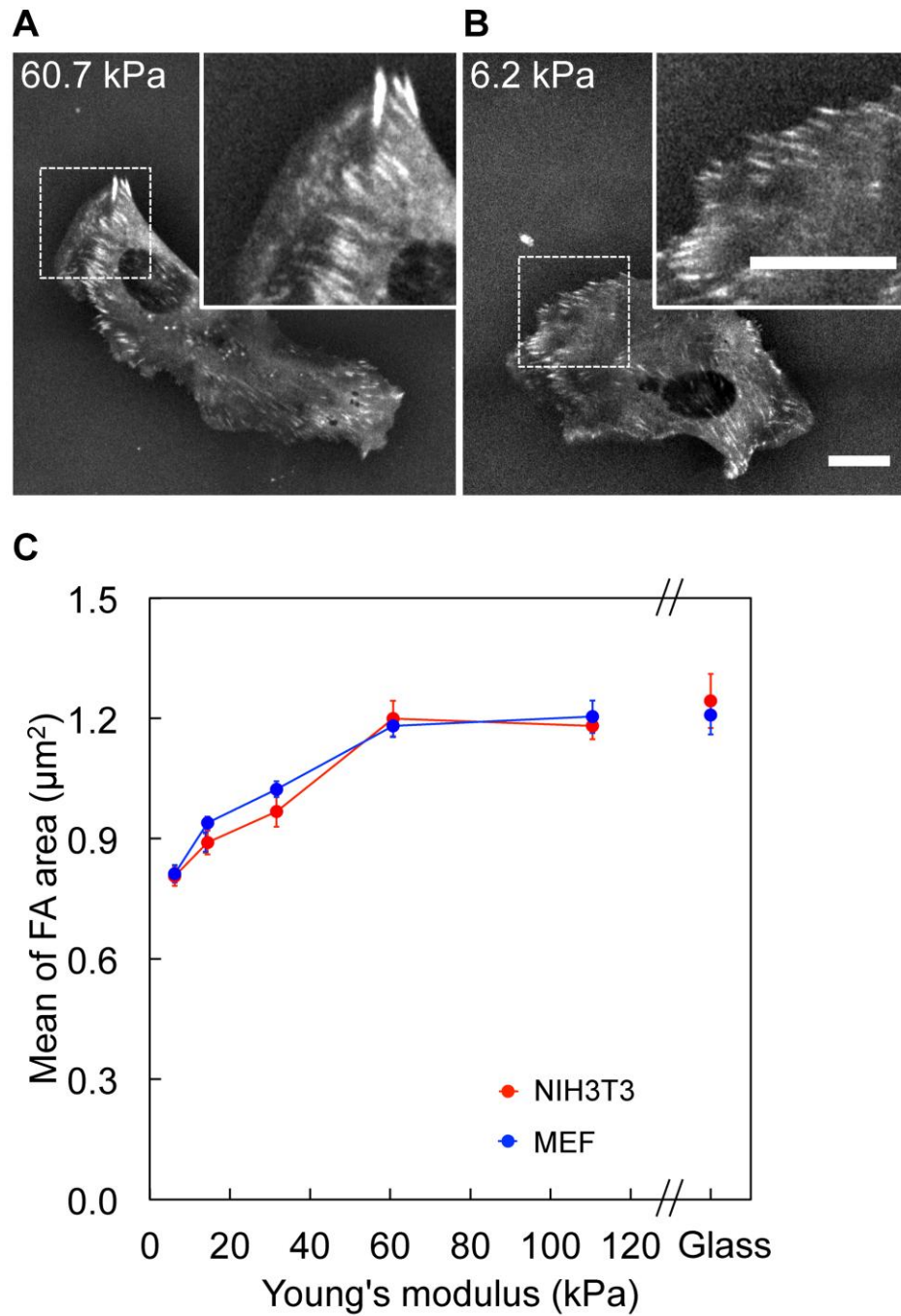
Figure 9 Relationship between focal adhesion area and substrate rigidity. MEFs stably expressing mCherry-tagged paxillin on polyacrylamide gels with Young's modulus of (*A*) 60.7 kPa and (*B*) 6.2 kPa, both with 0.2 mg/ml of collagen coating. Scale bar represents 20 μm. (*C*) Graph of mean focal adhesion area vs. substrate elasticity: mCherry-tagged zyxin in NIH3T3 cells (*red solid circles*) and mCherry-tagged paxillin in MEFs (*blue solid circles*). Error bars represent SE of the mean. For each substrate rigidity value, 10-20 cells were analyzed.

57
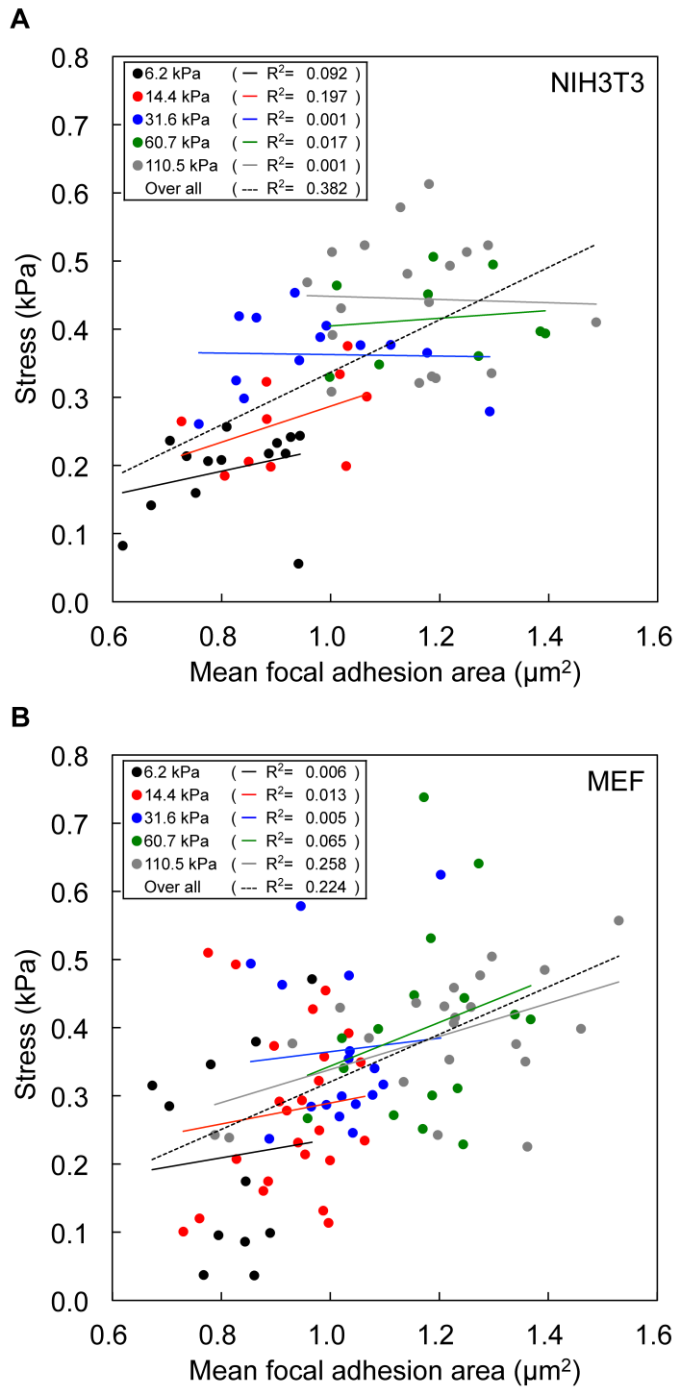
Figure 10 Relationship between focal adhesion area and traction stress magnitude.
Scatter plot of mean traction stress vs. mean focal adhesion area for (*A*) NIH3T3 cells
and (*B*) MEFs. Each point plots the mean traction stress value vs. mean focal adhesion
area value of a particular cell on polyacrylamide gels with Young's modulus of 6.2 kPa,
14.4 kPa, 31.6 kPa, 60.7 kPa and 110.5 kPa. Lines represent the linear fits to points of
the corresponding stiffness. The dashed lines represent the overall linear fitting of mean
traction stress to mean focal adhesion area for all cells.

2.4 Discussions

2.4.1 Cell migration is a balance between cell traction force and cell-substrate adhesion

The initial observations show good agreement with experimental results published by other research groups. For example, when fibronectin concentration was varied from 0.01-0.1 mg/ml cells were found to migrate fastest on substrates with intermediate fibronectin concentration (between 0.025 – 0.075 mg/ml depending on substrate rigidity). This is in agreement with previous studies by Palecek et al. (32) who reported that cell migration speed of Chinese hamster ovary cells on glass exhibits a biphasic dependence on ECM ligand concentration with maximal cell speed occurring at 10 µg/ml fibronecting coating concentration. DiMilla et al. (92) explained using a mathematical model that a balance of contractile with adhesion forces is required for maximal migration speed. At low ECM ligand concentration, not enough adhesion bonds form at the cell front to resist contraction thus resulting in low migration speed. However, at higher ECM ligand concentration the cell adheres too strongly to the substratum, preventing it from detaching from the substratum at the trailing edge of the cell, thus retarding migration.

However, the biphasic relationship is not exclusive to cell migration on ECM of different fibronectin concentration but also with substrate rigidity.

When substrate rigidity is varied from 1-31 kPa, while keeping the fibronectin concentration constant, it was found that cell migration speed exhibits a biphasic relation with ECM rigidity with maximum speed recorded at intermediate substrate rigidity (6-16 kPa). Pelham et al. (61) observed that normal rat kidney epithelial cells migrate fastest on collagen coated substrates with rigidity of 15 kPa as compared to cells on stiffer substrates. However, the authors did not report cell migration speeds for substrate rigidity lesser than 15 kPa, and hence did not observe the biphasic relationship between cell migration velocity and substrate stiffness as observed in our experiments. In a separate study, Peyton and Putnam (93) similarly reported an optimal intermediate substrate rigidity whereby smooth muscle cell migration speed is maximal (on substrates with Young's modulus of 20 kPa and 8 μg/ml fibronectin coating). The biphasic relationship between cell migration speed and substrate rigidity was also found to be removed by inhibiting ROCK activity. However, how increased ROCK activity leads to the biphasic relationship between cell migration speed and substrate rigidity remains hypothetical.

Attempts have also been made, by employing computational models, to explain cell migration behavior on substrates with varying rigidities. These models typically assume that traction forces increase with an increase in substrate rigidity up to 100 kPa, beyond which they stay constant (89,90). However, these studies were based on limited data: previous traction force

analyses on continuous substrates have been limited to substrates with Young's moduli below 50 kPa (65,66,71). Therefore, we have performed traction force microscopy on continuous polyacrylamide substrates with rigidities from 6-110 kPa, which spans the entire range of physiologically relevant matrix rigidities from brain tissue (1 kPa) to bone (100 kPa) (55).
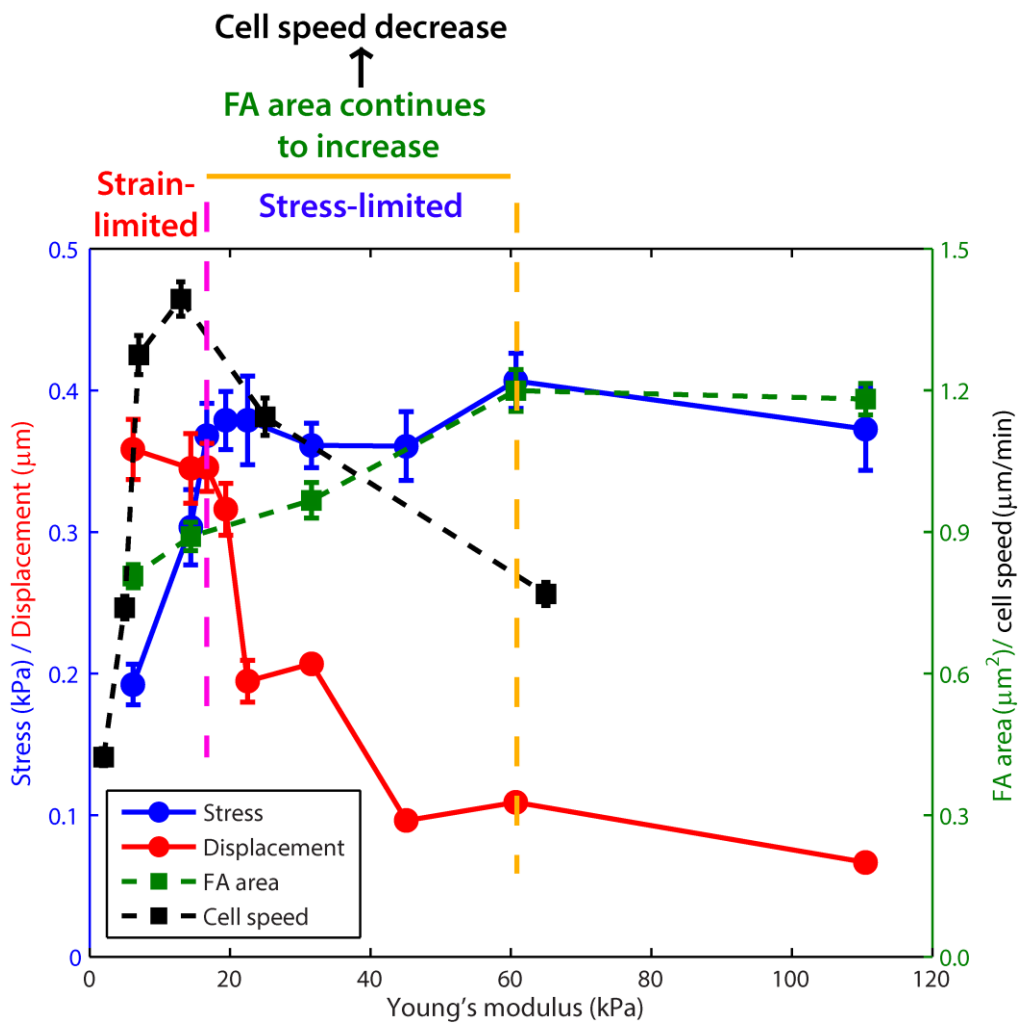
Figure 11 Graph of mean substrate stress, substrate displacement, focal adhesion area and cell speed vs Young's modulus of the polyacrylamide substrate.

61

We observed that both traction stress magnitude and mature focal adhesion areas increased with increasing substrate rigidity but in distinct fashions. Fibroblastic cells exerted larger traction forces and formed larger focal adhesions with increasing substrate rigidity up to 20 kPa. Beyond 20 kPa, traction stresses remained at a constant value while focal adhesion sizes continued to increase (Figure 11). We propose that at substrate rigidities below 20 kPa, the increasing cell traction force, probably a result of increased ROCK activity (98), allowed cells to migrate faster with increasing substrate rigidities. However, at substrate rigidity larger than 20 kPa, the larger focal adhesions caused cell migration to slow down as traction forces remained constant, hence giving rise to the biphasic relationship between cell speed and substrate rigidity.

2.4.2 Cells are strain-limited on soft substrate and stress-limited on stiff substrates

Although many studies have shown that cells sense and respond to rigidity of the ECM, the mechanisms underlying how cells sense the ECM rigidity are still poorly understood. In particular, there is no clear consensus as to whether cells sense the strain or the stress of their immediate environment. Freyman et al. have proposed that fibroblasts are force limited and generate a constant contractile force regardless of the surrounding matrix rigidity (87).

To the contrary, experiments using micropillars showed that Madin-Darby canine kidney (MDCK) epithelial cells and fibroblasts maintained constant deformations on those substrates to which these cells adhered (69,70,88,107). Oakes et al. have also reported that human neutrophils exerted constant deformations on polyacrylamide substrates (66). Discher et al. have also proposed that cells respond to substrate rigidity by producing constant substrate strain (63). Cell traction stresses are expected to increase with increasing substrate rigidity if the cells are to sense their external environments by responding to substrate strains.

We have shown using traction force microscopy that fibroblasts exert traction stresses on substrates softer than 20 kPa to maintain constant strains. However, at rigidities beyond 20 kPa, stress appears to be limiting as traction stress reaches a plateau (Figure 11). The cellular response of maintaining constant strain, which we observed on substrates having Young's moduli below 20 kPa, does not explain our observation that traction stress appears to be independent of the substrate rigidity for substrates with Young's moduli above 20 kPa. Our results instead suggest that depending on the substrate rigidity, either substrate strain or substrate stress tends to be conserved.

Similarly, in another study on fibroblasts which used micropillar arrays, Ghibaudo et al. (69) reported two distinct regimes in the traction force-pillar stiffness relationship. A linear increase in both traction force and pillar stiffness was observed at corresponding Young's moduli below 100 kPa whilst

63

at higher Young's moduli, traction forces plateaued. In our study we employed continuous substrates to reach similar conclusions, although we observed that traction stresses leveled out at a much lower rigidity (20 kPa). This difference could be due to confounding effects of micropillar size, location and density, which may affect focal adhesion areas. In experiments using polyacrylamide gels these limitations do not exist. This notion is supported by reports that total traction forces and focal adhesion areas for cells on micropillars can be increased by increasing micropillar density (108). In addition, micropillars have a different substrate topology that may also modify cell responses in terms of focal adhesion kinase activity and cell contractility (108,110). Therefore, traction stress measurements using micropillars may not be directly comparable to measurements using continuous substrates with which 2D cell migration is commonly studied.

2.4.3 Actin reorganization may be involved in strain-conservation at low substrate rigidity

A substrate rigidity value of 20 kPa appears to be important in regulating the fibroblast mechano-response as it is around this value that a switch from conservation of strain to conservation of stress appears to occur (Figure 11). Interestingly, Solon et al. have reported that fibroblasts tend to match their internal stiffness to that of their substrates up to 20 kPa (111). They have also found that actin cross-linking in cells is enhanced with increasing substrate rigidity, suggesting that actin fibers may play a role in

rigidity sensing. Consistent with this notion, Trichet et al. have shown that more actin stress fibers align along the long axis of the cell when substrate rigidity is increased, and proposed that stress fibers may act as force sensors by transmitting tension from myosin motors to the focal adhesion complexes (70). The alignment of the stress fibers possibly facilitates transmission of forces, from the contractile units within the cells to sites of cell-substrate adhesions (focal adhesions), which then allows the cell to exert traction forces on the substrates.

Relevant to these observations, Zemel et al. have shown both experimentally and theoretically that stress fiber organization can be regulated by physical factors such as matrix rigidity and cell shape, with maximum stress fiber alignment occurring along the long axis of the cell when cellular and matrix rigidity values are related by an optimal ratio (82). Considering that fibroblasts originate from connective tissues which are approximately 8-17 kPa in rigidity (55), the switch from conservation of strain to conservation of stress in fibroblasts, which we observe at a substrate rigidity of 20 kPa, seems to be born out of the interplay of inherent mechano-responsive processes that the fibroblasts are commonly expected to face. At substrate rigidities below 20 kPa, which is similar in rigidity to the matrix rigidity that fibroblasts are physiologically found, fibroblasts may reorganize their actin stress fiber alignment to sustain substrate strains, with maximum stress fiber alignment occurring at 20 kPa.

Interestingly, although physical mechanisms proposed by Zemel et al. (82) and Walcott and Sun (81), seems to explain the relation between stress fiber alignment and matrix rigidity, these theoretical models assume that there is a crosstalk between elastic stresses within the cell as the cell adhere to the cell matrix and stretch, and the active forces generated by the cell acto-myosin machinery to oppose the stretch. It remains unclear however, how, if at all, the cell 'feels' the stretch and translate the mechanical signal to a biochemical signal that subsequently results in an increased acto-myosin contractility. For example, some intracellular signaling proteins such as the mitogen-activated proteins kinases (155) have been shown to be activated as the cell is stretched, resulting in increased alignment of the stress fibers.

On the other hand, Mitrossilis et al. proposed that the acto-myosin interactions can provide a simple mechanistic explanation for rigidity sensing by the cell (113). During acto-myosin contraction, the sliding of actin filaments requires the detachment of myosin heads from the actin filaments, thereby imposing an internal load or friction which dissipates into heat and limits the speed of contractile shortening. The authors hypothesized that when ECM rigidity is low, the higher speed of shortening will cause more energy to be dissipated as heat, and hence less force can be transmitted by the cell to the softer substrates as compared to another cell on a stiffer substrate.

2.4.4 Stress-conservation may arise due to limitations in the acto-myosin contraction machinery

The contractile activity of the acto-myosin units that transmit tension to the focal adhesion through actin stress fibers has also been shown to be important in stress fiber formation and alignment (81,82). It is likely that the substrate rigidity-gated switch between the sustained substrate strain and the sustained substrate stress at substrate Young's modulus of 20 kPa, results from an inherent limit to the quantity of contraction that these acto-myosin units can generate.

Marcq et al. have explained that contractile molecular motor activity plays a central role in reproducing the increase in traction force with increasing substrate rigidity for low rigidity values and the leveling off of traction force at larger rigidity values (112). Using microplates of variable stiffness, Mitrossilis et al. also found that myoblast cells contract and pull on the microplates as they spread between the microplate up till an equilibrium force value where cells stop spreading and contracting (113). This equilibrium traction force was found to increase with increasing microplate stiffness until a maximum force point (about 300 nN) is reached at microplate stiffness of approximately 100 nN/µm, beyond which the equilibrium traction force did not increase further. The results hence suggest that there is a maximum traction force with which the acto-myosin units in myoblasts can generate before the acto-myosin machinery stalls and force saturates.

In a separate study, Aratyn-Schaus et al. compared stress fiber remodeling and traction force buildup in osteosarcoma cells after washing out blebbistatin-containing cell media which inhibits myosin contraction in the cells (156). The authors observed that rapid recovery of cell-exerted traction forces slows down actin retrograde flow at the cell's leading edge, and F-actin stress fibers were seen to form after the contractile forces saturates. The author also hypothesized that this stall force triggers a transition actin network contraction to actin network organization into stress fiber bundles.

Taken collectively, these studies revealed that the acto-myosin machinery is crucial in determining stress fiber organization and potentially the cellular response to the underlying substrate rigidity. It would therefore be of interest to investigate if an increase in this acto-myosin stall force (possibly through overexpressing proteins such as myosin IIb in the cell) can increase the value of the substrate rigidity where maximal stress fiber alignment, and the transition from strain-limited to stress-limited cellular response, occurs.

2.4.5 Strain or stress sensing mechanisms are likely to be independent from mechanisms regulating mature focal adhesion sizes

Previous reports have demonstrated that focal adhesion areas increase with increasing substrate rigidity (61,65,71,72,64). Balaban et al. have found that adhesion areas are linearly dependent on local traction forces exerted by the cells, and have proposed that traction force is closely related to focal

adhesion assembly (73). Nicolas and Safran have also reported that focal adhesion areas reach a finite size which can be altered by changing substrate rigidity (83,84). Many studies have also shown that larger mechanical forces at the focal adhesion sites can induce focal adhesion complexes to increase in size and facilitate actin polymerization at the focal adhesion complexes (106,157-160). These observations suggest that the rigidity sensor could be located within the focal adhesion complexes which connects the actin cytoskeleton to the sites of focal adhesions.

By contrast, we found that although cells responded to increasing substrate rigidity by increasing the focal adhesion area and traction stress magnitude (Figure 11), the mean focal adhesion area was poorly correlated with mean traction stress magnitude (Figure 10). Our findings also revealed that between 20-60 kPa, mean focal adhesion areas continue to increase even when mean traction forces saturate, thus suggesting that additional factors other than traction forces could be involved in the regulation of focal adhesion sizes.

We prostulate that while traction stress is important in the growth of focal adhesion sizes initially, maturation of focal adhesion could be influenced by other factors such as rate of focal adhesion assembly and disassembly, possibly separately regulated by the substrate elasticity. Similarly, observations by Stricker et al. (68) indicate that focal adhesion area and traction stress magnitude are strongly correlated only during the initial phases

69

of myosin-mediated adhesion maturation and growth. Upon the maturation of focal adhesions, their sizes stabilize and no longer correlate with traction stress magnitude. Beningo et al. have also shown that small focal adhesions at the cell's leading edge transmit strong propulsive forces while large mature focal adhesions exert weaker tractions on the substrate (114). Consistent with these findings, Trichet et al. have reported that focal adhesions of a similar area can sustain a wide range of force (70).

Although focal adhesion areas have been shown to be poorly correlated to traction stress magnitude, focal adhesion proteins could still be important in transmitting traction stresses to the substrate. Gardel et al. have found that traction stresses at focal adhesions correlate biphasically with the speed of actin retrograde flow (115). They have proposed that focal adhesions at the cell front function as a molecular clutch to slow down the actin retrograde flow and that further polymerization of actin can contribute to the cell protrusion, resulting in large traction stresses on the substrates. On the other hand, at a very low actin flow rate, the linkages between F-actin and focal adhesions are disrupted, resulting in small traction stresses on the substrate.

In addition to such actin reorganization, ion channels located at or near focal adhesions may also play a role in mechano-sensing. Kobayashi and Sokabe have demonstrated that different mechano-sensitive ion channels located in the vicinity of focal adhesion form molecular complexes with both stress fibers and focal adhesion to control the level of cytoplasmic Ca^{2+}, which

subsequently induces acto-myosin contraction or facilitates further cell signaling events (85).

2.5 Conclusions

In conclusion, sustained substrate strain on soft substrates and sustained traction stress on stiff substrates suggests that depending on the substrate rigidity, either the strain or the stress might critically influence the behavior of fibroblasts. We propose that on substrates softer than 20 kPa, strain-sensing machinery of cells is active and governs cellular functions to maintain constant substrate deformations. Considering that traction forces are likely to be transmitted along actin filaments, a global response such as F-actin reorganization may be the factor responsible for conserving strain on soft substrates.

On the other hand, on substrates stiffer than 20 kPa, fibroblast behavior switches to be governed by stresses defined by the force-generating machinery within cells. Limitations in the force-generating capacity of the cell's acto-myosin units may be responsible for the plateau of cell-generated traction stress on stiff substrates. We speculate that the threshold value of substrate rigidity, where the switch between sustaining constant substrate deformation to sustaining constant traction stress occurs (20 kPa), is determined by the coordination of strain-sensing and force-generating machineries. This threshold value may be relevant to the physical properties of fibrous tissues.

In addition, we found focal adhesion areas to be weakly correlated to traction stresses, suggesting that local responses to substrate rigidity may not be involved in the mechanism regulating mature focal adhesion sizes in its entirety. We propose that rigidity sensing machineries are distinct from the mechanisms primarily regulating maturation of the focal adhesion. However, individual focal adhesion proteins or associated ion channels may still contribute to the cellular response to substrate rigidity. Although detailed processes of cellular responses to substrate rigidity remain to be elucidated by future studies, the findings and tools presented here can provide valuable clues to deciphering the complex regulatory mechanisms behind cellular mechano-sensing.

3 INVESTIGATING MECHANISTIC DIFFERENCES BETWEEN AMOEBOID AND MESENCHYMAL MIGRATION

3.1 Amoeboid and mesenchymal cell migration – distinguishing between the two

Cell migration has been widely studied on 2D surfaces and usually, movement is predominantly driven by actin polymerization at the cell's leading edge producing structures known as lamellipodia and filopodia (14,23-25,122). Integrin-mediated cell-substrate adhesion also plays an important role during cell migration, with the cell adhering to the ECM through structures known as focal adhesion complexes (14,29-31). Cell migration also requires the generation of large traction forces on both the front and rear ends of the cell (123). In 3D environments, cells may also secrete proteases which cleave surrounding fibrils to overcome the physical barriers impeding cell movement (14,26-28,35). This mode of migration has been termed mesenchymal cell migration and mesenchymal cells such as fibroblasts, smooth muscle cells, and cancer cells from epithelial cancers are known to exhibit this migration mode (14).

However, some cell types, such as zebrafish PGCs, leukocytes, and some tumor cells, seem to employ a different migration mechanism altogether. Instead of adhering to the substrate and forming lamellipodia at the cell front,

these cells move via rapid shape changes, alternating cycles of morphological bleb-like expansion and contraction, and relatively low-affinity substrate binding (35-40). Cytoplasmic streaming was also observed, whereby a pseudopodium forms during migration and a stream of granular material flows into the growing protrusions (40). This is similar to the early observations of amoebae movement (2-4,45-49). This type of migration is hence termed amoeboid cell migration and cells exhibiting this mode of motility are called amoeboid cells. However, mechanisms involved in amoeboid migration in mammalian cells remain unclear and amoeboid migration is sometimes used to describe any mode of migration that does not exhibit characteristics of mesenchymal migration.

In addition, it has been reported that inhibiting mesenchymal cell migration in 3D matrices is not sufficient to stop cancer cells, which normally migrate using the mesenchymal mode, from metastasizing (14,35). Wolf et al. (35) observed that when protease inhibitors was added to cancer cells in 3D collagen matrix to prevent cells from cleaving physical barriers impeding cell movement, cells undergo MAT. These cells, which used to migrate using the mesenchymal mode, can continue to move by amoeboid migration in the presence of protease inhibitors. Instead of degrading the matrix to create space for migration, cells change their shape in an amoeba-like manner to squeeze through pre-existing gaps between collagen fibers. This reiterates the importance of understanding amoeboid cell migration and how external

factors in the ECM influence the migration mechanism cells use, especially in developing therapies to inhibit metastasis of cancerous cells completely.

Neutrophil-like, differentiated human promyelocytic leukemia (HL60) cells were chosen for this study as neutrophils have been postulated to be capable of both amoeboid and mesenchymal cell migration (14). Neutrophils were observed to migrate using lamellipodia-like structures in the presence of substrate ligands such as intercellular adhesion molecule 1 (ICAM-1) and fibronectin (41,66,124). However, a few studies have also shown that neutrophils could migrate in the absence of integrin-mediated cell-substrate adhesion (52,125). This adhesion-independent migration mechanism had been loosely termed amoeboid migration.

To the best of our knowledge, we have for the first time, compared and quantified differences in the amoeboid and mesenchymal migration behavior of differentiated HL60 (dHL60) cells. In our setup, dHL60 cells were confined between two pieces of polyacrylamide gels embedded with fluorescent beads, thereby allowing us to monitor gel deformation and hence gel stresses during cell migration. By imaging F-actin distribution in the dHL60 cells, we have shown that these cells showed distinctly different migration mechanism in the absence and presence of integrin-fibronectin mediated cell-substrate adhesion: by producing bleb-like features (amoeboid mode) and lamellipodia (mesenchymal mode) respectively.

We have observed that cells exhibiting the amoeboid and mesenchymal mode of migration exerted different stress patterns on the gels, and suggested a quantitative measure to distinguish between the two migratory modalities. In addition, we also varied the width of the separation between the two gels, thus controlling the extent of cell deformation during migration, and the stiffness of the substrates. We found that, unlike mesenchymal cell migration, amoeboid cell migration speed is fastest at an intermediate gap size and is not affected by gel rigidity. Our computational model of amoeboid cell migration in a confined environment also revealed that the strength of membrane-cortex adhesion is a crucial factor in determining the gap size at which amoeboid migration speed is the maximal.

3.2   Methods and materials

3.2.1   Cell culture, differentiation and transfection of HL60 cells

Human promyelocytic leukemia HL60 cells (ATCC, Manassas, VA) were maintained at 37°C and 5% CO_2 in Roswell Park Memorial Institute medium (ATCC) supplemented with 10% fetal bovine serum (GIBCO, Grand Island, NY) and 1% penicillin-streptomycin (GIBCO). The HL60 cells were differentiated into neutrophils (dHL60 cells) by culturing cells in culture media containing 1.3% dimethyl sulfoxide (DMSO) for 6 days following the protocols reported in literatures (126,127,128). Following this protocol,

76

approximately 72% of 300 cells counted had differentiated into neutrophils as revealed by the nitroblue tetrazolium (NBT) reduction test described in (127,128) (see Fig. S1. in the Supporting Material)..

The dHL60 cells were transfected with Lifeact-GFP via electroporation with the Neon Transfection System (1350 V, 35 ms, 1 pulse) to visualize the F-actin localization within the cells without compromising actin dynamics (135). In separate experiments, cell migration speeds were obtained either immediately after cells were treated with 50 μM of blebbistatin (Tocris Bioscience, Bristol, United Kingdom) or 24 h after cells were treated with 20 μM of baicalein (Sigma-Aldrich, St. Louis, MO), to study to role of myosin contractility, or ezrin mediated membrane-cortex adhesion strength during cell migration respectively.
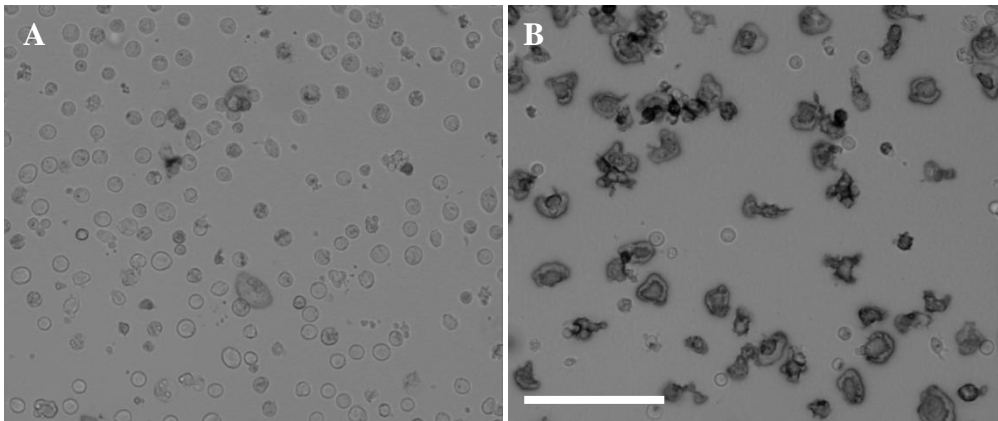
Figure 12 Transmitted light image of HL60 after adding 0.1% NBT. (*A*) Undifferentiated HL60: nuclei were not stained by NBT. (*B*) HL60 after incubating 6 days with 1.3% DMSO: differentiated cells' nuclei were stained. Scale bar represent 100 μm.

3.2.2   Preparation of polyacrylamide gels

Polyacrylamide gels were prepared and attached to glass-bottomed culture dishes (bottom gels), and coverslips (top gels) by a method previously described in (61). Glass-bottomed dishes (20 mm glass diameter; ibidi GmbH, Planegg, Germany) or coverslips (15 mm diameter) were treated with 3-aminopropyltrimethoxysilane (Sigma-Aldrich) for 5 min to activate the glass surfaces for gel attachment. The glass surfaces were then washed with distilled water, and covered with 0.5% glutaraldehyde (Sigma-Aldrich) in phosphate buffered saline (PBS) for 30 min.

The pre-polymerized acrylamide gel solutions were prepared with varying concentrations of acrylamide (Bio-Rad, Hercules, CA) and bisacrylamide (bis, Bio-Rad) to vary the polymerized gels' rigidity. Specifically, gel solutions were prepared with concentrations of acrylamide to bis at 8% acrylamide: 0.2% bis, 8% acrylamide: 0.1% bis, and 5% acrylamide: 0.05% bis, to obtain polymerized gels with rigidity of 16.6 ± 0.36 kPa (mean $\pm$ SE), 6.19 ± 0.13 kPa, and 1.25 ± 0.037 kPa respectively. The Young's moduli were obtained through measurements by an atomic force microscope on the polymerized gels (Fig. S2), and values corresponded well with values reported in previous literatures (124,61).

Prior to polymerization of the acrylamide gel solutions, 1/25 volume of red fluorescent beads (excitation and emission wavelength of 580 nm and 605

nm respectively) with 0.2 µm diameter (FluoSpheres; Invitrogen, Carlsbad, CA) were added to the pre-polymerized acrylamide gel solutions. Polymerization was initiated with 10% ammonium persulfate (Bio-Rad) and catalyzed with N,N,N',N'-Tetramethylethlenediamine (Bio-Rad). 6 µl of gel solution was placed onto the treated glass-bottomed dish or coverslip, and another untreated circular coverslip (12 mm diameter) created a sandwich over the drop. After polymerization, the top coverslip was carefully removed and the gel was rinsed with 50 mM 4-(2-hydroxyethyl)-1-piperazineethanesulfonic acid (HEPES, pH 8.5; Sigma-Aldrich). The thicknesses of fully hydrated gels made with this protocol were approximately 50-60 µm.

To functionalize polyacrylamide gels with fibronectin (fibronectin coated gels), 0.5 mg/ml sulfo-succinimidyl-6-(4-azido-2-nitrophenyl-amino) hexanoate (sulfo-SANPAH; Pierce, Rockford, IL) in HEPES was placed onto the surface of each gel and exposed to ultra-violet (UV) light in a sterile hood for 15 min. The darkened sulfo-SANPAH solution was removed and gels were rinsed with HEPES twice for 15 min. The gels were then covered by 100 µg/ml fibronectin (Sigma-Aldrich) for 2 h at room temperature on a rocker. For gels not functionalized with fibronectin (non-fibronectin coated gels), cell-matrix adhesion was further prevented by immersing gels in 0.1% pluronic F127 (BASF, Ludwigshafen, Germany) for 1 h at room temperature on a rocker (131).

79

Gels were then rinsed with PBS and sterilized by exposure to UV light in a sterile hood for 15 min. The gels were then incubated for 30 min in cell culture medium at 37°C before cells were transferred to the gels.

3.2.3 Measurement of Young's moduli of polyacrylamide gels

The Young's moduli of the polyacrylamide gels were measured using an atomic force microscope (AFM) to indent the gels. The spherical tip of the AFM cantilever was slowly pushed into the surface of the gels by the piezoelectric stage and the position of the piezoelectric stage is denoted by Z_p, where $Z_p = 0$ at the surface of the gel (Figure 13*A*). The deflection of the tip (Z_c) can be determined by the displacement of the position sensitive photo-detector signal (V_{PSPD}). For a small deflection of the cantilever, we can assume a linear relationship where

$$Z_c = s \cdot V_{PSPD}. \qquad (4)$$

The value of s was first obtained by pushing the AFM tip on a hard surface (glass) where $Z_p = Z_c$ (Figure 13*B*). The slope of a linear fit of Z_p vs. V_{PSPD} curve obtained from the AFM will give us the value of s. On the other hand, on a soft surface, the AFM tip may indent into the substrate and the indentation depth δ is given by $\delta = Z_p - Z_c$ (Figure 13*C*). The force (F) which the tip exert on the surface can be obtained from the deflection of the

tip, where $F = kZ_c$ and k represents the stiffness of the AFM cantilever as specified by the tip manufacturer.
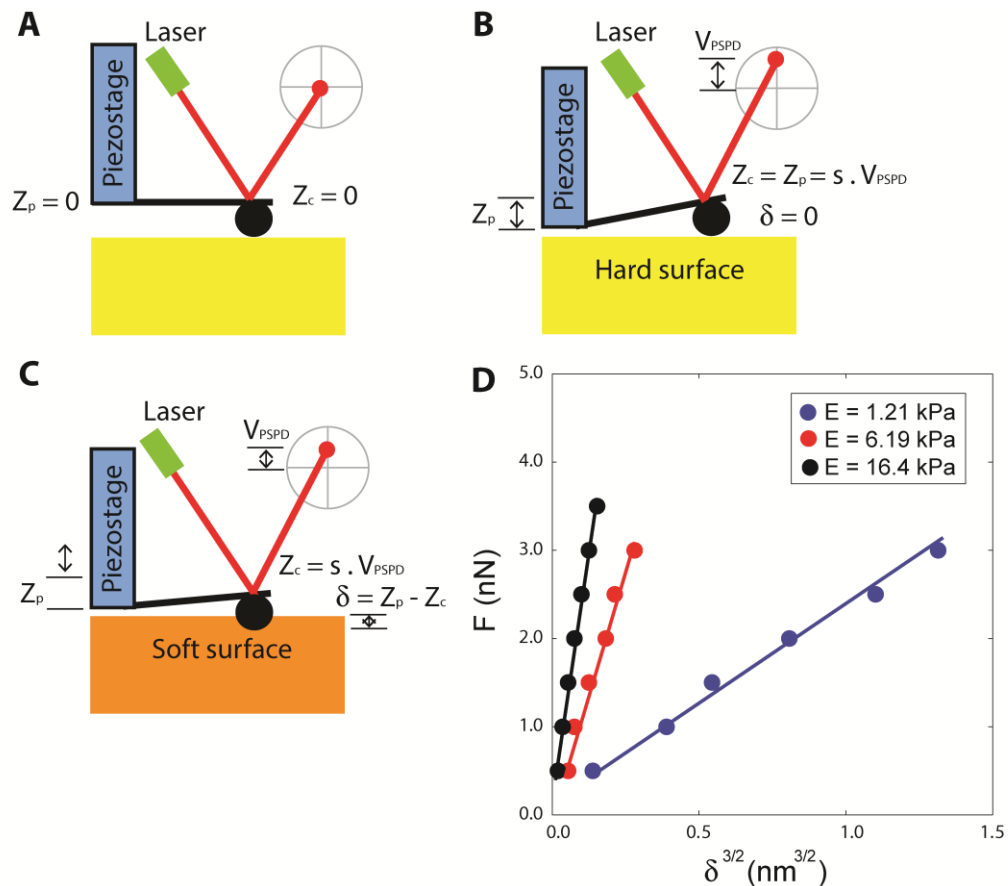
Figure 13 (*A-C*) **Schematic illustrations of gel rigidity measurement using AFM.** (*A*) **When the cantilever tip just contacts the surface, there is no deflection of the cantilever tip, i.e.** $Z_p = Z_c = 0$. (*B*) **When the tip touches a hard surface, the tip does not penetrate into the surface, thereby deflecting the cantilever tip and the** V_{PSPD}. (*C*) **When the tip touches a soft surface the tip penetrates into the surface, thereby deflecting the cantilever tip and the** V_{PSPD} **less as compared to the case in** (*B*). (*D*) **A linear fit of the graph of** F **vs.** $\delta^{3/2}$ **allows the calculation of the gel's Young's moduli.**

A Hertzian model was used to obtain the Young's moduli (E) of the gels, where

$$F = \frac{4E}{3(1-v^2)} D^{\frac{1}{2}} \delta^{\frac{3}{2}}$$

(5)

D represents the diameter of the spherical tip specified by the tip manufacturer and v is the Poisson's ratio of the gel. The Young's moduli of the gels can thus be obtained from the slope of the curves of F vs. $\delta^{3/2}$ (Figure 13D). Measurements were conducted at several points on the gel and an averaged value was obtained as the Young's moduli of the gel.

3.2.4   Assembly of confined environment for cell migration

In order to mimic 3D environment where cells have to squeeze through gaps in the ECM to move from a place to another, a confined environment was created by placing cells in between two polyacrylamide gels (Figure 14A-B). Red fluorescent beads were embedded in the gels for force calculations.
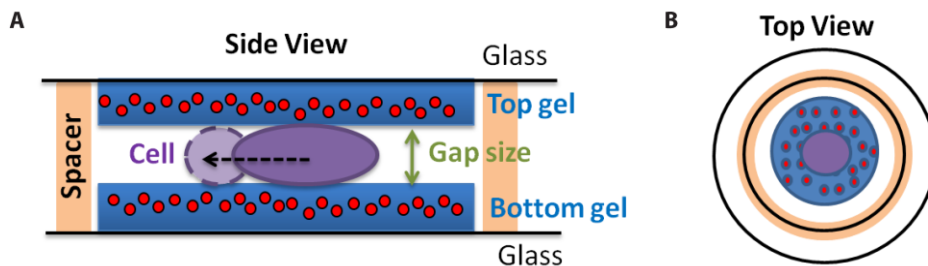
Figure 14 Side (*A*) and top (*B*) view of experimental setup. The cell is confined between two gels. Spacers are used to separate between the top and bottom coverslips, thereby creating a gap with variable heights between the two gels. Fluorescence beads (*circles*) are embedded within gels for calculation of traction stresses.

Cells were allowed to settle to the gel surface on non-fibronectin coated bottom gels before placing another non-fibronectin coated top gel over the cells. For fibronectin coated gels, cells were allowed to adhere to the top gel for 15 minutes before placing the top gel over the bottom gel such that only adhered cells were transferred to setup.

The two glass surfaces were separated by a spacer (120 μm Secure-Seal; Invitrogen) and the height of the separation between the top and bottom gels was defined as the gap size. Due to slight differences in gel thickness across the whole sample, which varies from approximately 50-60 μm, a variation of gap sizes can be achieved within the same sample. The gap size was determined using a confocal microscope with the fluorescent beads as markers on the surface of the top and bottom gels. A small weight (3 g) was placed on the top coverslip to minimize drifting of the top gel during image acquisition.

3.2.5   Live cell imaging

Live cell imaging was performed immediately after fMLP (Formyl-Methionyl-Leucyl-Phenylalanine; Sigma-Aldrich) was introduced (final concentration of 100 nM) to dHL60 cells cultured on the polyacrylamide gel. fMLP is a chemokine which activate and induce neutrophil migration (66,129,130). DIC images were obtained at regular intervals (every 30 seconds for 10 minutes) with PerkinElmer Ultraview at 60x water objective lens (NA

1.2) and a stage incubator. The cell nuclei were also stained with Hoechst 34580 (1 μg/ml, Invitrogen) to enable cell tracking and speed calculations. 3D image stacks of the fluorescent bead positions embedded within the polyacrylamide gel were also acquired for 3D traction stress calculations.

3.2.6 Quantification of cell migration speed

Cell migration speed was determined with time-lapse images of the cell nucleus recorded every 30 seconds, over a period of 10 minutes. Using the Image Processing Toolbox in MATLAB, images were thresholded, using a value determined by the Otsu's method (132), to define the cell nuclei regions. Nuclei which were connected to the borders were removed and nuclei centroid positions were determined. A MATLAB tracking program which compute the correlation of centroid positions between time frames was then used to find the nuclei displacement and hence the cell speeds (133). For each data point, at least 20 dHL60 cells were counted.

3.2.7 Quantification of number of blebs and protrusion asymmetry

The number of blebs within a cell was evaluated by counting the total number of blebs produced per cell from time-lapse images recorded every 30 seconds. The centroid of each bleb was estimated manually and angles between neighboring blebs were obtained by calculating the angles enclosed between the bleb centroids with the cell centroid as reference. For each cell,

the coefficient of variance (CV) of angles between neighboring blebs was evaluated as the ratio of the standard deviation to the mean angles between neighboring blebs. This CV was used as a measure of protrusion asymmetry, with a value of 0 indicating perfect protrusion symmetry and a larger value indicating more asymmetric protrusions.

3.2.8   3D traction stress calculations

2D traction force microscopy has been widely reported and protocols of conducting experiments and calculations are well established (60-62,64-66,68,71,72). However, in recent years, many research groups have extended the 2D calculation to find the 3D forces that cell exerts on the substrates (74-80).

We use the digital volume correlation (DVC) first applied to traction force microscopy by Franck et al. (78-80). Two 3D volume of images of the polyacrylamide gels without and with the cell were obtained and the volumes were divided into sub-volumes Ω. The fluorescence intensity of the fluorescent beads in each 3D sub-volume of the unstrained and strain gel was represented by $f(x_1, x_2, x_3)$ and $g(x_1, x_2, x_3)$ respectively, where x_1, x_2, and x_3 correspond to the Cartesian coordinates along the x, y, and z axes.

The displacement vector u between each corresponding sub-volume was estimated from the location of the cross-correlation peak, defined by:

$$m(\mathbf{u}) = \int f(\mathbf{x})g(\mathbf{x}+\mathbf{u})d\Omega_x \qquad (6)$$

The cross correlation function can be efficiently computed using Fourier transforms as denoted by Eq. (7).

$$m(\mathbf{u}) = F^{-1}\{F[f(\mathbf{x})]*F[g(\mathbf{x})]\}, \qquad (7)$$

where the Fourier transform of $f(\mathbf{x})$ is defined by $F[f(\mathbf{x})] = \int f(\mathbf{x})e^{-i\,\mathbf{k}}d\Omega_{\mathbf{x}}$, $*$ denotes the complex conjugate, and F^{-1} denotes the inverse Fourier transform.

The mean displacement at cell-free regions, where the cell was at least 5 μm away, was subtracted from the calculated displacements, to correct for sample drift during image acquisition. The resultant displacement matrix approximates the local gel deformation for each sub-volume which best fit the strained image to the unstrained image. After obtaining $\mathbf{u}$, a displacement-gradient technique was used to obtain the strain tensor $\boldsymbol{\varepsilon}$ by minimizing the vector $\mathbf{S}$ in a least square fashion (80),

$$\mathbf{S} = \sum_{i=1}^{3}\sum_{j=1}^{3}\sum_{k=1}^{3}\left(\hat{u}_{ijk}-u_{ijk}\right)^2, \qquad (8)$$

where $u_{ijk}(x_1, x_2, x_3) = ax_1 + bx_2 + cx_3 + d$. Constants a, b, c, and d were determined by the least square minimization of Eq. (8) using a 3×3×3 pixel kernel. The strain tensor $\boldsymbol{\varepsilon}$ was obtained from the constants a, b, c, and d and can be written in a matrix form:

$$\boldsymbol{\varepsilon} = \begin{pmatrix} \varepsilon_{11} & \varepsilon_{12} & \varepsilon_{13} \\ \varepsilon_{21} & \varepsilon_{22} & \varepsilon_{23} \\ \varepsilon_{31} & \varepsilon_{32} & \varepsilon_{33} \end{pmatrix} = \begin{pmatrix} a & \frac{1}{2}(a+b) & \frac{1}{2}(a+c) \\ \frac{1}{2}(a+b) & b & \frac{1}{2}(b+c) \\ \frac{1}{2}(a+c) & \frac{1}{2}(b+c) & c \end{pmatrix}. \tag{9}$$

Assuming that the material is linearly elastic, isotropic and incompressible, the material stress tensor $\boldsymbol{\sigma}$ can then be determined from the materials constitutive relation

$$\boldsymbol{\sigma} = E\boldsymbol{\varepsilon}/(1+v), \tag{10}$$

where E is the Young's modulus of the gel and v the Poisson's ratio of the gel.

The stress or traction vector $\boldsymbol{F}$ was calculated at the surface of the gel using the Cauchy relationship,

$$\boldsymbol{F} = \boldsymbol{\sigma} \cdot \boldsymbol{n}, \tag{11}$$

where $\boldsymbol{n}$ is the surface normal vector (78).

To quantify the differences between stresses exerted by an amoeboid and a mesenchymal cell, we summed the stresses in the z-direction ($\vec{F}_z$) vectorially over the cell area at the gel's first z-plane, which is immediately next to the cell ($k = 0.25\mu m$) to obtain the magnitude of the resultant $\vec{F}_z$ acting on the surface of the gel (F_{net}):

$$F_{net} = \left| \sum_{i=1}^{m} \sum_{j=1}^{n} \vec{F}_z(i, j, 0.25) \right| \tag{12}$$

where *m* and *n* denotes the number of sub-volumes in the *x* and *y* directions respectively.

We also defined another measure called the penetration depth as the depth of gel whereby the magnitude of the average gel stress ($F_{x,y,z}$) first decreased below 100 Pa where

$$F_{x,y,z}(k) = \frac{\sum_{i=1}^{m}\sum_{j=1}^{n}\sqrt{\vec{F}_x(i,j,k)^2 + \vec{F}_y(i,j,k)^2 + \vec{F}_z(i,j,k)^2}}{mn} \quad (13)$$

3.2.9 Modeling of amoeboid motility in confined environments

A computational model of blebbing cell motility has been developed by our collaborator Dr Fong Yin Lim and details of the computational method have been described elsewhere (134). A schematic of the model is also shown in Figure 15. For completeness, details of the computational model have been summarized in this thesis.

The cell was modeled in 2D and surrounded by an incompressible viscous fluid. A cell was represented by an elastic actin cortex with cortical tension T_c and bending stiffness B_c, enclosed by an elastic cell membrane characterized by membrane tension T_m and bending stiffness B_m. The cell membrane was uniformly adhered to the actin cortex and the membrane-cortex adhesion was assumed to be Hookean with a spring constant k_{ad}. The cytoplasm and extracellular fluid were assumed to be incompressible and with

the same viscosity μ. Due to the low Reynolds number of the cytoplasm, the cytoplasmic velocity field u and pressure field p at any instant of time can be described by the Stokes equation and the equation of continuity,

$$\nabla p = \mu \nabla^2 u + f, \text{ and} \qquad (14)$$

$$\nabla \cdot u = 0. \qquad (15)$$

f represents the body force on either the membrane (f_m) or the actin cortex (f_c).

The cell membrane was parameterized in the deformed configuration by $r_m(\zeta_m) = (x_m(\zeta_m); y_m(\zeta_m))^T$, with $\zeta_m = [0; L_m]$ where L_m was the perimeter of the membrane. Similarly, the actin cortex was parameterized in the deformed configuration by $r_c(\zeta_c) = (x_c(\zeta_c); y_c(\zeta_c))^T$, with $\zeta_c = [0; L_c]$ where L_c was the perimeter of the cortex.

The body force f_m on the membrane results from membrane bending f_{bm}, membrane tension f_{tm}, and membrane-cortex adhesion f_{ad}, as shown in Eq. (16).

$$\mathbf{f}_m(\mathbf{r}_m) = \int_0^{Lm} [\mathbf{f}_{bm}(\mathbf{r}_m) + \mathbf{f}_{tm}(\mathbf{r}_m) + \mathbf{f}_{ad}(\mathbf{r}_m)]\delta(\mathbf{r} - \mathbf{r}_m)d\zeta_m, \qquad (16)$$

where $\delta(r)$ is the two-dimensional Dirac delta function. The motion of the membrane at position r_m can be obtained from the no-slip boundary condition imposed on the Stokes equation, i.e.,

$$\mathbf{u} = \frac{d\mathbf{r}_m}{dt} \qquad (17)$$

The body force f_c on the cortex results from the cortex bending f_{bc}, cortex tension f_{tc}, membrane cortex adhesion f_{ad} and f_{com} which mimics the acto-myosin contraction. f_{com} was exerted on each of the membrane-cortical springs, in the direction tangent to the springs, thus giving rise to a uniform intracellular pressure that was higher than the surroundings.

$$\mathbf{f}_c(\mathbf{r}_c) = \int_0^{Lc} [\mathbf{f}_{bc}(\mathbf{r}_c) + \mathbf{f}_{tc}(\mathbf{r}_c) + \mathbf{f}_{ad}(\mathbf{r}_c) + \mathbf{f}_{com}(\mathbf{r}_c)]\delta(\mathbf{r} - \mathbf{r}_c)d\zeta_c \qquad (18)$$

The actin cortex is assumed to be permeable and to interact with the cell membrane only via the membrane-cortex adhesion term f_{ad}. The motion of the actin cortex at position r_c is obtained by solving for the force balance on a cortical element, assuming a uniform cortical viscosity v_c, i.e.,

$$\mathbf{f}_c = v_c \frac{d\mathbf{r}_c}{dt} \qquad (19)$$

Initial detachment of membrane-cortex adhesion resulted in nucleation of a bleb. In addition, the membrane-cortex adhesive springs would break if the spring energy exceeds the membrane-cortex adhesion energy (i.e. length of the spring is greater than a critical length l_c). To account for retraction, a second imaginary cortical element termed the diffusive cortex element was introduced. These diffusive cortical elements exist only when a region of the membrane was detached from the cortex. Upon breakage of membrane-cortex

90

adhesive springs, these elements would move towards the bleb membrane with a speed V_c. In reality, these diffusive cortical elements represent the actin monomers that reform the cortex underneath the bleb membrane during bleb retraction. Once the diffusive cortex elements were within a distance D_{equil} from the membrane, membrane-cortex adhesive springs that were previously broken will be reattached.

Boundary integral method with regularized Stokeslets was used to solve Eq. (14) - (16), and (18). Having solved for the fluid velocity field u, the membrane markers positions r_m and cortical markers positions r_c can be updated according to Eq. (17) and Eq. (19) using the forward Euler method with a time step δt.

We considered the case of bleb nucleation of a cell confined between two rigid walls. We assumed that the cell does not adhere to these obstacles. Therefore, the interaction between the cell and obstacles was purely hydro-dynamical. The boundary integral method with regularized Stokeslets can be easily adapted to the case when fixed obstacles exist. This was done by imposing zero velocity boundary conditions on the obstacles and finding the forces exerted by the obstacles on the fluid.

The average cell migration speed was obtained by taking the average of the difference of the cell's center of mass between adjacent time steps divided by the value of the time step. The intracellular pressure was defined as the cytoplasmic fluid pressure prior to any blebbing events.
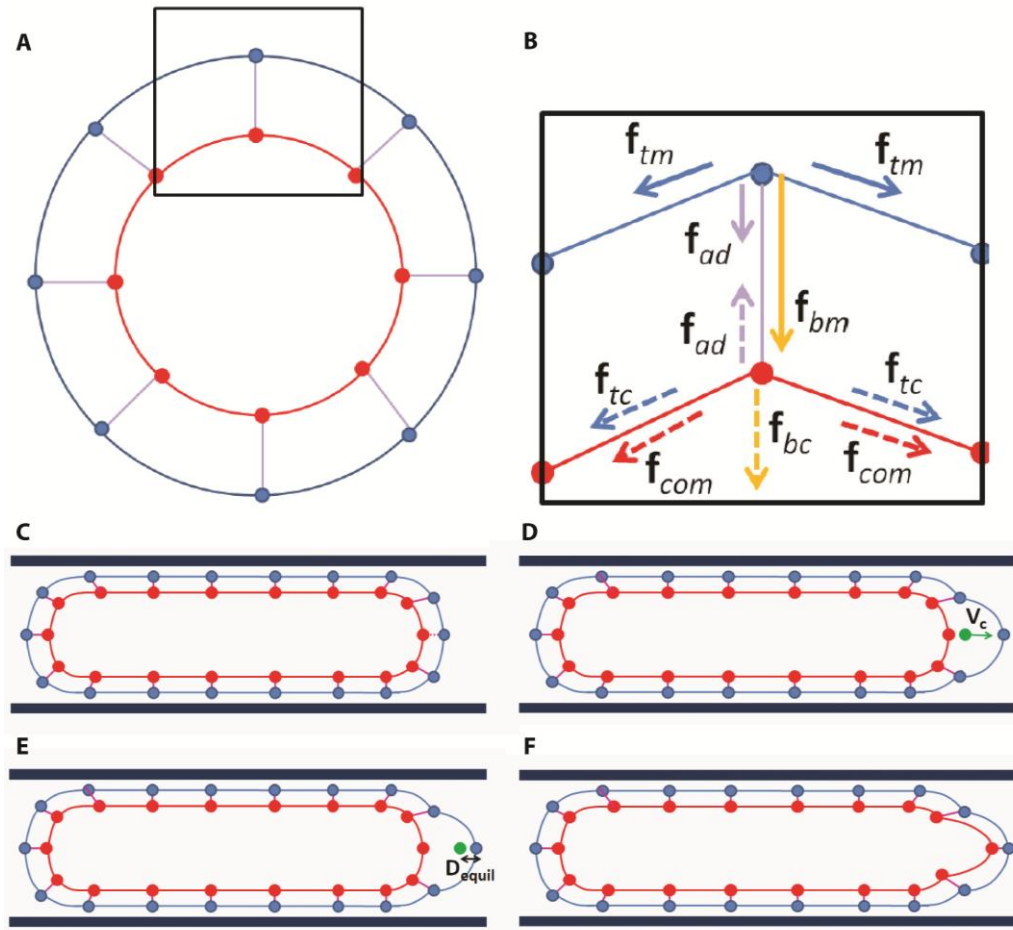
Figure 15 Schematic illustrations of model. (*A*) **A cell is made up of the cell membrane (*blue*) and the actin cortex (*red*), connected to each other via membrane-cortex springs (*purple*).** (*B*) **Detailed drawing of boxed region in (*A*), with the forces acting on each point shown.** (*C*) **A local rupture of membrane-cortex bond (*dashed magenta line*) causes a drop in local pressure at that point.** (*D*) **Fluid flows into the region, down a pressure gradient, to initiate bleb formation. As fluid flows into the bleb, the free actin cortex elements (*green*) are moved into the bleb with a speed V_c.** (*E*) **Once the actin cortex elements are within a distance of D_{equil} from the membrane, the connections between the cortex and the membrane will reform.** (*F*) **This cause a retraction of the bleb and the cells' centre of mass will move. Black lines in (*C*)-(*F*) represents the rigid walls of the channel.**

3.3 Results

3.3.1 dHL60 cells confined between two gels without fibronectin coating form blebs and migrate in the amoeboid mode

Neutrophil-like, dHL60 cells that were obtained by differentiating HL60 cells, were observed to form both bleb-like protrusions and lamellipodia when cells were cultured on unconfined fibronectin coated polyacrylamide gels. However, on unconfined non-fibronectin coated polyacrylamide, most of the cells remained in suspension and formed blebs. After confining the cells, rounded protrusions resembling blebs (Figure 16*A* and *B*) (amoeboid cell migration), and sheet-like protrusions resembling lamellipodia (mesenchymal cell migration) was observed (Figure 16*C* and *D*). To clearly differentiate whether cells were moving using blebs or lamellipodia, the dHL60 cells were transfected with Lifeact-GFP which labels the F-actin present in the cells with GFP without compromising actin dynamics (135).

We observed that on non-fibronectin coated gels, cells produced protrusions that separate from the actin cortex. These protrusions are initially devoid of F-actin, until subsequently, the actin cortex reforms underneath the cell membrane (Figure 16*E* and *F*). This is similar to observations of blebbing cells reported in previous literatures (40,39). On the other hand, on fibronectin coated gels, cells formed sheet like protrusions known as lamellipodia, where F-actin is always enriched at the cell front (Figure 16*G* and *H*).
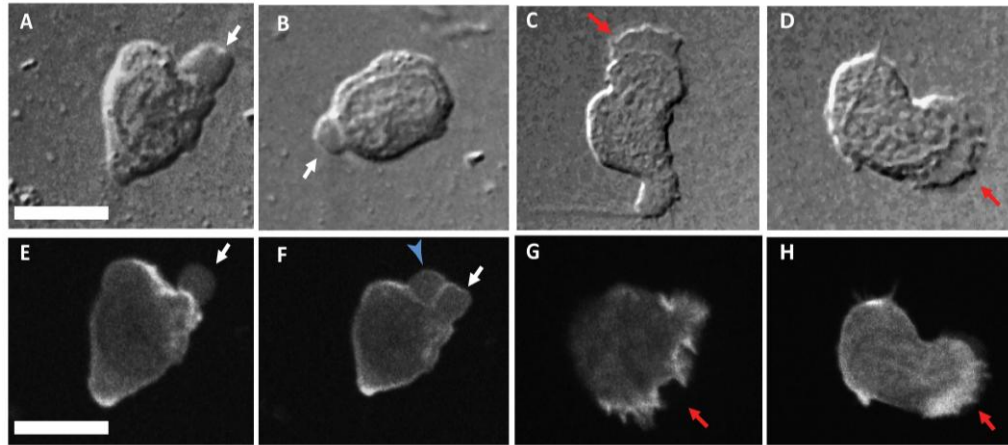
Figure 16 (*A-D*) DIC images of dHL60 cells confined between two gels: (*A-B*) Cells showing bleb-like protrusions (*arrows*) when confined between two pieces of non-fibronectin coated gels with Young's modulus of 1.25 kPa, and gap size 2 µm; (*C-D*) Cells showing sheet-like protrusion (*arrows*) when confined between two pieces of gels with Young's modulus of 1.25 kPa, 100 µg/ml fibronectin coating, and gap size 2 µm. (*E-H*) dHL60 transfected with LifeAct-GFP. (*E-F*) Cells confined between non- fibronectin coated gels (Young's modulus of 1.25 kPa and gap size 2 µm) formed protrusions (*arrow*) which separate from actin cortex. Actin cortex subsequently reforms under cell membrane, and another bleb is formed (*arrowhead*). (*G-H*) Cells formed lamellipodia (*arrows*) when confined between gels coated with 100 µg/ml fibronectin (gel rigidity of 1.25 kPa and gap size 2 µm). F-actin in these cells is always localized at cell front. Scale bars represent 10 µm.

3.3.2 dHL60 cells switch from migrating using the amoeboid mode to the mesenchymal mode when gels are coated with fibronectin

The fraction of dHL60 cells exhibiting blebs or lamellipodia during migration, on non-fibronectin and fibronectin coated gels, was quantified (Figure 17*A*). We found that on non-fibronectin coated gels, with Young's modulus of 16.63 kPa, cells forming blebs (amoeboid mode) made up 59.1% of the cell population, while cells forming lamellipodia (mesenchymal mode) formed 5.5% of the cell population. Conversely, in the presence of 100 µg/ml

94

of fibronectin coating, only 0.8% of the cell population formed blebs, while 60.3% of the cell population formed lamellipodia. There were also some cells which formed blebs at one moment and lamellipodia at another time point, making up about 35.4% and 38.9% of the cell population for non-fibronectin and fibronectin coated gels respectively.

3.3.3 Amoeboid cell migration speed is not affected by gel rigidity

The cell speeds on non-fibronectin coated gels were found to be independent of gel rigidity over the range of Young's moduli from 1.25-16.63 kPa, where cell speeds remained approximately constant at 3.6 µm/minutes (Figure 17*B*). However, in the presence of cell-substrate adhesion, cells were most motile when embedded within gels with Young's modulus of 6.19 kPa (cell speed of 3.4 ± 0.2 µm/minutes (mean ± SE)), as compared to cells on gels with Young's moduli of 1.25 kPa (cell speed of 3.1 ± 0.1 µm/minutes) and 16.63 kPa (cell speed of 1.9 ± 0.1 µm/minutes) (Figure 17*B*). This observation is similarly reported in (124,136), where cells on 4-7 kPa gels coated with 100 µg/ml fibronectin were found to move the fastest as compared to cells on other gel rigidities with similar fibronectin coating. The magnitudes of our migration speeds are also comparable to neutrophil migration speeds reported elsewhere (66,124,136).
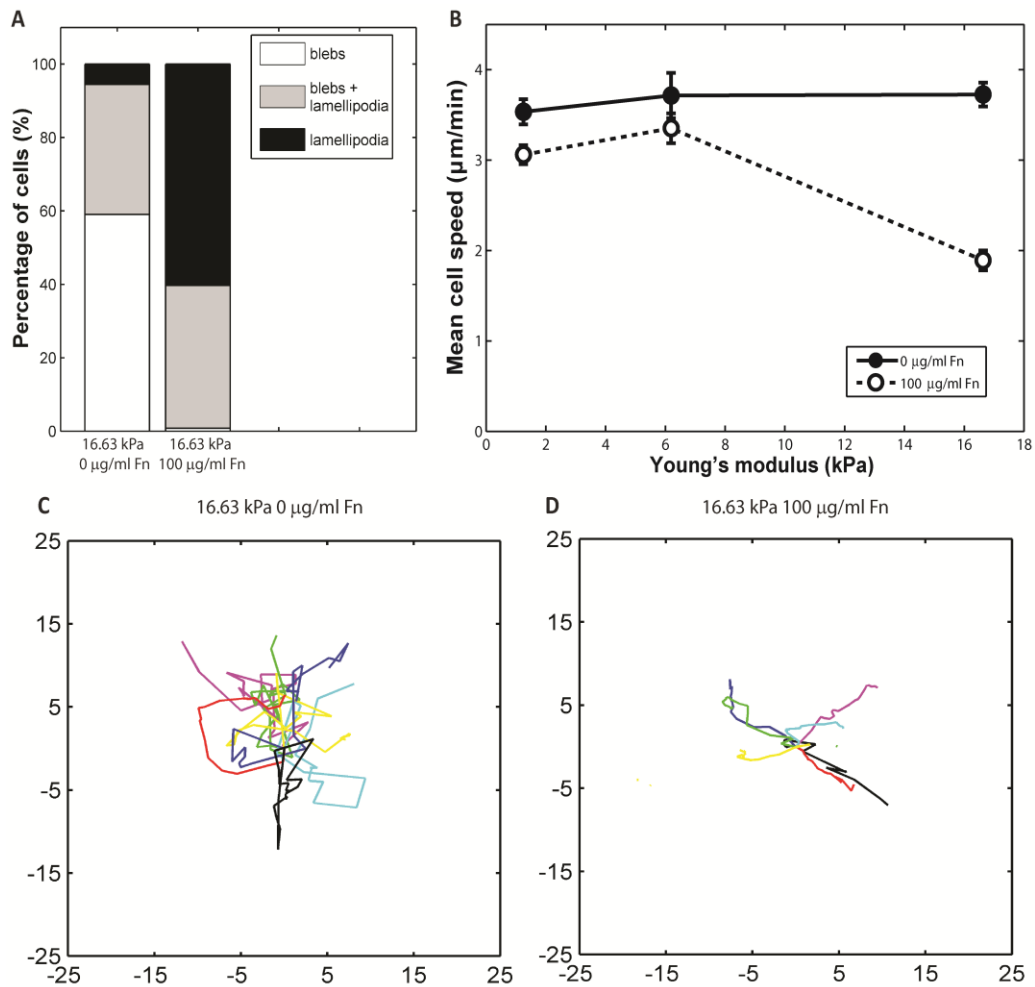
Figure 17 (A) Percentage of cells which formed bleb (white), lamellipodia (black) or both (grey) when embedded between two non-fibronectin (0 µg/ml Fn) and two fibronectin (100 µg/ml Fn) coated gels with Young's modulus of 16.63 kPa. (B) Speed of migrating cells on gels vs. gel rigidity for non-fibronectin (0 µg/ml Fn, solid circles) and fibronectin (100 µg/ml Fn, open circles) coated gels. Error bars represent SE of the mean. (C) Trajectories of cells embedded within non-fibronectin coated gels with gel rigidity of 16.63 kPa. (D) Trajectories of cells embedded within gels with gel rigidity of 16.63 kPa and 100 µg/ml fibronectin coating. x- and y-axis are in units of µm. Each colored line in (*C-D*) represents the track of an individual cell.

In addition, we observed faster migration on non-fibronectin coated gels as compared to fibronectin coated gels (Figure 17*B*). Although amoeboid cells moved quickly on non-fibronectin coated gels, amoeboid cells generally showed little persistence as they changed directions often (Figure 17*C*). In contrast, on fibronectin coated gels, mesenchymal cells moved slowly albeit with more persistence, when compared to amoeboid cells, as they changed directions less frequently (Figure 17*D*).

3.3.4 Amoeboid cells generate normal stresses to anchor to the gel and shear stresses at cell front during bleb protrusions

In the absence of cell-substrate adhesion, we found that amoeboid cells exert mainly normal stresses on the gel, acting in a direction perpendicular (along the *z*-axis) to both gel surfaces (Figure 18*E-G*). This indicates that during amoeboid migration, cells anchor themselves, in the absence of cell-substrate adhesion, by pushing on opposing gel surfaces as they migrate ($\vec{F}_{anchor}$). We also observed that as the cells produced blebs at the cell front during migration, cells exerted a shearing stress in the *xy*-plane at the cell front where blebs were formed, in the direction of cell migration (Figure 18*B-D*, $\vec{F}_{protrusion \, //}$). In addition to the shearing stresses, we also observed that the bleb exerts a normal stress component on the gels in some cases (Figure 18*G*, $\vec{F}_{protrusion \, \perp}$). Collectively, these observations suggest that during amoeboid migration, cells anchor itself between the two gels such that any bleb

protrusions will result in a net translation and a subsequent shift of the anchoring stress forward as the cell rear retracts.

Conversely, mesenchymal cells were found to exert large opposing tractional stresses at the cell front and rear (Figure 19*B-C*) ($\vec{F}_{protrusion\,/\!/}$ and $\vec{F}_{retraction\,/\!/}$ respectively), similar to what is commonly reported in 2D traction studies of fibroblasts (64,65,71,72,78,115). The mesenchymal cells also showed a push-pull dynamics, with the front of the cells applying a downward stress, along the *z*-axis, into the gel, and the rear of the cell applying an upward force, along the *z*-axis, out of the gel (Figure 19*C*, $\vec{F}_{protrusion\,\perp}$ and $\vec{F}_{retraction\,\perp}$ respectively). This push-pull dynamics corresponds to traction stress measurements reported in previous studies using fibroblasts (80).

In addition, we calculated the vector sum of the normal stresses over the whole cell at the first *z*-plane of the gels (immediately above the cell), as defined by F_{net} in the methods. We found that in amoeboid cells, F_{net} decreased as the gap size between the gels increased (Figure 20*A solid circles*, *C*, *E*, *G*). Similarly, we observed that the penetration depth of cell imposed stresses, as defined in the methods, also decreased when gap size is increased (Figure 20*B solid circles*, *C*, *E*, and *G*). On the other hand, in mesenchymal cells, we found that F_{net}, and the penetration depth were maintained around a constant value, of 2.6 kPa and 18 μm respectively, when gap size is increased (Figure 20*A-B open circles*, *D*, *F*, and *H*). F_{net} for mesenchymal cells were

also found to be generally lower than F_{net} for amoeboid cells (Figure 20*A*), while penetration depths of cell imposed stresses were higher for mesenchymal cells as compared to amoeboid cells (Figure 20*B*).
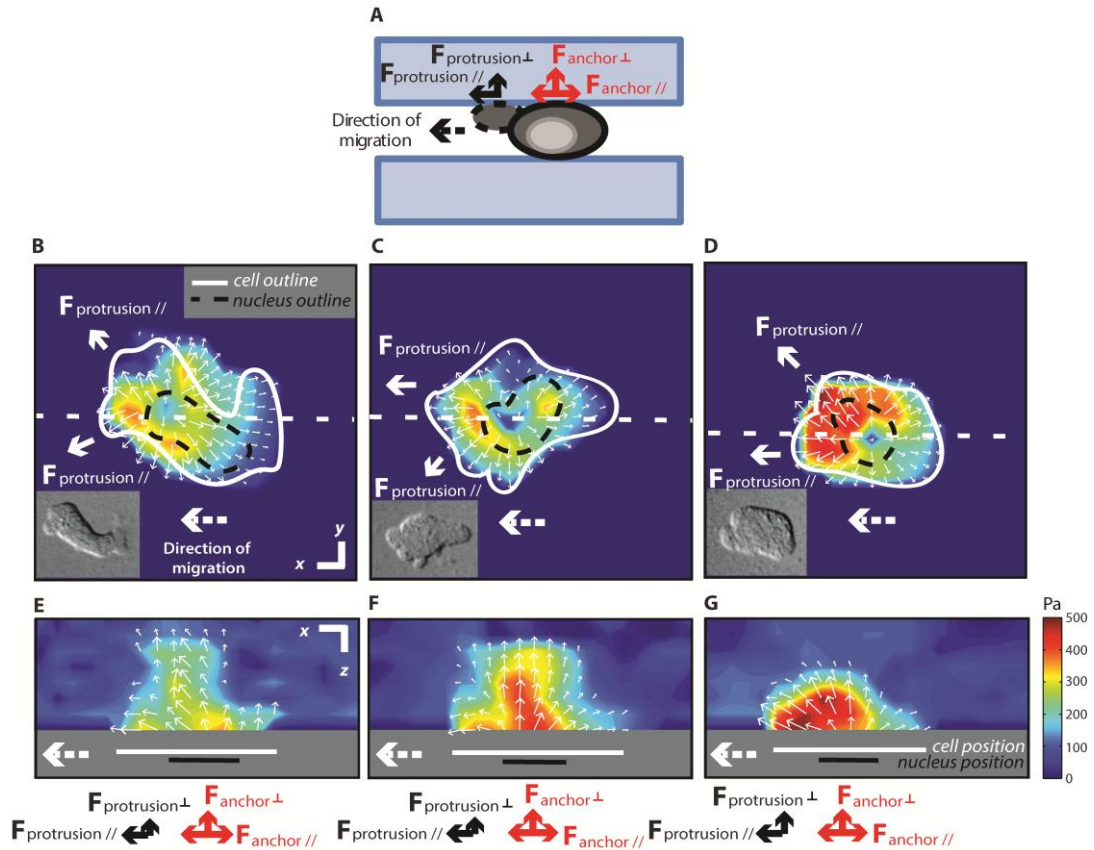
Figure 18 (*A*) **Schematic illustration of the stresses exerted by an amoeboid cell on the top gel. A bleb produced at the cell front (*dashed outline*) exerts a stress ($\vec{F}_{protrusion}$) on the gel in the direction of the bleb growth. Cell drifting is minimized as the cell body pushes into the gel thereby anchoring the cell between the two gels ($\vec{F}_{anchor}$). (*B-G*) Stress maps showing the stresses exerted by the cell on the top gel when the cell is confined between two pieces of non-fibronectin coated gels with Young's modulus of 1.25 kPa. (*B-D*) *xy*-stress maps of the top gel in the *xy*-plane immediately above the cell for three different dHL60 cells. Insets at the lower left are DIC images of the respective cells. Cell and nucleus boundaries are indicated by the white solid lines and black dashed lines respectively. (*E-G*) Corresponding *xz*-stress maps of the gel at the planes denoted by the white dashed lines in (*B-D*) respectively. Dashed arrows denote direction of cell migration. Cell and nucleus positions are indicated by the white and black lines respectively. Scale bars represent 5 μm in the *x*, *y* and *z* directions.**
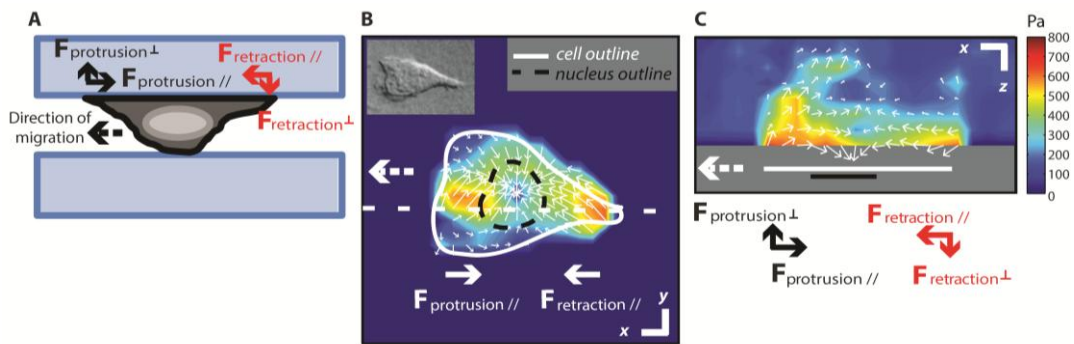
Figure 19(*A*) **Schematic illustration of the stresses exerted by a mesenchymal cell on the top gel. The cell adheres to the gel and exerts large contractile shearing stresses at the cell front and rear (** $\vec{F}_{\text{protrusion}}$ **and** $\vec{F}_{\text{retraction}}$ **respectively).** (*B*) *xy*-**stress map of the top gel in the** *xy*-**plane immediately above the cell when the cell is confined between two pieces of gels with Young's modulus 1.25 kPa and coated with 100 µg/ml of fibronectin. Inset at the top left in (***B***) is the DIC image of the cell. Cell and nucleus boundaries are indicated by the white solid lines and black dashed lines respectively.** (*C*) **Corresponding** *xz*-**stress map of the top gel at the plane denoted by the white dashed line in (***B***). Dashed arrows denote direction of cell migration. Cell and nucleus positions are indicated by the white and black lines respectively. Scale bars represent 5 µm in the** *x*, *y* **and** *z* **directions.**
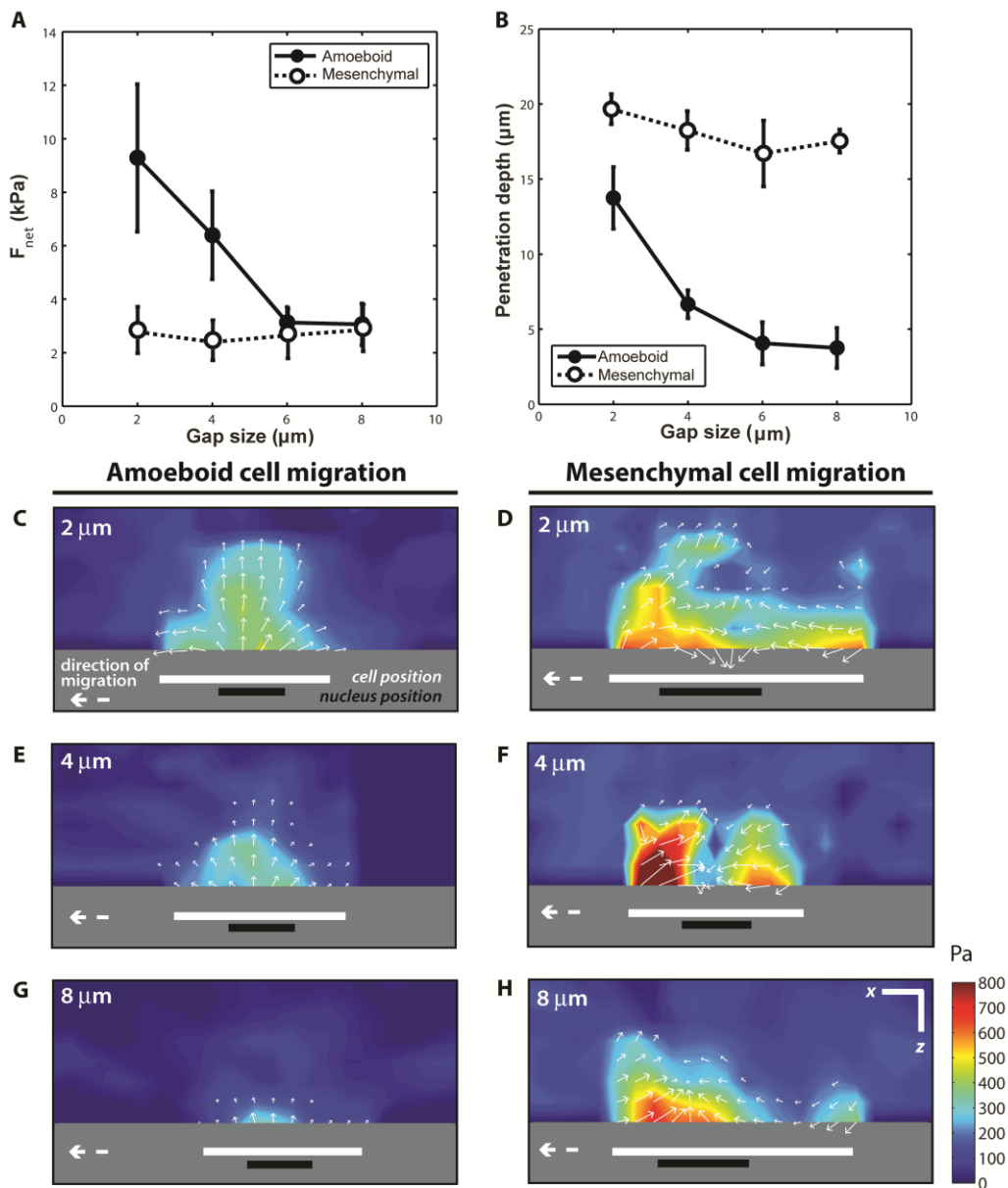
Figure 20 (*A*) **Magnitude of the vector sum of normal stresses (F_{net}) on the gels vs. gap size.** (*B*) **Penetration depth of cell imposed stresses on the gel vs. gap size. Error bars represent SE of the mean.** (*C-H*) **xz-stress map of the top gel for amoeboid** (*C, E, G*) **and mesenchymal** (*D, F, H*) **cells with varying gap sizes between the gels:** (*C-D*) **2 μm,** (*E-F*) **4 μm, and** (*G-H*) **8 μm. The gels have a Young's modulus of 1.25 kPa and cells were on non-fibronectin or fibronectin coated gels for amoeboid and mesenchymal cells respectively. Dashed arrows denote direction of cell migration. Cell and nucleus positions are indicated by the white and black lines respectively. Scale bars represent 5 μm in the *x*, *y* and *z* directions.**

101

3.3.5 Amoeboid cell migration speed is biphasic with respect to gap size and is fastest at an intermediate gap size

We also found that on non-fibronectin coated gels, cell migration speeds showed a biphasic relationship with gap size as speed peaks at an intermediate gap size of 6 µm (Figure 21*A solid squares*). However, on fibronectin coated gels, gap size did not significantly affect cell speeds (Figure 21*A open squares*). To verify that the dependence of cell speed on gap size on the non-fibronectin coated gels were indeed due to bleb formation, we added a myosin II inhibitor, blebbistatin, which prevents bleb formation but does not affect lamellipodia-driven migration (41,98). We observed that adding a concentration of 50 µM of blebbistatin slowed down cell migration by up to 80% on non-fibronectin coated gels (Figure 21*A*). In addition, blebbistatin removed any dependence of cell speed on gap size on non-fibronectin coated gels (Figure 21*A solid circles*), suggesting that the biphasic relationship of cell speed with gap size is predominantly due to bleb formation. In contrast, cell speed was not significantly changed with the addition of blebbistatin on fibronectin coated gels (Figure 21*A open circles*).
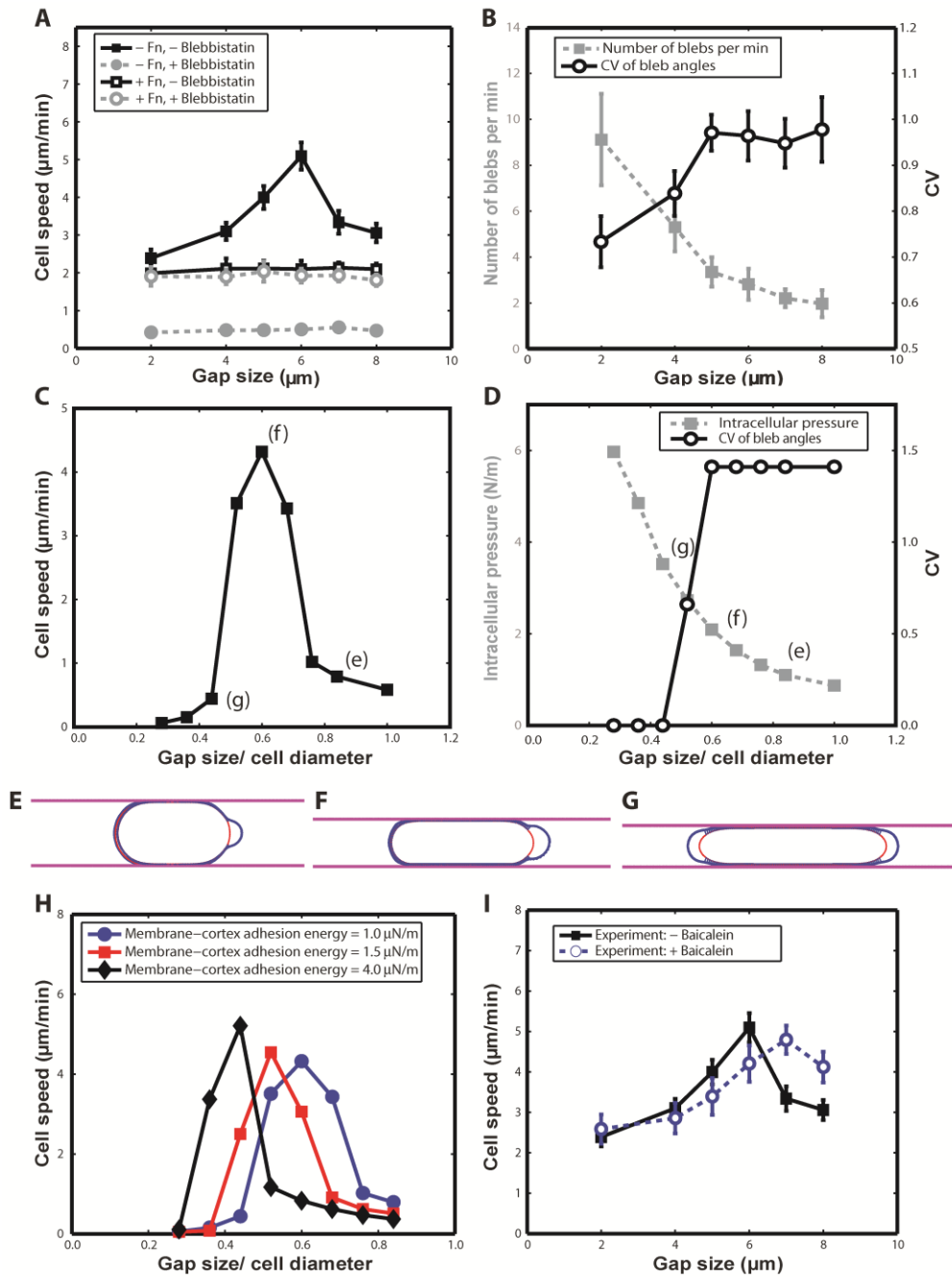
Figure 21 (*A-B*) **Experimental results:** (*A*) **Cell speed vs. gap size on non-fibronectin (*solid squares*) and fibronectin coated (*open squares*) gels with gel rigidity 16.63 kPa. Cell speed vs. gap size after addition of 50 µM blebbistatin, on non- fibronectin (*solid circles*) and fibronectin coated (*open circles*) gels with Young's modulus of 16.63 kPa. (*B*) Average number of blebs formed per minutes vs. gap size (*solid squares*), and mean CV of angles between neighboring blebs vs. gap size (*open circles*), of cells on non-fibronectin coated gels with rigidity of 16.63 kPa. Error bars represent SE of the mean. (*C-H*) Simulation results: (*C*) Cell speed vs. ratio of gap size and cell diameter (*G/D*). (*D*) Intracellular pressure vs. *G/D* (*solid squares*), and CV of angles between neighboring**

blebs vs. *G/D* (*open circles*). (*E-G*) Schematics of blebs formed by cells corresponding to points marked by (*e*) - (*g*) respectively, in graphs (*C-D*). (*E*) Cell in confinement produces a bleb at cell front. (*F*) As gap size decreases, intracellular pressure increases and bigger blebs are formed, leading to greater cell speed. (*G*) When intracellular pressure within the cell is too high, blebs are spontaneously formed at cell front and rear. This results in small net movement of the cell and slower cell speed. (*H*) Cell speed vs. *G/D* for various membrane cortex adhesion strengths used in simulation. (*I*) Experimental results: Cell speed vs. gap size for results in Figure 21A (*solid squares*) and after addition of 20 µM baicalein on non- fibronectin coated gel with Young's modulus of 16.63 kPa (*open circles*).

We then attempted to quantify the number and location of blebs produced by the dHL60 cells on non-fibronectin coated gels, and observed that cells produce more blebs at smaller gap sizes (Figure 21*B solid squares*). The larger number of blebs formed could have facilitated cell migration thus explaining the increase in cell speed as gap size decreased.

However, we also noticed that at extremely small gap sizes (2-4 µm), cells produced multiple blebs in opposing directions. As a measure of protrusion asymmetry, we quantified the CV of angles between neighboring blebs as described in the methods. A CV of 0 indicates protrusions are symmetrically distributed around the cell (symmetric protrusions), while larger CV values indicate bleb protrusions with increasing occurrence on a particular side of the cell (asymmetric protrusions). We found that the CV of angles between blebs decreased at small gap sizes (Figure 21*B open circles*), thus indicating that bleb formation were located less asymmetrically around the cell with decreasing gap size. As there were no asymmetric shape changes which will cause a cell to move in any particular direction, effective cell

104

migration could have been hindered, leading to a decrease in cell speed as gap size decreased beyond 6 µm.

3.3.6 Computational modeling reveals that intracellular pressure and membrane-cortex adhesion determine optimum gap size

To help us further understand the mechanisms involved in amoeboid migration, we used a computational model to investigate how formation of cellular blebs translates to movement in a confined environment.

When there was slight confinement (ratio of gap size to cell diameter (G/D) > 0.6), cell speeds increased as cells became more confined (Figure 21C). This may be attributed to the increase in intracellular pressure caused by the confinement (Figure 21D *solid squares*), leading to formation of a larger bleb (compare Figure 21E and F). In the case where there was extreme confinement (G/D < 0.6), cell speeds decreased as cells became more confined (Figure 21C). This is because the nucleation of a bleb at the cell front was insufficient to release the high intracellular pressure and blebs formed spontaneously at the cell rear, hence lowering the CV of the angles between blebs (Figure 21D *open circles*), and hindering directed cell movement (Figure 21G). These observations are in agreement with our experimental data (dHL60 cell diameter is approximately 10 µm).

Another model parameter which affected cell speed is the strength of membrane-cortex adhesion. We found that increasing membrane-cortex

linkers' strength in our model prevents blebs from forming at both ends of the cell under very small confinement. The stronger membrane-cortex linkers serve to tether the membrane to the cortex even when intracellular pressure is high, thus reducing bleb formation at the cell rear. The model predicts that the optimum gap size at which maximal migration speed occurs can be decreased or increased by strengthening or weakening membrane-cortex adhesion strength respectively (Figure 21*H*). This may be achieved experimentally, through altering the activity of ERM proteins.

To verify this model prediction, we added an inhibitor of ezrin, baicalein (20 μM) which has been reported to reduce ezrin RNA expression levels (137), to dHL60 cells for 24 hours, prior to image acquisition. We observed that treated cells generally produced blebs more frequently than untreated cells. Although cell speeds for treated cells were not significantly different at gap sizes between 2-5 μm, cell speed decreased at gap size of 6 μm, and increased at gap sizes of 7-8 μm, as compared to untreated cells (Figure 21*I*). The optimum gap size where cell speed peaked was also increased from 6 to 7 μm. This increase in the optimum gap size corresponds to the prediction from the computational model that optimum gap size increases with decreasing membrane-cortex adhesions.

3.4   Discussions

In recent years, amoeboid-like migration was observed in mammalian cells such as leukocytes, zebrafish PGCs and in some tumor cells (14,36-42) migrating in 3D environments. These cells were found to migrate using bleb-like protrusions which were initially devoid of F-actin (amoeboid cell migration). This type of motility is significantly different from that commonly exhibited by fibroblasts and keratocytes cultured on 2D gels where lamellipodia formation and integrin-mediated cell-substrate adhesion are often implicated during cell migration (mesenchymal cell migration) (14).

Amoeboid pseudopodium or bleb growth is proposed to be driven by hydrostatic pressure generated by myosin contraction which leads to a local weakening of the cell's membrane-cortex adhesion. Bleb formation is initiated when the cell membrane detaches from the actin cortex. The membrane subsequently expands as cytoplasmic fluid flows towards the site of membrane-cortex detachment due to the pressure difference between the intracellular pressure exerted by the actin cortex, and the lower pressure at the site of membrane-cortex detachment. This pressure driven bleb growth is not supported by an actin cytoskeleton initially, but an actin cortex subsequently reassemble under the cell membrane, leading to bleb retraction (43). However, how bleb formation translates to cell migration remains hypothetical due to a lack of quantitative experimental data.

3.4.1 Confined amoeboid cells migrating via chimneying requires an anchoring and a protrusive force

Charras and Paluch (43) hypothesized that for cells in confined environments (e.g. between two glass coverslips or in a thin micro-fluidic channel), the blebbing cell can migrate in the absence of receptor-ligand mediated cell–substrate adhesion as the cell exerts forces perpendicularly to the surfaces and squeezes itself forward. This observation was reported by Malawista et al. (52) as they observed that leukocytes with β2-integrin adhesion deficiency were able to migrate efficiently in confined environment, between two coverslips.

To explain their experimental observations, Malawista et al. (52) proposed a mechanism known as chimneying, where in the absence of cell-substrate adhesion, cells in confined environments press on opposing surfaces to generate forces for locomotion. Motivated by this hypothesis, we seek to validate, using 3D traction stress analysis, that amoeboid cells uses this chimneying mechanism during migration. To the best of our knowledge, we have shown for the first time, the 3D stresses imposed by the amoeboid cell on its surrounding in a confined environment and compared these stresses to that imposed by a mesenchymal cell.

Based on our 3D traction stress measurements, we proposed that the mechanism of chimneying, during amoeboid cell migration, comprises two

main components: namely forces to anchor the cell to the gels, and forces due to bleb protrusions (Figure 18*A* and Figure 22). Cells were found to exert large normal stresses (along the *z* axis) acting into the gel (Figure 18, $\vec{F}_{anchor}$). The magnitude of these stresses (approximately 200-400 Pa) corresponds to measurements of intracellular pressure reported elsewhere (138). This suggests that as the gel press onto cells in confinement, the cells react by producing an opposing stress on the gel due to the cell's intracellular pressure, which allows cells to anchor themselves between the two gels. Any protrusions (e.g. blebs) can then lead to a net translation of the cell in the absence of cell-substrate adhesion.

In addition to these anchoring stresses, we observed that the production of cellular blebs also generates shearing in-plane stresses (*xy*-plane) at the cell front, in the direction of the bleb protrusion (Figure 18*B-G*, $\vec{F}_{protrusion\,//}$). In some cases, we also observed that the bleb exert some normal stresses on the gels (Figure 18*G*, $\vec{F}_{protrusion\,\perp}$). We propose that this feature is important for cells to progressively move forward, as it allows the anchoring of the cell at the locations where the blebs were formed, while the cell rear retracts.

3.4.2 Tractional stresses exerted by amoeboid cells are distinct from that exerted by mesenchymal cells

In contrast, mesenchymal cells pushed and pulled on the gel at the cell front and cell rear during cell protrusion and retraction respectively (Figure

19*B-C*), similar to that reported by Franck et al. (80). It has been established that mesenchymal cells move via a five step migration cycle: actin-driven protrusion of the cell's leading edge; cell-matrix interaction via integrins and its ligands in ECM, and recruitment of adaptor and signaling proteins; recruitment of surface proteases to cleave ECM proteins; contraction of acto-myosin; and focal contact disassembly and detachment at the cell rear (14).

Our 3D stress maps revealed a similar dynamics as we observed that cells exert a contractile in-plane (*xy*-plane) stress on the gel to which cells adhered (Figure 19*B*, $\vec{F}_{protrusion\,/\!/}$ and $\vec{F}_{retraction\,/\!/}$). In addition, we noticed that as the cells protrude at the cell front, cells push into the gel, exerting normal stresses (along the *z*-axis) acting into the gel (Figure 19*C*, $\vec{F}_{protrusion\,\perp}$). On the other hand, as cells detach from the gel at the cell rear, cells pull on the gel, generating normal stresses acting out of the gel (Figure 20*C*, $\vec{F}_{retraction\,\perp}$).

These observations from the 3D stress analysis clearly showed that amoeboid and mesenchymal cells exert distinct mechanical stresses on the cell's surroundings during migration. These differences not only offer us a mechanistic understanding of the migration processes, it could also be a quantitative classification between mesenchymal and amoeboid migration. Very often, morphological differences such as cell shape and the presence of constriction rings are used to classify mesenchymal and amoeboid migration (35), which may be subjective. F-actin may also be labeled to determine if blebs or lamellipodia are formed, but the method would be challenging in cell-

types that are hard to transfect. In contrast, it could be easier to classify amoeboid and mesenchymal migration by looking at the nature of 3D traction stresses on the gels. Experimentally, it is easy to embed fluorescent beads to track gel displacements in both 2D and 3D matrices and many groups have published protocols detailing 2D and 3D traction stress analysis (62,64-66,71-80).

As a quantitative measure, we proposed that the magnitude of the vector sum of normal stresses exerted over the cell area (F_{net}) and the penetration depth of cell imposed stresses can aid in distinguishing amoeboid and mesenchymal cell migration quantitatively. Using our setup, at small gap sizes (2 μm), amoeboid cells exerted a larger F_{net} on the gel (approximately 9.2 kPa) than the mesenchymal cell (approximately 2.8 kPa) (Figure 20*A*). This is because in mesenchymal cells, the normal stresses due to protrusion and retraction of the cells are in opposing directions, resulting in a small value when the stresses are summed vectorially. In contrast, the normal stresses due to amoeboid cells during chimneying are always directed in the same direction, away from the cell body and pointing into the gels. This results in a larger F_{net} in amoeboid cells, as compared to that in the mensenchymal cells.

We also observed that in amoeboid cells, F_{net} and the penetration depth of the overall stress ($F_{x,y,z}$), decreased with increasing gap size between the two gels (Figure 20*C*, *E*, *G*). The decrease in F_{net} and penetration depth is likely due to the smaller contact area of the cell, and possibly a decreasing

intracellular pressure (as predicted by our computational model), when gap size increases. On the other hand, in mesenchymal cells, F_{net} and penetration depth remained constant with increasing gap size between the two gels (Figure 20*D*, *F*, *H*), as cells remain adhered to the gels regardless of gap size (Figure 22). These two measures (F_{net} and penetration depth) thus potentially offer us a quantitative classification for amoeboid and mesenchymal cells, particularly in identifying factors resulting in mesenchymal to amoeboid transitions.

3.4.3 Amoeboid and mesenchymal cell migration are influenced by different physical parameters of the ECM

Reviews of previous literatures have shown that the choice of migration mechanism employed by the cells may be influenced by physical cues in the ECM, such as ECM pore size, adhesiveness through binding of integrin receptors to ligand proteins in the ECM, and ECM rigidity (refer to Section 1.5). We hypothesize that amoeboid and mesenchymal migration could be independently regulated by different parameters in the ECM and cells may choose to employ a migratory mode which is most favorable to navigate the ECM. However, in 3D collagen matrices studies, it is not possible to study the independent effects of changing ECM stiffness from pore size and ligand concentration as changing one parameter, for example, collagen concentration, often cause a change in ECM rigidity and pore size as well (89). This problem was overcame by confining cells between 2 pieces of deformable polyacrylamide gels, thus allowing ECM rigidity, pore size (gap size between

the top and bottom gels) and ECM ligand concentration to be altered independently.

We have also studied how gap size and gel rigidity alter migration speeds of amoeboid and mesenchymal cells, through varying the distance between the two gels and the gel rigidity of our setup. Our results suggest that unlike mesenchymal cell migration, whose speeds show biphasic relationships with gel rigidity and ECM ligand concentrations (refer to Section 2.3.1), amoeboid cell migration speeds was maintained at a constant level regardless of gel rigidity (Figure 17*B*). Instead, amoeboid migration speed exhibits a biphasic relationship with gap size as migration speeds reached a maximal value at an intermediate gap size between the two gels (Figure 21*A*).

3.4.3.1   Mesenchymal cells sense gel rigidity and ECM adhesiveness

Mesenchymal cell migration is known to be influenced by cell-substrate adhesion. Many studies have shown that cell speed exhibits a biphasic dependence on ECM fibronectin concentration and gel rigidities during mesenchymal migration (refer to Section 2.3.1, and references 32,89,93,124). Previous reports have also demonstrated that increasing gel rigidity increases the area of individual focal adhesion. This indicates that cells alter their cell-substrate adhesion in response to ECM rigidity (refer to Section 2.3.3 and references 61,63-65,71,72). Mesenchymal cell migration is also known to involve a highly complicated signaling network which requires as

many as 160 distinct proteins related to the formation of focal adhesion and nearly 700 known interactions between different signaling components (29). Hence, our observations of lamellipodia formation on fibronectin coated gels and the dependence of mesenchymal cell speed with gel rigidity, further suggest that mesenchymal cell migration is likely to be regulated by mechanisms which influence integrin-mediated cell-substrate adhesiveness.

On the other hand, the independence of cell speed with cell-substrate adhesion and gel rigidity implied that integrin-mediated cell-substrate interactions are unlikely to play a crucial role in amoeboid migration mechanism. We propose that in the absence of cell-substrate adhesion, signaling proteins responsible for mesenchymal cell migration could not be recruited and dHL60s preferentially form blebs to explore its environment. Similarly, Bergert et al. reported that a suspension subline of Walker 256 carcinosarcoma cells were able to transit from bleb-like to lamellipodia-like protrusions when cultured on adhesive gels (54).

In addition, the authors also demonstrated that cells can switch from lamellipodia to bleb-based migration by either decreasing Arp2/3 mediated actin polymerization or increasing myosin activity. These suggest that mechanisms leading to bleb and lamellipodia formation are mutually exclusive. However, the molecular mechanism of amoeboid migration is not well understood other than the importance of myosin contractility (36,40,53) and ERM proteins which links the cell membrane to the actin cortex

(39,44,50,51). Further studies would be required to elucidate the molecular components of amoeboid cell migration.
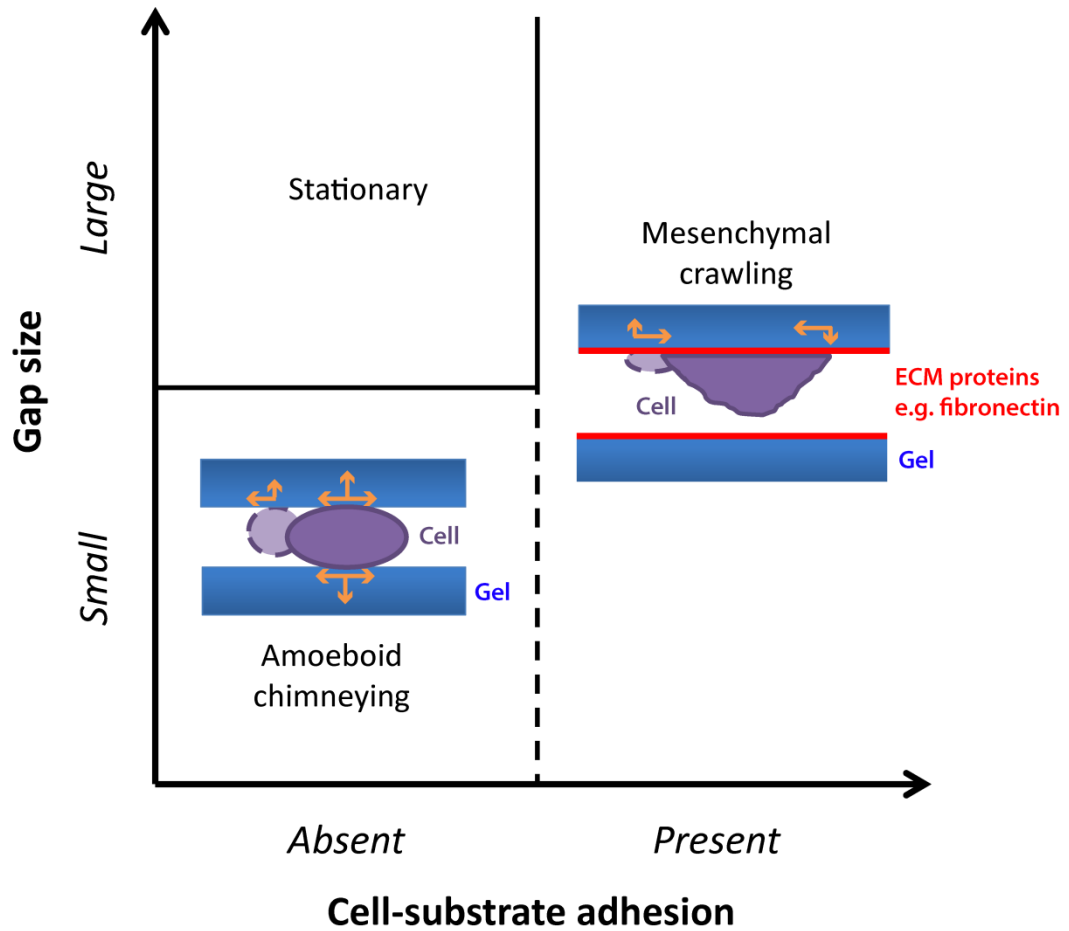
Figure 22 Phase diagram of cell phenotype as a function of gap size and cell-substrate adhesion. Arrows denote the direction of stresses which the cells impose on the gels.

3.4.3.2 Cells migrating with the amoeboid mode sense ECM pore size through changes in the cells' intracellular pressure

In addition, we were also able to see cell blebbing even when the dHL60s are in suspension, but these cells were not able to migrate effectively without pushing off a surface. In the presence of confinement, cells are now able to anchor themselves against the walls and translate blebbing into effective locomotion (Figure 22). We explained that decreasing gap size increases the number of blebs formed, while the asymmetric distribution of cellular protrusions reduced (Figure 21*B*). This explains the biphasic relationship between cell speed and gap size (Figure 21*A*) and were reproduced using the computational model which we have proposed (Figure 21*C-D*). From our model, we observed that gap size contributes to bleb formation by changing the intracellular pressure. Cells would feel a larger pressure exerted on itself as the gap sizes decreased, causing larger and more blebs to form, thus increasing migration speeds. At very small gap sizes however, the high intracellular pressure caused blebs to form at opposing ends, hence reducing cell migration speed.

In a separate study, Hawkins et al. (139) proposed a different mechanism to explain cell migration in narrow channels without specific adhesion proteins or myosin contraction. The cell was able to migrate in the model due to actin polymerization against the channel walls. Hawkins also predicted that myosin contraction only serves to speed up velocity of motion

by approximately two times but is not crucial to cell migration in the narrow channel. However we see that Hawkins' prediction does not apply in our case because in our experiments when cells are confined between two substrates, inhibiting myosin II contraction with blebbistatin reduces cell migration drastically by up to 80% in the absence of cell-substrate adhesion (Figure 21*A*). Hawkins' model also assumed actin polymerization at the cell front, which, we have shown is not the case in the amoeboid blebbing cells. We think Hawkins' model does not apply in describing amoeboid cell migration as what was observed in our experiments, but rather modeled a different type of cell migration in confined geometries.

3.4.4 Membrane-cortex adhesion provides a mechanism to sense intracellular pressure

Experimentally, our observations of increased blebbing frequency when gap size is decreased suggests that more membrane-cortex adhesions were broken. In our computational model, the larger intracellular pressure was found to drive the breakage of more membrane-cortex adhesions resulting in the formation of a larger bleb, as the gap size decreased (Figure 21*C-G*). Interestingly, the model predicts that when intracellular pressure exceeds a critical threshold when gap size becomes very small, the nucleation of a bleb at the front of the cell is insufficient to release the intracellular pressure and a bleb forms spontaneously at the rear of the cell. This is because membrane-cortex springs that mimics the cell membrane to the cell cortex adhesions are

stretched beyond their threshold lengths, resulting in their breakages and spontaneous formation of blebs. It is possible that a stronger membrane-cortex adhesion strength will tether the membrane to the cortex more strongly and discourage bleb formation, thereby changing the cell migration speed.

In fact, the model predicted that the gap size where migration speed peaks can be increased by decreasing the membrane-cortex adhesion strength as this adhesion strength determines the gap size where blebs begin to form at both ends of the cell. We have verified this prediction experimentally, by weakening the membrane-cortex adhesion strength by incubating cells for 24 hours in culture media containing baicalein which is an inhibitor of ezrin, one of the ERM proteins (137). We observed that the gap size where fastest migration speed occurs is increased, as predicted by the computational model.

Taken collectively, our results point to ERM proteins as a possible sensor of intracellular pressure in amoeboid cells. Amoeboid cells may also regulate their membrane-cortex adhesion strength to help a cell migrate directionally in confined environment.

In a separate study, Diz-Munoz et al. have demonstrated that zebrafish mesoderm-endoderm germ-layer progenitor cells which possess a dominant-negative ezrin domain are less directed than wild-type cells as these cells produced more blebs (39). The authors attributed this observation to the lower occurrence of lamellipodia and filopodia formation in these cells, which they proposed are responsible for the directionality of cell migration. We would

like to suggest that in addition to the change in the mode of migration, the loss in cell migration directionality when membrane-cortex adhesion strength is weakened could also be attributed to the loss of asymmetric bleb protrusions.

We propose that heightened ERM activity may play a beneficial role in cell migration by inhibiting the production of cellular blebs in opposing directions. Indeed, ezrin has been identified as a crucial molecule in the dissemination of two pediatric tumors (rhabdomyosarcoma and osteosarcoma) and has been found to be significantly over-expressed in pancreatic and breast cancer (140-143). However, research on the ERM proteins with regards to cancer progression thus far, has focused mainly on modulation of cell survival pathways due to ezrin signaling (144), and ezrin's role on cell migration particularly during cancer metastasis remains largely unknown. We hypothesize that by tethering the actin cortex more strongly to the cell membrane, over-expression of ezrin allows directional bleb protrusion thereby increasing directional migration and more efficient extravasation of cancer cells during metastasis. We predict that by inhibiting ERM activity, cells' ability to squeeze through narrow pores in the ECM in a directed manner, through amoeboid migration, will be significantly hampered, thereby providing a potential target for inhibiting cancer cell metastasis.

It is also possible that cells sense and react to cues in the ECM by redistributing the localization of ERM proteins responsible for membrane-cortex adhesions, hence allowing directed cell migration. External factors such

119

as chemoattractant may trigger biochemical signaling pathways within the cell to weaken membrane-cortex adhesions at the cell front by reducing ERM protein localization at the cell front, or enhancing ERM protein localization at the cell rear. This hypothesis is supported by a few studies which showed that erzin and moesin localize at the rear of amoeboid cells (50,51). However, the mechanisms of how ERM proteins are localized to the cell rear remains unknown and further experiments will be required to prove conclusively that ezrin localization at the cell rear is due to the cell's response to external factors such as chemoattractant or possibly changes in ECM porosity.

3.5 Conclusions

We have shown that neutrophils migrate using two distinct mechanisms of migration, by producing bleb-like protrusions and lamellipodia, the latter when cell-substrate adhesion are present. These two distinct mechanisms are termed amoeboid and mesenchymal cell migration respectively. We have shown that amoeboid cell migrate by pushing off the surface of the gel in contact with the cells, thus generating normal stresses which act into the gels, while blebs protrude at the cell front. Conversely, mesenchymal cells push and pull on the gels in contact during cell protrusion and retraction, generating normal stresses that point into and out of the gel respectively. Based on these differences in the 3D traction stress, we have

proposed quantitative measures which may be used to classify cells into the amoeboid or mesenchymal mode of migration.

We have also showed that the two modes of migration are regulated by different physical properties of the extracellular environment. Mesenchymal cell migration was found to be regulated by changes in gel rigidity, as cell speed showed a biphasic relationship with gel rigidity. On the other hand, changes in cell confinement affect amoeboid cell migration as cell speed showed a biphasic relationship with gap size. We propose that decreasing gap size increases the intracellular pressure (and hence number and size of blebs produced), and decreases the asymmetry of bleb protrusions, thus resulting in an intermediate optimum gap size through which cell migration is the fastest. The value of this optimum gap size can be increased by inhibiting membrane-cortex adhesion. Collectively, our results offer clear mechanistic insights regarding amoeboid migration, which is often implicated in cancer cell metastasis.

4   CONCLUSIONS AND FUTURE DIRECTIONS

4.1   Summary

In summary, the work presented in this thesis have provided a platform to improve our understanding of how mechanical cues present in the cell's ECM can influence the cell's migration strategy. I have shown that mesenchymal and amoeboid cells sense different physical parameters in their environment: Mesenchymal cell migration speed shows a biphasic relationship with the substrate adhesiveness and rigidity, while amoeboid cell migration speed shows a biphasic relationship with the degree of cell confinement.

I have shown that mesenchymal cell migration speed exhibits a biphasic relationship with cell-matrix adhesiveness and substrate rigidity. While larger cell traction force may allow cells to migrate faster with increasing substrate rigidities, cell migration at higher substrate rigidities where traction stresses saturates is likely slowed down by the larger mature focal adhesions formed. I have proposed that on soft substrates, mesenchymal cells are likely to sense substrate rigidities, through mechano-sensors related to actin stress fiber organization that allow cells to sense ECM strains, and bring about changes in the cell traction force. However, on stiffer substrates, mesenchymal cells are likely limited by the saturation of acto-myosin machinery responsible for cell contractility and hence cell traction forces. Although cell-matrix adhesions may also play an important role in

mesenchymal cell migration through signaling events triggered by formation of focal complexes and focal adhesions, traction force generation and maturation of focal adhesions in response to substrate rigidity seems to be independently regulated given the weak linear correlation between the two measurements.

On the other hand, I have showed that amoeboid cell migration speed is independent of ECM rigidity. The presence of cell-matrix adhesion also caused amoeboid cells to switch to using the mesenchymal mode of migration. This is likely due to the activation of signaling pathways involved in mesenchymal migration, initiated by the formation of cell-substrate adhesions.

Instead of sensing ECM rigidity and adhesiveness, I have shown that amoeboid cells sense the degree of cell confinement via changes in their intracellular pressure and possibly through proteins involved in regulating the cell membrane to actin cortex adhesion strength. I have also shown that the strength of membrane-cortex adhesions may determine the polarization of bleb formation and directionality of migration. It is possible that cells respond to cues in the ECM by redistributing the localization of ERM proteins responsible for membrane-cortex adhesions, hence allowing directed cell migration.

By sensing different parameters in the cell's mechanical environment, the cell can then choose the most favorable mode of migration depending on the conditions of the ECM. However, before the molecular mechanism can be

elucidated, it is important for researchers to be able to quantitatively distinguish between the two modes of migration. Classification of mesenchymal and amoeboid cell migration cannot remain vague and qualitative. In view of this, I have shown that 3D traction force microscopy can help to quantitatively distinguish between mesenchymal and amoeboid cell migration as the two distinct mechanisms produce different stresses on the ECM. In the amoeboid mode, cells migrate via a chimneying mechanism by generating anchoring stresses normal to the confining gels, and shearing stresses at bleb protrusions. Bleb growth shifted the anchoring stress forward resulting in cell movement. On the other hand, cells in the mesenchymal mode generated contractile, opposing shearing stresses at the cell front and rear during protrusion and retraction, respectively. These traction stress differences allowed me to quantitatively distinguish between the two migratory modes, with potential applications to high throughput studies to elucidate the molecular components involved during MAT in cancer cell metastasis. Collectively, the results and tools for quantitative analysis presented in this thesis can contribute towards understanding the complex mechanisms behind the regulation of cell migration strategies

4.2   Future works

Although the work in this thesis offers us a mechanistic insight into the cell's migratory responses to mechanical factors present in the ECM, many questions remain to be answered by future studies.

4.2.1 Elucidating the mechano-sensor in mesenchymal cell migration

For instance, although I have demonstrated that mesenchymal cells respond to increasing substrate rigidity by conserving strains on soft substrates and stress on stiffer substrates, the identity of the mechano-sensor remains elusive.

Past studies have suggested that the acto-myosin machinery is crucial in determining stress fiber organization on soft substrates and becomes limiting on stiffer substrates. It would therefore be interesting to investigate if an increase in the acto-myosin stall force can increase the value of the substrate rigidity where the transition from strain-limited to stress-limited cellular response, occurs. This may be done possibly through overexpressing proteins implicated in the acto-myosin machinery in the cell, such as myosin IIb.

Kobayashi and Sokabe have also proposed that different mechano-sensitive ion channels located at or near focal adhesions could be possible sensor of substrate rigidity (85). These ion channels may form a molecular complex with stress fibers and focal adhesions to control the level of cytoplasmic Ca^{2+}, which in turn can phosphorylate myosin light chain kinase, induce acto-myosin contractility or activate further cell signaling events.

In addition to these mechano-sensitive ion channels, non-channel type mechano-sensors have also been associated with cell mechano-sensing

mechanisms. For example, many studies have shown that actin stress fiber organization in cells is crucial for the cells to sense and respond to substrate rigidity (refer to Section 2.4.3). It seems probable that the mechano-sensors are associated with stress fiber organization as cells were found to reorganize their actin cytoskeleton to sustain substrate strains, and transmit traction forces generated by the cell's acto-myosin motors to the ECM. Hayakawa et al. proposed that tension in the actin stress fibers reduces cofilin binding which in turn prevents the stress fibers disassembly through the severing action of cofilin (147). However, this hypothesis is mainly based on in vitro studies.

Focal adhesion proteins such as talin and p130Cas have also been proposed to act as mechano-sensors, through the mechanical unfolding of these proteins which allows tyrosine phosphorylation and activation of the signaling pathways involved in cell mechano-sensing (146).

Although many mechano-sensors have been proposed, the research community has not sufficiently established the mechanism which cells use in sensing mechanical factors in the ECM. I propose that the identity of these proposed mechano-sensors can be further proven through the application of traction force analysis as applied in this thesis work. By analyzing the substrate strains in the presence or absence of these possible mechano-sensors, we can study the conditions in which substrate strains are conserved and arrive at a possible mechano-sensing mechanism.

4.2.2   Elucidating the molecular mechanism of amoeboid cell migration

Another important future work would also include elucidating the molecular mechanism involved in amoeboid cell migration. The molecular requirements for amoeboid migration is not well understood other than the importance of myosin II contractility mediated by ROCK and RhoA (reviewed in Section 1.5.2), and the ERM proteins which are responsible for cell membrane to actin cortex adhesions (reviewed in Section 1.4.3). Whether and how an amoeboid cell alter its contractility or ERM protein localization in response to a chemoattractant or mechanical perturbations in the ECM remains to be answered by future experiments.

In addition, the question on whether myosin II contractility is coupled to ERM protein localization to produce blebs polarized in a particular direction in response to chemo-attractants or ECM cues present in the external environment remains elusive. Amoeboid cells seemed to produce localized myosin II contractions at the cell front where bleb forms (40), while ezrin is localized at the cell rear (50,51). Whether these observations are merely coincidences or born out of an inherent cross-talk between signaling pathways involved in myosin II contractility and ezrin localization could be further investigated.

Plasma membrane tension has also been shown to reduce when the cell membrane detaches from the actin cortex during bleb expansion, while

membrane tension increases when the actin cortex reforms underneath the bleb during bleb retraction (151). This suggests that decrease in membrane tension could play a role in cortex reformation through the recruitment of proteins to the plasma membrane to physically link the plasma membrane to the cell cytoskeleton (149). How cells sense the decrease in membrane tension during bleb protrusion, and what proteins are being recruited to the membrane during bleb protrusion can help us better understand the molecular requirements for amoeboid cell motility.

Interestingly, increased membrane tension has also been associated with increased motility during mesenchymal cell migration by enhancing lamellipodia formation (148-150). It will be interesting to study the differences in membrane tension regulation during amoeboid and mesenchymal cell migration and whether these differences can trigger distinct signaling pathways which cause the cells to migrate using either the amoeboid or mesenchymal mode of migration.

4.2.3 Elucidating the requirements for MAT

One of the fundamental reasons of understanding mesenchymal and amoeboid migration is to enhance our understanding of cancer cell metastasis and propose possible drug targets to inhibit cancer cell metastasis. This can only be possible if the interplay between ECM factors, and signaling pathways leading to the different cell migration strategies, are known.

Currently, it is known that a tight interplay between Rho and Rac signaling is important in determining the different strategies tumor cell employ during cell migration. Sanz-Moreno et al. have demonstrated in melanoma cells that mesenchymal cell migration is driven by activation of Rac which directs mesenchymal movement (152). Rac was also shown to suppress amoeboid movement by reducing acto-myosin contractility. On the other hand, during amoeboid cell migration, it was shown that increased ROCK signaling activates a Rac GTPase-activating protein which suppressed mesenchymal cell migration by inactivating Rac.

However, how external factors in the cell's ECM, particularly factors such as ECM rigidity, adhesiveness, and pore size, can translate to molecular signals leading to the activation of one pathway and the inactivation of another remains to be answered by future studies. This interplay between the cell's ECM and the migration strategies is important as it has been shown that during cancer progressions, abnormal changes occur in the biochemical and biomechanical properties of the ECM which could potentially deregulate the cell's behavior during malignant transformation (154). For example, it has been reported that breast cancer tissues can be 10 times more rigid than the normal breast tissues (153). The stiffer tissues were also shown to promote tumor cell invasion and progression (153). The ECM architecture, for example collagen fibrils, in cancerous tissues are also found to be highly orientated, which is fundamentally different from that in the normal tissue stroma which

consist of relaxed non-oriented fibrils (154). Knowledge of how these changes

in the ECM can lead to changes in cell migration strategies will benefit the

research community by aiding in the design of anti-metastatic drugs.

BIBLIOGRAPHY

1. Chicurel, M. 2002. Cell migration research is on the move. *Science*. 295:606-609.

2. Jeon, K. W. 1973. The Biology of Amoeba. Academic Press, New York, USA.

3. Allen, R. D. 1981. Motility. *J. Cell Biol*. 91:148-155.

4. Allen, R. D., N. Kamiya. 1964. Primitive Motile Systems in Cell Biology. Academic Press, New York, USA.

5. Nobelprize.org. Ilya Mechnikov - Nobel Lecture: On the Present State of the Question of Immunity in Infectious Diseases. http://www.nobelprize.org/nobel_prizes/medicine/laureates/1908/mechnikov-lecture.html. Accessed on 12 Feb, 2013.

6. Keller, R. 2005. Cell migration during gastrulation. *Curr. Opin. Cell Biol*. 17:533-41.

7. Keller, R. 2002. Shaping the Vertebrate Body Plan by Polarized Embryonic Cell Movements. *Science*. 298:1950-1954.

8. Weiser, D. C., U. J. Pyati, an D. Kimelman. 2007. Gravin regulates mesodermal cell behavior changes required for axis elongation during zebrafish gastrulation. *Genes and Dev*. 21:1559-1571.

9. Shaw, T. J., and P. Martin. 2009. Wound repair at a glance. J. Cell Sci. 122:3209-3213.

10. Singer, A. J., and R. A. F. Clark. 1999. Cutaneous wound healing. N. Engl. J. Med. 341:738-746.

11. Friedl, P., and B. Weigelin. Interstitial leukocyte migration and immune function. 2008. *Nature Immunol*. 9:960-969.

12. Anderson, A. O., and N. D. Anderson. 1976. Lymphocyte emigration from high endothelial venules in rat lymph nodes. *Immunology*. 31:731-48.

13. Friedl, P., and D. Gilmour. 2009. Collective cell migration in morphogenesis, regeneration and cancer. *Nat. Rev. Mol. Cell Bio.* 10: 445-457.

14. Friedl, P., and K. Wolf. 2003. Tumour-cell invasion and migration: diversity and escape mechanisms. *Nat. Rev. Cancer.* 3:362-374.

15. Boyle, P. and B. Levin. 2008. World Cancer Report 2008. International Agency for Research on Cancer.

16. Suresh, S. 2007. Biomechanics and biophysics of cancer cells. *Acta Biomater*. 3:413-438.

17. Abercrombie, M., and J. E. Heaysman. 1953. Observations on the social behaviour of cells in tissue culture. I. Speed of movement of chick heart fibroblasts in relation to their mutual contacts. *Exp. Cell. Res*. 5:111-131.

18. Abercrombie, M., J. E. Heaysman, and S. M. Pegrum. 1970. The locomotion of fibroblasts in culture. I. Movements of the leading edge. *Exp. Cell Res*. 59:393-398.

19. Abercrombie, M., J. E. Heaysman, and S. M. Pegrum. 1970. The locomotion of fibroblasts in culture. II. "Ruffling". *Exp. Cell Res*. 60:437-444.

20. Abercrombie, M., J. E. Heaysman and S. M. Pegrum. 1970. The locomotion of fibroblasts in culture. III. Movements of particles on the dorsal surface of the leading lamella. *Exp. Cell Res*. 62:389-398.

21. Abercrombie, M., J. E. Heaysman and S. M. Pegrum. 1971. The locomotion of fibroblasts in culture. IV. Electron microscopy of the leading lamella. *Exp. Cell Res*. 67:359-367.

22. Giannone, G., B. J. Dubin-Thaler, O. Rossier, Y. Cai, O. Chaga, G. Jiang, W. Beaver, H.-G. Dobereiner, Y. Freund, G. Borisy, and M. P. Sheetz. 2007. Lamellipodial actin mechanically links myosin activity with adhesion-site formation. *Cell*. 128:561-575.

23. Pollard, T. D., G. G. Borisy. 2003. Cellular motility driven by assembly and disassembly of actin filaments. *Cell*. 112:453-465.

24. Mattila, P. K., and P. Lappalainen. 2008. Filopodia: molecular architecture and cellular functions. *Nat. Rev. Mol. Cell Biol.* 9:446-454.

25. Davenport, R. W., P. Dou, V. Rehder, and S. B. Kater. 1993. A sensory role for neuronal growth cone filopodia. *Nature*. 361:721-724.

26. Murphy, D. A., and S. A. Courtneidge. 2011. The 'ins' and 'outs' of podosomes and invadopodia: characteristics, formation and function. *Nat. Rev. Mol. Cell Biol.* 12:413-26.

27. Clainche, C. L., and M.-F. Carlier. 2008. Regulation of actin assembly associated with protrusion and adhesion in cell migration. *Physiol. Rev.* 88:489-513.

28. Yilmaz, M., and G. Christofori. 2009. EMT, the cytoskeleton, and cancer cell invasion. *Cancer Metast. Rev*. 28:15-33.

29. Geiger, B., J. P. Spatz, and A. D. Bershadsky. 2009. Environmental sensing through focal adhesion. *Mol. Cell Biol.* 10:21-33.

30. Zaidel-Bar, R., C. Ballestrem, Z. Kam, and B. Geiger. 2003. Early molecular events in the assembly of matrix adhesion at the leading edge of migrating cells. *J. Cell. Sci*. 116:4605-4613.

31. Zaidel-Bar, R., M. Cohen, L. Addadi, and B. Geiger. 2004. Hierarchical assembly of cell-matrix adhesion complexes. *Biochem. Soc. T*. 32:416-420.

32. Palecek, S. P., J. C. Loftus, M. H. Ginsberg, D. A. Lauffenburger, and A. F. Horwitz. 1997. Integrin-ligand binding properties govern cell migration speed through cell-substratum adhesiveness. *Nature* 385:537-540.

33. Palecek, S. P., A. F. Horwitz, and D. A. Lauffenburger. 1999. Kinetic model for integrin-mediated adhesion release during cell migration. *Ann Biomed Eng.* 27:219-235.

34. Palecek, S. P., C. E. Schmidt, D. A. Lauffenburger, and A. F. Horwitz. 1996. Integrin dynamics on the tail region of migrating fibroblasts. *J. Cell Sci*. 109:941-952.

35. Wolf, K., I. Mazo, H. Leung, K. Engelke, U. H. von Andrian, E. I. Deryugina, A. Y. Strongin, E. B. Bröcker, and P. Friedl. 2003. Compensation mechanism in tumor cell migration: mesenchymal– amoeboid transition after blocking of pericellular proteolysis. *J. Cell Biol.* 160:267-277.

36. Pinner, S., and E. Sahai. 2008. Imaging amoeboid cancer cell motility in vivo. *J. Microsc.* 231:441-445.

37. Lammermann, T., B. L. Bader, S. J. Monkley, T. Worbs, R. Wedlich-Soldner, K. Hirsch, M. Keller, R. Forster, D. R. Critchley, R. Fassler, and M. Sixt. 2008. Rapid leukocyte migration by integrin independent flowing and squeezing. *Nature.* 453:51-55.

38. Wolf, K., R. Müller, S. Borgmann, E.-B. Bröcker, and P. Friedl. 2003. Amoeboid shape change and contact guidance: T-lymphocyte crawling through fibrillar collagen is independent of matrix remodeling by MMPs and other proteases. *Blood*. 102:3262-3269.

39. Diz-Munoz, A., M. Krieg, M. Bergert, I. Ibarlucea-Benitez, D. J. Muller, E. Paluch, and C. P. Heisenberg. 2010. Control of directed cell migration in vivo by membrane-to-cortex attachment. *PLoS Biol.* 8:e1000544.

40. Blaser, H., M. Reichman-Fried, I. Castanon, K. Dumstrei, F. L. Marlow, K. Kawakami, L. Solnica-Krezel, C. Heisenberg, and E. Raz. 2006. Migration of zebrafish primordial germ cells: A role for myosin contraction and cytoplasmic flow. *Dev. Cell.* 11:613-627.

41. Jacobelli, J., F. C. Bennett, P. Pandurangi, A. J. Tooley, and M. F. Krummel. 2009. Myosin-IIA and ICAM-1 regulate the interchange between two distinct modes of T cell migration. *J. Immunol.* 182:2041-2050.

42. Lammermann, T., and M. Sixt. 2009. Mechanical modes of 'amoeboid' cell migration. *Curr. Opin. Cell Biol.* 21:636–644.

43. Charras, G., and E. Paluch. 2008. Blebs lead the way: how to migrate without lamellipodia. *Nat. Rev. Mol. Cell Biol.* 9:730-736.

44. Charras, G. T., M. Coughlin, T. J. Mitchison, and L. Mahadevan. 2008. Life and times of a cellular bleb. *Biophys. J.* 94:1836-1853.

45. Allen, R. D., and N. S. Allen. 1978. Cytoplasmic streaming in amoeboid movement. *Annu. Rev. Biophys & Bioeng.* 7:469-495.

46. Bruyn, P. 1947. Theories of Amoeboid Movement. *Q. Rev. Biol.* 22:1-24.

47. Mast, S. O. 1926. Structure, movement, locomotion, and stimulation in amoeba. *J. Morphol. Physiol.* 41:347-425.

48. Taylor, D. L., M. Fechheimer, and D. M. Shotton. 1982. Cytoplasmic structure and contractility: The solation-contraction coupling hypothesis [and discussion]. *Philos. Trans. R. Soc. Lond. B. Biol. Sci.* 299:185-197.

49. Odell, G. M., and H. L. Frisch. 1975. A continumn theory of the mechanics of amoeboid pseudopodium extension. *J. Theor. Biol.* 50:59-86.

50. Rossy, J., M. C. Gutjahr, N. Blaser, D. Schlicht, and V. 2007. Niggli. Ezrin/moesin in motile Walker 256 carcinosarcoma cells: signal-

dependent relocalization and role in migration. *Exp. Cell Res.* 313:1106-1120.

51. Lorentzen, A., J. Bamber, A. Sadok, I. Elson-Schwab, and C. J. Marshall. 2010. An ezrin-rich, rigid uropod-like structure directs movement of amoeboid blebbing cells. *J. Cell Sci.* 124:1256-1267.

52. Malawista, S. E., A. B. Chevance, and L. A. Boxer. 2000. Random locomotion and chemotaxis of human blood polymorphonuclear leukocytes from a patient with leukocyte adhesion deficiency-1: normal displacement in close quarters via chimneying. *Cell Motil. Cytoskel.* 46:183-189.

53. Sahai, E., and C. J. Marshall. 2003. Differeing modes of tumour cell invasion have distinct requirements for Rho/ROCK signalling and extraceelular proteolysis. *Nat. Cell Biol*. 5:711-720.

54. Bergert, M., S. D. Chandradoss, R. A. Desai, and Ewa Paluch. 2012. Cell mechanics control rapid transitions between blebs and lamellipodia during migration. *Proc. Natl. Acad. Sci. USA*. 109:14434-14439.

55. Engler, A. J., S. Sen, H. L. Sweeney, and D. E. Discher. 2006. Matrix Elasticity Directs Stem Cell Lineage Specification. *Cell.* 126:677–689.

56. Tang, X., Q. Wen, T. B. Kuhlenschmidt, M. S. Kuhlenschmidt, P. A. Janmey, and T. A. Saif. 2012. Attenuation of cell mechanosensitivity in colon cancer cells during in vitro metastasis. *PLoS One*. 7:e50443.

57. Tang, X., T. B. Kuhlenschmidt, J. Zhou, P. Bell, F. Wang, M. S. Kulenschmidt, and T. A. Saif. 2010. Mechanical force affects expression

of an in vitro metastasis-like phenotype in HCT-8 cells. *Biophys. J.* 99:2460-2469.

58. Harris, A. K., P. Wild, and D. Stopak. 1980. Silicone rubber substrata: A new wrinkle in the study of cell locomotion. *Science*. 208:177-179.

59. Lee, J., M. Leonard, T. Oliver, A. Ishihara, and K. Jacobson. 1994. Traction forces generated by locomoting keratocytes. *J. Cell Biol.* 127:1957-1964.

60. Wang, J. H.-C., J.-S. Lin,and Z.-C. Yang. 2007. Cell traction force microscopy. *In* Advanced Bioimaging Technologies in Assessment of the Quality of Bone and Scaffold Materials Techniques and Applications, L. Qin, H. K. Genant, J. Griffith, and K.-S. Leung, editors, Springer, 227-235.

61. Pelham, R. J., and Y-L. Wang. 1997. Cell locomotion and focal adhesion are regulated by substrate flexibility. *Proc. Natl. Acad. Sci. USA*. 94:13661–13665.

62. Dembo, M., and Y-L. Wang. 1999. Stresses at the cell-to-substrate interface during locomotion of fibroblasts. *Biophys J.* 76:2307–2316.

63. Discher, D. E., P. Janmey, and Y-L. Wang. 2005. Tissue cells feel and respond to the stiffness of their substrate. *Science.* 310:1139–1143.

64. Guo, W. H., M. T. Frey, N. A. Burnham, and Y-L. Wang. 2006. Substrate rigidity regulates the formation and maintenance of tissues. *Biophys. J.* 90:2213–2220.

65. Lo, C. M., H. B. Wang, M. Dembo, and Y-L. Wang. 2000. Cell movement is guided by the rigidity of the substrate. *Biophys. J.* 79:144 – 152.

66. Oakes, P. W., D. C. Patel, N. A. Morin, D. P. Zietterbart, B. Fabry, J. S. Reichner, and J. X. Tang. 2009. Neutrophil morphology and migration are affected by substrate elasticity. *Blood.* 114:1387–1395.

67. Delanoë-Ayari, H., S. Iwaya, Y. T. Maeda, J. Inose, C. Rivière, M. Sano, and J.-P. Rieu. 2008. Changes in the Magnitude and Distribution of Forces at Different Dictyostelium Developmental Stages. *Cell Motil. Cytoskeleton.* 65:314–331.

68. Stricker, J., Y. Aratyn-Schaus, P. W. Oakes, M. L. Gardel. 2011. Spatiotemporal constraints on the force-dependent growth of focal adhesion. *Biophys. J.* 100:2883–2893.

69. Ghibaudo, M., A. Saez, L. Trichet, A. Xayaphoummine, J. Browaeys, P. Silberzan, A. Buguinb, and B. Ladoux. 2008. Traction forces and rigidity sensing regulate cell functions. *Soft Matter.* 4:1836–1843.

70. Trichet L., J. L. Digabel, R. J. Hawkins, S. R. K. Vedula, M. Gupta, C. Ribrault, P Hersen, R Voituriez, and B. Ladoux. 2012. Evidence of a large-scale mechanosensing mechanism for cellular adaptation to substrate stiffness. *Proc. Natl. Acad. Sci. USA.* 109:6933–6938.

71. Califano, J. P., and C. A. Reinhart-King. 2010. Substrate stiffness and cell area predict cellular traction stresses in single cells and cells in contact. *Cell. Mol. Bioeng.* 3:68–75.

72. Prager-Khoutorsky, M., A. Lichtenstein, R. Krishnan, K. Rajendran, A. Mayo, Z. Kam, B. Geiger, and A. D. Bershadsky. 2011. Fibroblast polarization is a matrix-rigidity-dependent process controlled by focal adhesion mechanosensing. *Nat. Cell Biol.* 13:1457–1466.

73. Balaban, N.Q., U. S. Schwarz, D. Riveline, P. Goichberg, G. Tzur, I. Sabanay, D. Mahalu, S. Safran, A. Bershadsky, L. Addadi, and B. Geiger. 2001. Force and focal adhesion assembly: a close relationship studied using elastic micropatterned substrates. *Nat. Cell Biol.* 3:466–72.

74. Koch, T. M., S. Munster, N. Bonakdar, J. P. Butler, and B. Fabry. 2012. 3D Traction Forces in Cancer Cell Invasion. *PLoS One.* 7:e33476.

75. Hur, S. S., Y. Zhao, Y.-S. Li, E. Botvinick, and S. Chien. 2009. Live Cells Exert 3-Dimensional Traction Forces on Their Substrata. *Cell. Mol. Bioeng.* 2:425-436.

76. Legant, W. R., J. S. Miller, B. L. Blakely, D. M. Cohen, G. M. Genin, and C. S. Chen. 2010. Measurement of mechanical tractions exerted by cells in three-dimensional matrices. *Nat. Methods.* 7:969-973.

77. Legant, W. R. C. K. Choi, J. S. Miller, L. Shao, L. Gao, E. Betzig, and C. S. Chen. 2013. Multidimensional traction force microscopy reveals out-of-plane rotational moments about focal adhesions. *Proc. Natl. Acad. Sci. USA.* 110:881-886.

78. Maskarinec, S. A., C. Franck, D. A. Tirell, and G. Ravichandran. 2009. Quantifying cellular traction forces in three dimensions. *Proc. Natl. Acad. Sci. USA.* 106:22108- 22113.

79. Franck, C., S. Hong, S. A. Maskarinec, D. A. Tirell, and G. Ravichandran. 2007. Three-dimensional full-field measurements of large deformations in soft materials using confocal microscopy and digital volume correlation. *Exp. Mech.* 47:427-438.

80. Franck, C., S. A. Maskarinec, D. A. Tirrell, and G. Ravichandran. 2011. Three-dimensional traction force microscopy: a new tool for quantifying cell-matrix interactions. *PLoS One*. 6: e17833.

81. Walcott S., and S. X. Sun. 2010. A mechanical model of actin stress fiber formation and substrate elasticity sensing in adherent cells. *Proc. Natl. Acad. Sci. USA*. 107:7757–7762.

82. Zemel A., F. Rehfeldt, A. E. X. Brown, D. E. Discher, and S.A. Safran. 2010. Optimal matrix rigidity for stress-fibre polarization in stem cells. *Nat. Phys.* 6: 468–473.

83. Nicolas A., and S. A. Safran. 2006. Limitation of cell adhesion by the elasticity of the extracellular matrix. *Biophys. J.* 91:61–73.

84. Nicolas A., A. Besser, and S. A. Safran. 2008. Dynamics of cellular focal adhesion on deformable substrates: Consequences for cell force microscopy. *Biophys. J.* 95:527–539.

85. Kobanyashi T., M. Sokabe. 2010. Sensing substrate rigidity by mechanosensitive ion channels with stress fibers and focal adhesion. *Curr. Opin. Cell Biol.* 22: 669–676.

86. De R., A. Zemel, and S. A. Safran. 2008. Do cells sense stress or strain? Measurement of cellular orientation can provide a clue. *Biophys. J.* 94:L29–L31.

87. Freyman, T. M., I. V. Yannas, R. Yokoo, and L. J. Gibson. 2002. Fibroblast contractile force is independent of the stiffness which resist the contractions. *Exp. Cell Res*. 272:153–162.

88. Saez, A., A. Buguin, P. Silberzan, and B. Ladoux. 2005. Is the mechanical activity of epithelial cells controlled by deformations or forces? *Biophys. J.* 86:L52–L54.

89. Zaman, M. H., R. D. Kamm, P. Matsudaira, and D. A. Lauffenburger. 2005. Computational model for cell migration in 3D matrices. *Biophys. J.* 89:1389 – 1397.

90. Dokukina, I. V., and M. E. Gracheva. 2010. A model of fibroblast motility on substrates with different rigidities. *Biophys. J.* 98:2794–2803.

91. Pless, D. D., Y. C. Lee, S. Roseman, and R. L. Schnaar. 1983. Specific cell adhesion to immobilized glycoproteins demonstrated using new reagents for protein and glycoprotein immobilization. *J. Biol. Chem.* 258: 2340–2349.

92. DiMilla, P.A., K. Barbee, and D. A. Lauffenburger. 1991. Mathematical model for the effects of adhesion and mechanics on cell migration speed. *Biophys. J.* 60:15-37.

93. Peyton, S. R., and A. J. Putnam. 2005. Extracellular matrix rigidity governs smooth muscle cell motility in a biphasic fashion. *J. Cell. Physiol.* 204:198-209.

94. Kandow, C. E., P. C. Georges, P.A. Janmey, and K. A. Beningo. 2007. Polyacrylamide Hydrogels for Cell Mechanics: Steps Toward Optimization and Alternative Uses. *Methods Cell Biol.* 83:29–46.

95. Landau, L. D., and E. M. Lifshitz. 1986. Theory of Elasticity, 3rd ed. J. B. Sykes, and W. H. Reid, translators. Pergamon Press, Oxford, UK.

96. Araki, K., K. Kawauchi, and N. Tanaka. 2008. IKK/NF-kB signaling pathway inhibits cell cycle progression via a novel Rb-independent suppression system for E2F transcription factors. *Oncogene.* 112:5878–5884.

97. Katz, B.-Z., E. Zamir, A. Bershadsky, Z. Kam, K. M. Yamada, and B. Geiger. 2000. Physical state of the extracellular matrix regulates the structure and molecular composition of cell-matrix adhesion. *Mol Biol Cell.* 11:1047–1060.

98. Beningo, K. A., K. Hamao, M. Dembo, Y-L. Wang, and H. Hosoya. 2006. Traction forces of fibroblasts are regulated by the Rho-dependent kinase but not by the myosin light chain kinase. *Arch. Biochem. Biophys.* 456:224–231.

99. Dembo, M., T. Oliver, A. Ishihara, and K. Jacobson. Imaging the traction stresses exerted by locomoting cells with the elastic substratum method. *Biophys. J.* 70:2008–2022.

100. Butler, J. P., I. M. Tolic-Nørrelykke, B. Fabry, and J. J. Fredberg. 2002. Traction fields, moments, and strain energy that cells exert on their surroundings. *Am. J. Physiol. Cell Physiol.* 282:C595–605.

101. Maskarinec, S. A., C. Franck, D. A. Tirell, and G. Ravichandran. 2009. Quantifying cellular traction forces in three dimensions. *Proc. Natl. Acad. Sci. USA.* 106:22108–22113.

102. Franck, C., S. Hong, S. A. Maskarinec, D. A. Tirell, and G. Ravichandran. 2007. Three-dimensional full-field measurements of large deformations in soft materials using confocal microscopy and digital volume correlation. *Exp. Mech.* 47:427–438.

103. Pankov, R., E. Cukierman, B. Katz, K. Matsumoto, D. C. Lin, S. Lin, C. Hahn, and K. M. Yamada. 2000. Integrin Dynamics and Matrix Assembly: Tensin-dependent Translocation of a5b1 Integrins Promotes Early Fibronectin Fibrillogenesis. *J. Cell Biol.* 148:1075–1090.

104. Avnur, Z., and B. Geiger. 1981. The Removal of Extracellular Fibronectin from Areas of Cell-Substrate Contact. *Cell.* 25:121–132.

105. Andrew, D. R., W. H. Guo, and Y-L. Wang. 2011. The regulation of traction force in relation to cell shape and focal adhesion. *Biomaterials.* 32:2043–2051.

106. Sawada, Y., and M. P. Sheetz. 2002. Force transduction by Triton cytoskeletons. *J. Cell Biol.* 156:609–615.

107. Saez, A., E. Anon, M. Ghibaudo, O. Roure, J. M. Di Meglio, P. Hersen, P. Silberzan, A. Buguin, and B. Ladoux. 2010. Traction forces exerted by epithelial cell sheets. *J. Phys. Condens. Matter.* 22:194119.

108. Han, S. J., K. S. Bielawski, L. H. Ting, M. L. Rodriguez, and N. J. Sniadecki. 2012. Decoupling substrate stiffness, spread area and micropost density: A close spatial relationship between traction forces and focal adhesion. *Biophys. J.* 103: 640–648.

109. Tzvetkova-Chevolleau T., A. Stéphanou, D. Fuard, J. Ohayon, P. Schiavone, and P. Tracqui. 2008. The motility of normal and cancer cells in response to the combined influence of the substrate rigidity and anisotropic microstructure. *Biomaterials.* 29: 1541–1551.

110. Frey M. T., I. Y. Tsai, T. P. Russell, S. K. Hanks, and Y-L. Wang. 2006. Cellular Responses to Substrate Topography: Role of Myosin II and Focal Adhesion Kinase. Biophys. J. 90: 3774–3782.

111. Solon, J., I. Levetal, K. Sengupta, P. C. Georges, and P. A. Janmey. 2007. Fibroblast Adaptation and Stiffness Matching to Soft Elastic Substrates. *Biophys. J.* 93:4453–4461.

112. Marcq P., N. Yoshinaga, and J. Prost. 2011. Rigidity sensing explained by active matter theory. *Biophys. J.* 101:L33–L35.

113. Mitrossilis D., J. Fouchard, A. Guiroy, N. Desprat, N. Rodriguez, B. Fabry, and A. Asnacios. 2009. Single-cell response to stiffness exhibit muscle-like behavior. *Proc. Natl. Acad. Sci. USA.* 106:18243–18248.

114. Beningo K. A., M. Dembo, I. Kaverina, J. V. Small, and Y-L. Wang. 2001. Nascent focal adhesion are responsible for the generation of strong propulsive forces in migrating fibroblasts. *J. Cell Biol.* 153: 881–887.

115. Gardel M. L., S. Benedikt, L. Ji, G. Danuser, U. S. Schwarz, and C. M. Waterman. 2008. Traction stress in focal adhesion correlates biphasically with actin retrograde flow speed. *J. Cell Biol.* 183:999–1005.

116. Califano, J. P., and C. A, Reinhart-King. 2008. A balance of substrate mechanics and matrix chemistry regulates endothelial cell network assembly. *Cell. Mol. Bioengin,* 1: 122–132.

117. Reinhart-King, C. A., M. Dembo, and D. A. Hammer. 2003. Endothelial cell traction force on RGD-derivatized polyacrylamide substrata. *Langmuir.* 19: 1573-1579.

118. Reinhart-King, C. A., M. Dembo, and D. A. Hammer. 2008. Cell-cell mechanical communication through compliant substrates. *Biophys. J.* 95: 6044–6051.

119. Reinhart-King, C. A., M. Dembo, and D. A. Hammer. 2005. The dynamics and mechanics of endothelial cell spreading. *Biophys. J.* 89: 676–689.

120. Leach, J. B., X. Q. Brown, J. G. Jacot, P. A. DiMilla, and J. Y. Wong. 2007. Neurite outgrowth and branching of PC12 cells on very soft substrates sharply decreases below a threshold of substrate rigidity. *J. Neural Eng.* 4: 26–34.

121. Paszek, M. J., N. Zahir, K. R. Johnson, J. N. Lakins, G. I. Rozenberg, A. Gefen, C. A. Reinhart-King, S. S. Margulies, M. Dembo, D. Boettiger, D. A. Hammer, and V. M. Weaver. 2005. Tensional homeostasis and the malignant phenotype. *Cancer Cell*. 8: 241–254.

122. Giannone, G., B. J. Dubin-Thaler, O. Rossier, Y. Cai, O. Chaga, G. Jiang, W. Beaver, H. G. Dobereiner, Y. Freund, G. Borisy, and M. P. Sheetz. 2007. Lamellipodial Actin Mechanically Links Myosin Activity with Adhesion-Site Formation. *Cell.* 128:561-575.

123. Munevar, S., Y.L. Wang, and M. Dembo. 2001. Distinct roles of frontal and rear cell-substrate adhesion in fibroblast migration. *Mol. Biol. Cell.* 12:3947-3954.

124. Stroka, K. M., and H. Aranda-Espinoza. 2009. Neutrophils display biphasic relationship between migration and substrate stiffness. *Cell Motil. Cytoskel.* 66:328-341.

125. Jannat, R. A., M. Dembo, and D. A. Hammer. 2010. Neutrophil adhesion and chemotaxis depend on substrate mechanics. *J. Phys. Condens. Matter.* 22:194117.

126. Martin, S. J., J. G. Bradley, and T. G. Cotter. 1990. HL-60 cells induced to differentiate towards neutrophils subsequently die via apoptosis. *Clin. Exp. Immunol.* 79:448-453.

127. Wei, C. W., C. C. A. Hu, C. H. A. Tang, M. C. Lee, and J. J. Wang. 2002. Induction of differentiation rescues HL-60 cells from Rana catesbeiana ribonuclease-induced cell death. *FEBS Lett.* 531:421-426.

128. Gieseler, F., P. Meyer, D. Schiffmann, and K. Wilms. 1989. Granulocytic differentiation of HL-60 cells is not regulated by DNA de novo methylation. *Blut.* 58:159-163.

129. Eddy, R. J., L. M. Pierini, F. Matsumura, and F. R. Maxfield. 2000. Ca^{2+}-dependent myosin II activation is required for uropod retraction during neutrophil migration. *J. Cell Sci.* 113:1287-1298.

130. Mitchell, M. J., and M. R. King. 2012. Shear-Induced Resistance to Neutrophil Activation via the Formyl Peptide Receptor. *Biophys. J.* 102:1804-1814.

131. Tan, J. L., J. Tien, D. M. Pirone, D. S. Gray, K. Bhadriraju, and C. S. Chen. 2002. Cells lying on a bed of microneedles: An approach to isolate mechanical force. *Proc. Natl. Acad. Sci. USA.* 100:1484-1489.

132. Otsu, N. 1979. A Threshold Selection Method from Gray-Level Histograms. IEEE T. Syst. Man Cyb. 9:62-66.

133. Crocker, J. C., and E. R. Weeks. Particle tracking using IDL. http://www.physics.emory.edu/~weeks/idl/. Accessed 12 September, 2009.

134. Lim, F. Y., Y. L. Koon. K.-H. Chiam. A computational model of amoeboid cell migration. 2013. *Comput. Method Biomec.* 1-12.

135. Riedl, J., A. H. Crevenn, K. Kessenbrock, J. H. Yu, D. Neukirchen, M. Bista, F. Bradke, D. Jenne, T. A. Holak, Z. Werb, M. Sixt, and R. Wedlich-Soldner. 2008. Lifeact: a versatile marker to visualize F-actin. *Nat. Methods.* 5:605- 607.

136. Jannat, R. A., M. Dembo, and D. A. Hammer. 2010. Neutrophil adhesion and chemotaxis depend on substrate mechanics. *J Phys. Condens. Matter.* 22:194117.

137. Wu, B., J. Li, D. Huang, W. Wang, Y. Chen, Y. Liao, X. Tang, H. Xie, and F. Tang. 2011. Baicalein mediates inhibition of migration and invasiveness of skin carcinoma through ezrin in A431 cells. *BMC Cancer.* 11:527.

138. Stewart, M. P., J. Helenius, Y. Toyoda, S. P. Ramanathan, D. J. Muller, and A. A. Hyman. 2011. Hydrostatic pressure and the actomyosin cortex drive mitotic cell rounding. *Nature.* 469:226-230.

139. Hawkins, R. J., M. Piel, G. Faure-Andre, A.M. Lennon-Dumenil, J.F. Joanny, J. Prost and R. Voituriez. 2009. Pushing off the walls: A mechanism of cell motility in confinement. *Phys. Rev. Lett.* 102:058103.

140. Khanna, C., J. Khan, P. Nguyen, J. Prehn, J. Caylor, C. Yeung, J. Trepel, P. Meltzer, and L. Helman. 2001. Metastasis-associated differences in gene expression in a murine model of osteosarcoma. *Cancer Res.* 61:3750-3759.

141. Yu, Y., J. Khan, C. Khanna, L. Helman, P. S. Meltzer, and G. Merlino. 2004. Expression profiling identifies the cytoskeletal organizer ezrin and the developmental homeoprotein Six-1 as key metastatic regulators. *Nat. Med.* 10:175-81.

142. Elliott, B. E., J. A. Meens, S. K. SenGupta, D. Louvard, and M. Arpin. 2005. The membrane cytoskeletal crosslinker ezrin is required for metastasis of breast carcinoma cells. *Breast Cancer Res.* 7:R365-R373.

143. Meng, Y., Z. Lu, S. Yu, Q. Zhang, Y. Ma, and J. Chen. 2010. Ezrin promotes invasion and metastasis of pancreatic cancer cells. *J. Transl. Med.* 8:61.

144. Gautreau, A., P. Poullet, D. Louvard, and M. Arpin. 1999. Ezrin, a plasma membrane–microfilament linker, signals cell survival through the phosphatidylinositol 3-kinase/Akt pathway. *Proc. Natl. Acad. Sci. USA.* 96:7300-7305.

145. Friedl, P., and K. Wolf. 2009. Plasticity of cell migration: a multiscale tuning model. *J. Cell Biol.* 188:11-19.

146. Hayakawa, K., H. Tatsumi, and M. Sokabe. 2012. Mechano-sensing by actin filaments and focal adhesion proteins. *Commun. Integr. Biol.* 5:572–577.

147. Hayakawa, K., H. Tatsumi, and M. Sokabe. 2011. Actin filaments function as a tension sensor by tension-dependent binding of cofilin to the filament. J. Cell Biol. 195:721–727.

148. Batchelder, E. L., G. Hollopeter, C. Campillo, X. Mezanges, E. M. Jorgensen, P. Nassoy, P. Sens, and J. Plastino. 2011. Membrane tension regulates motility by controlling lamellipodium organization. *Proc. Natl. Acad. Sci. USA.* 108:11429-11434.

149. Keren, K. 2011. Cell motility: the integrating role of the plasma membrane. *Eur. Biophys. J.* 40:1013-1027.

150. Gauthier, N. C., M. A. Fardin, P. Roca-Cusachs, M. P. Sheetz. 2011. Temporary increase in plasma membrane tension coordinates the activation of exocytosis and contraction during cell spreading. *Proc Natl Acad Sci USA.* 108:14467-14472.

151. Norman, L. L., J. Brugés, K. Sengupta, P. Sens, and H. Aranda-Espinoza. 2010. Cell blebbing and membrane area homeostasis in spreading and retracting cells. *Biophys. J.* 99:1726-1733.

152. Sanz-Moreno, V., G. Gadea, J. Ahn, H. Paterson, P. Marra, S. Pinner, E. Sahai, and C. J. Marshal. 2008. Rac activation and inactivation control plasticity of tumor cell movement. *Cell.* 135:510-523.

153. Levental, K. R., H. Yu, L. Kas, J. N. Lakins, M. Egeblad, J. T. Erler, S. F. Fong, K. Csiszar, A. Giaccia, W. Weninger, M. Yamauchi, D. L. Gasser, and V. M. Weaver. 2009. Matrix crosslinking forces tumor progression by enhancing integrin signaling. *Cell.* 139:891-906.

154. Lu, P., V. M. Weaver, and Z. Werb. 2012. The extracellular matrix: A dynamic niche in cancer progression. *J. Cell Biol.* 196:395-406.

155. Hsu, H. J. , C. F. Lee, A. Locke, S. Q. Vanderzyl, and R. Kaunas. 2010. Stretch-induced stress fiber remodeling and the activations of JNK and ERK depend on mechanical strain rate, but not FAK. *PLoS ONE.* 5:e12470.

156. Aratyn-Schaus, Y., P. W. Oakes, and M. L. Gardel. 2011. Dynamic and structural signatures of lamellar actomyosin force generation. *Mol. Biol. Cell*. 22:1330-1339.

157. Gupton, S. L., and C. M. Waterman-Storer. 2006. Spatiotemporal feedback between actomyosin and focal-adhesion systems optimizes rapid cell migration. *Cell.* 125:1361–1374.

158. Hirata, H., H. Tatsumi, and M. Sokabe. 2008. Mechanical forces facilitate actin polymerization at focal adhesions in a zyxin-dependent manner. *J. Cell Sci*. 121:2795-2804.

159. Pasapera, A. M., I. C. Schneider, E. Rericha, D. D. Schlaepfer, and C. M. Waterman. 2010. Myosin II activity regulates vinculin recruitment to focal adhesions through FAK-mediated paxillin phosphorylation. *J Cell Biol.* 188:877-890.

160. Wolfenson, H., A. Bershadsky, Y. I. Henis, and B. Geiger. 2011. Actomyosin-generated tension controls the molecular kinetics of focal adhesions. *J. Cell Sci*., 124:1425-1432.